Spring 5-31-2004

3-D numerical simulation of reactive extrusion and its application to polymerization of ε-caprolactone in co-rotating twin-screw extruders

Linjie Zhu
New Jersey Institute of Technology

ABSTRACT

3-D NUMERICAL SIMULATION OF REACTIVE EXTRUSION AND ITS APPLICATION TO POLYMERIZATION OF ε-CAPROLACTONE IN CO-ROTATING TWIN-SCREW EXTRUDERS

by
Linjie Zhu

A 3-D numerical simulation model was proposed to predict the polymerization of ε-caprolactone in fully-filled conveying elements and kneading blocks of co-rotating twin-screw extruders, in which the kinetics equation for polymerization is coupled with continuity equation, momentum equation, and energy equation. With the 3-D model, parametric studies have been carried out to investigate the effects of screw configurations, screw diameter, operational conditions, values of heat from reaction, initiator concentration, and heat transfer conditions at barrel surface upon the polymerization progress. Two simulation models for the polymerization in the partially-filled channels were developed based on the conveying mechanisms of the reaction system in the screw channels. Finally, a global model for reactive extrusion was proposed, combining the models for the fully-filled screw elements and the partially-filled channels.

The predicted conversion ratios at the die based on the 3-D model agree well with the experimental results from the literature, indicating that the proposed 3-D model for polymerization in twin-screw extruders is reliable. Three indices, i.e. flux-mixing coefficient, temperature mixing coefficient, and conversion ratio mixing coefficient, are defined for the first time to evaluate the axial mixing during reactive extrusion.

Moreover, transverse mixing is characterized with the ratio of pressure flow rate to net flow rate in axial cross sections.

The simulation results based on the 3-D model indicate that the polymerization of ε-caprolactone in screw elements depends not only on the mixing mechanism and flow behavior, but also on the heat generation in the reaction system and the heat transfer at the barrel surfaces. It is proposed that the optimization of polymerization in twin-screw extruders can be achieved by matching the flow and mixing mechanisms with the energy generation and energy loss. The application of 1-D model, a commonly used method in the simulation of reactive extrusion, in predicting the polymerization progress in reactive extrusion is acceptable only under certain conditions, such as a small screw diameter, a short fully-filled length, a low screw rotating speed, and a small heat from reaction.

The investigation in scaling up polymerization in twin-screw extruders with the 3-D model reveals that the polymerization is completed in shorter screw length (in unit of screw diameter) with increasing screw diameter, due to the non-uniformity in temperature in large extruders. The optimizations of screw configurations, operational conditions, and cooling systems are extremely important to the polymerization in large machines, in which 3-D model is a valuable tool.

3-D NUMERICAL SIMULATION OF REACTIVE EXTRUSION AND ITS APPLICATION TO POLYMERIZATION OF ε-CAPROLACTONE IN CO-ROTATING TWIN-SCREW EXTRUDERS

by
Linjie Zhu

A Dissertation
Submitted to the Faculty of
New Jersey Institute of Technology
in Partial Fulfillment of the Requirements for the Degree of
Doctor of Philosophy in Mechanical Engineering

Department of Mechanical Engineering

May 2004

APPROVAL PAGE

3-D NUMERICAL SIMULATION OF REACTIVE EXTRUSION AND ITS APPLICATION TO POLYMERIZATION OF ε-CAPROLACTONE IN CO-ROTATING TWIN-SCREW EXTRUDERS

Linjie Zhu

Dr. Kwabena A. Narh, Dissertation Advisor — Date
Associate Professor of Mechanical Engineering, NJIT

Dr. Kun S. Hyun, Dissertation Co-Advisor — Date
President of Polymer Processing Institute, Newark, NJ
Research Professor of Otto York Department of Chemical Engineering, NJIT

Dr. Marino Xanthos, Committee Member — Date
Professor of Otto York Department of Chemical Engineering, NJIT
Director of Polymer Processing Institute, Newark, NJ

Dr. Rong-Yaw Chen, Committee Member — Date
Professor of Mechanical Engineering, NJIT

Dr. I. Joga Rao, Committee Member — Date
Assistant Professor of Mechanical Engineering, NJIT

BIOGRAPHICAL SKETCH

Author: Linjie Zhu

Degree: Doctor of Philosophy

Date: May, 2004

Undergraduate and Graduate Education:

- Doctor of Philosophy in Mechanical Engineering, 2004
  New Jersey Institute of Technology, Newark, NJ

- Doctor of Philosophy in Chemical Processing and Machinery, 1999
  Beijing University of Chemical Technology, Beijing, China

- Master of Science in Polymer Processing, 1996
  Chengdu University of Science and Technology, Sichuan, China

- Bachelor of Engineering in Plastics Engineering/Processing Machinery, 1993
  Chengdu University of Science and Technology, Sichuan, China

Major: Mechanical Engineering

Publications and Presentations

L. Zhu, K. A. Narh, K. S. Hyun, "Scale-up Consideration for Polymerization in a Twin-screw Extruder using 3-D Numerical Simulation", Accepted by 62nd *SPE ANTEC*, 2004.

L. Zhu, K. A. Narh, "Investigation of Reinforcement Mechanisms of Carbon Nanotube-polymer Composites with Numerical Simulation", Accepted by 62nd *SPE ANTEC*, 2004.

L. Zhu, K. Narh, "Numerical Simulation of the Effect of Nanotube Orientation on Tensile Modulus of Carbon Nanotube Reinforced Polymer Composites", Accepted by *Polymer International.*

L. Zhu, K. Narh, "Modeling of Tensile Modulus of Polymer-clay Nanocomposites", Accepted by *Journal of Polymer Science, Part B, Polymer Physics.*

L. Zhu, M. Xanthos, "Effects of Process Conditions and Mixing Protocols on Structure of Extruded Polypropylene Nanocomposites", Accepted by *Journal of Applied Polymer Science.*

L. Zhu, X. Geng, "Experimental Investigation of Polymer Pellets Melting Mechanisms in Co-rotating Twin-screw Extrusion", *Advances in Polymer Technology*, 21, pp. 188-200, 2002.

L. Zhu, K. A. Narh, X. Geng, "Modeling of Particle-Dispersed Melting Mechanism and Its Application in Co-rotating Twin-Screw Extrusion", *Journal of Polymer Science, Part B, Polymer Physics*, 39, pp. 2461-2468, 2001.

L. Zhu, K. A. Narh, K. S. Hyun, "3-D Modeling of Polymerization in Conveying Element in Twin-screw Extruder", *Proceedings of 61st SPE ANTEC*, Nashville, TN, Society Plastics Engineers, Brookfield, CT, pp. 147 -151, 2003.

L. Zhu, K. S. Hyun, "Numerical Simulation of Bulk Polymerization of ε-Caprolactone in Extrusion", *Proceedings of 60th SPE ANTEC*, San Francisco, CA, Society Plastics Engineers, Brookfield, CT, pp. 204-208, 2002.

L. Zhu, K. S. Hyun, K. A. Narh, "Modeling of Bulk Polymerization of ε-Caprolactone in Shear Flow", *Proceedings of 18th Annual Meeting of Polymer Processing Society (PPS-18)*, Guimaraes, Portugal, 2002.

This dissertation is dedicated to my beloved wife, Ying Sun, and my parents.

ACKNOWLEDGMENT

I like to express my sincere appreciation to my advisors, Dr. K. A. Narh and Dr. K. S. Hyun, for their valuable guidance, supervision and friendship through this research. Special thanks are given to Dr. M. Xanthos, Dr. R. Chen, and Dr. I. J. Rao for serving as dissertation committee members, and providing helpful suggestions for this study. I also like to thank Dr. D. Todd from the Polymer Processing Institute, for his inspirational discussions with me about this research topic.

I am grateful for the financial support from the Department of Mechanical Engineering, NJIT, and the support from the Polymer Processing Institute (PPI) in the summer semesters of 2001 and 2002.

I owe a debt of gratitude to my wife, my parents, and my sisters, for their patience and understanding. Without their support, it would have been impossible for me to complete my academic pursuits smoothly.

Finally, I would like to extend a special thanks to my friends here at NJIT and PPI, who made my experience a most enjoyable one.

TABLE OF CONTENTS

TABLE OF CONTENTS
(Continued)

Chapter **Page**

TABLE OF CONTENTS
(Continued)

Chapter **Page**

LIST OF TABLES

LIST OF FIGURES

LIST OF FIGURES
(Continued)

Figure **Page**

LIST OF FIGURES
(Continued)

Figure **Page**

LIST OF FIGURES
(Continued)

Figure **Page**

LIST OF FIGURES
(Continued)

Figure **Page**

LIST OF FIGURES
(Continued)

Figure **Page**

LIST OF SYMBOLS

A	Area (m^2)
C, C_o	Conversion ratio and initial conversion ratio
C_p	Specific heat (J/kg K)
C_L	Centerline distance (mm)
D	Diameter (mm)
E_a	Activation energy (kJ/mol)
E_b, E_s	Activation energy for the bulk, and solution systems (kJ/mol)
$E_{monomer}$	Activation energy for monomer (kJ/mol)
F_r	Froude number
G_f	Flux mixing coefficient in axial direction
G_T	Temperature mixing coefficient in axial direction
G_c	Conversion ratio mixing coefficient in axial direction
G_{TV}	Transverse mixing coefficient
h_b, h_s	Heat transfer coefficients at barrel, and screw surface (W/m^2 K)
ΔH, H	Reaction heat (kJ/kg)
H_{ch}	Channel Depth (mm)
g	Gravitational constant
J_r	Jeffrey's number
k	Thermal conductivity (W/m K)
L, L_z	Channel Length (mm)
M_o	Monomer molecular weight (g)

LIST OF SYMBOLS
(Continued)

$\overline{M}_w$	Weight averaged molecular weight (g)
$[M]$, $[M]_o$	Monomer concentration and initial monomer concentration
N	Screw rotating speed (rpm)
N_b, N_f	Numbers of the cells with forward, and reversed axial velocity
n	Number of thread start of screw
ΔP	Pressure difference (Pa)
P	Pressure (Pa)
Q, Q_d,Q_p	Net flow rate, drag flow rate and Pressure flow rate (m^3/s)
Q_L	Leaking flow rate (m^3/s)
Q_{dmax}	Maximum drag flow capacity (m^3/s)
Q_v, Q_r	Viscous dissipation and reaction heat (W)
Q_B, Q_F	Back flow rate, and forward flow rate (m^3/s)
Q_{ch}	Volume of the screw channel (m^3)
Q_{pr}	Volumetric flow rate per revolution ($m^3/s/r$)
q	Heat flux (W/m^2)
R_b, R_s	Screw tip radius, and screw root radius (mm)
Re	Reynolds number
R	Universal gas constant (8.314 kJ/kg mol K)
r_r	Degree of reaction
S_b	Barrel surface area (m^2)

LIST OF SYMBOLS
(Continued)

T	Temperature (K)
$\overline{T}_f$	Average temperature of melt (K)
T_b, T_s	Barrel, and screw temperatures (K)
T_{fl}	Fluid temperature in the layer next to the barrel surface (K)
t	Reaction time (s)
t_p , t_f	Residence time in partially-, and fully-filled channels (s)
V	Velocity (m/s) or volume (m^3)
V_L	Leaking flow rate (m^3/s)
V_f	Volume of the flight (m^3)
X, Y, Z	x-, y- and z-coordinates
ΔZ	Axial length of the partially filled area (mm)
α	Tip angle or the partial order related to the initiator
λ, ξ, ζ	Constants
η	Viscosity (Pa - s)
ε	Degree of fill
ρ	Density (kg/ m3) or radius (m)
φ	Helical angle of the flight or constant
δ	Clearance (m)
Δ	Layer thickness (m)

CHAPTER 1

INTRODUCTION TO SIMULATION OF REACTIVE EXTRUSION

Reactive extrusion refers to the application of screw extruders as chemical reactors to deliberately perform chemical reactions, such as polymerization and chemical modification of polymers (1-3). This chapter gives a brief introduction to the structures of intermeshing co-rotating twin-screw extruders, features of reactive extrusion, and literature review of numerical simulation in reactive extrusion.

1.1 Co-rotating Twin-screw Extruder

As an important part of processing technology, the twin-screw extruder has a variety of geometries. The main geometrical features that distinguish various twin-screw extruders are the sense of rotation and the degree of intermeshing between two screws (4-9). There are three basic categories of twin-screw extruders nowadays, i.e. intermeshing co-rotating twin-screw extruder, intermeshing counter-rotating twin-screw extruder, and non-intermeshing counter-rotating twin-screw extruder.

Co-rotating intermeshing twin-screw extruders (CRTSEs) are the most important twin-screw machines. They are typically offered in modular screw and barrel designs (Figure 1.1), which allow for economical manufacturing as well as versatile mechanical configurations and operating conditions, dictated by the processing needs. Such design characteristics make CRTSEs a valuable part of manufacturing processes in the polymer, chemical, and food industries. However, the flexibilities in modular designs and operating condition selections can lead the inexperienced process engineer down the

wrong path. Therefore, to complete a complicated processing task successfully, a well-defined and focused approach to the problem must be pursued (10). This is the reason why lots of research efforts have been carried out to understand the conveying, melting and mixing mechanisms in CRTSEs in the last decades.

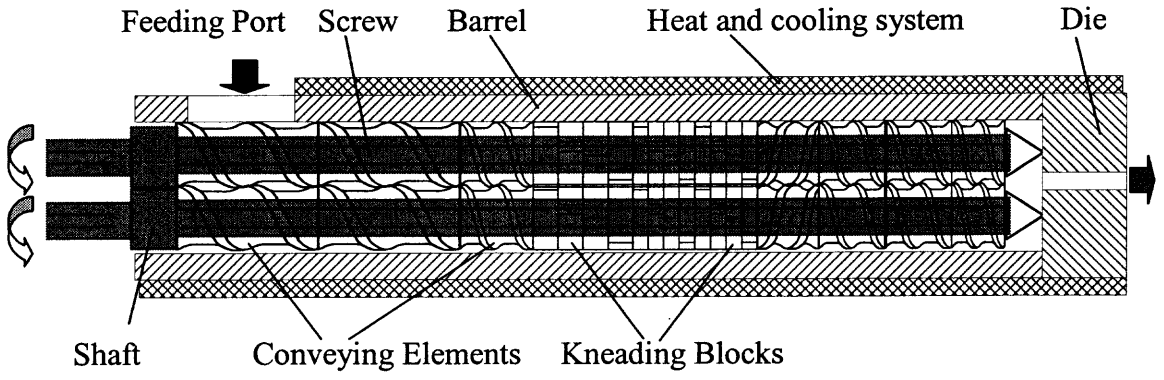

Figure 1.1 Schematic diagram for co-rotating twin-screw extruders.

There are two basic types of screw elements in co-rotating twin screw extruders: conveying elements and kneading blocks. The cross section of a conveying element is exactly the same as a kneading block. Figure 1.2 shows the typical cross section curves for a co-rotating twin screw extruder, in which the radius $\rho(\theta)$ is given as (11-12):

$$\rho(\theta)=\begin{cases} R_b & \begin{cases} -\frac{\alpha}{2}\le\theta\le\frac{\alpha}{2} \\ \pi-\frac{\alpha}{2}\le\theta\le\pi+\frac{\alpha}{2} \end{cases} \\ R_s Cos(\theta-\frac{\alpha}{2})+\sqrt{C_L{}^2-R_s{}^2 Sin^2(\theta-\frac{\alpha}{2})} & \begin{cases} \frac{\alpha}{2}\le\theta\le\frac{\pi}{2}-\frac{\alpha}{2} \\ \frac{\pi}{2}+\frac{\alpha}{2}\le\theta\le\pi-\frac{\alpha}{2} \\ \pi+\frac{\alpha}{2}\le\theta\le\frac{3\pi}{2}-\frac{\alpha}{2} \\ \frac{3\pi}{2}+\frac{\alpha}{2}\le\theta\le 2\pi-\frac{\alpha}{2} \end{cases} \\ R_s & \begin{cases} \frac{\pi}{2}-\frac{\alpha}{2}\le\theta\le\frac{\pi}{2}+\frac{\alpha}{2} \\ \frac{3\pi}{2}-\frac{\alpha}{2}\le\theta\le\frac{3\pi}{2}+\frac{\alpha}{2} \end{cases} \end{cases} \tag{1.1a}$$

where C_L is the centerline distance; R_b is the screw tip radius, and R_s the screw root radius. α is the tip angle, defined as:

$$\alpha = \pi/(n) - 2\cos^{-1}(C_L/2R_b) \tag{1.1b}$$

where n is the number of thread start of screw (n = 2 in Figure 1.2).

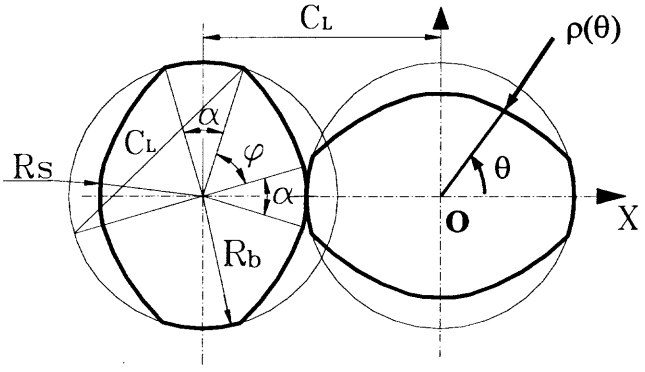

Figure 1.2 Cross sectional curves of screw elements.

The difference in geometries between conveying elements and kneading blocks is as follows: the conveying element is constructed by propagating the cross sectional curve (described in Equation 1.1) continuously along a helix, as shown in Figure 1.3a; the kneading blocks are built with a certain number of kneading discs at a constant stagger angle, in which the kneading disc is extruded from the cross sectional curve (with a zero helical angle) at a certain thickness. For instance, Figure 1.3b exhibits the configuration of a kneading block built by 4 pieces of kneading discs at a stagger angle of 60°.

The flow of polymer melt in screw channels can be described by a simplified equation:

$$Q = Q_d - Q_p - Q_L \tag{1.2a}$$

$$Q = \lambda N - \xi \frac{\Delta P}{\eta} - \zeta N \tag{1.2b}$$

in which Q is the net flow rate, and Q_d the drag flow rate; Q_p is the pressure flow rate and Q_L the leaking flow rate. Three terms on the right side of Equation 1.2b are the expressions for Q_d, Q_p and Q_L, respectively, where λ, ξ, and ζ are constants depending on the screw geometry (12). N is the screw rotational speed, and ΔP the pressure difference between the inlet and outlet of the screw element. η is the viscosity of the polymer melt.

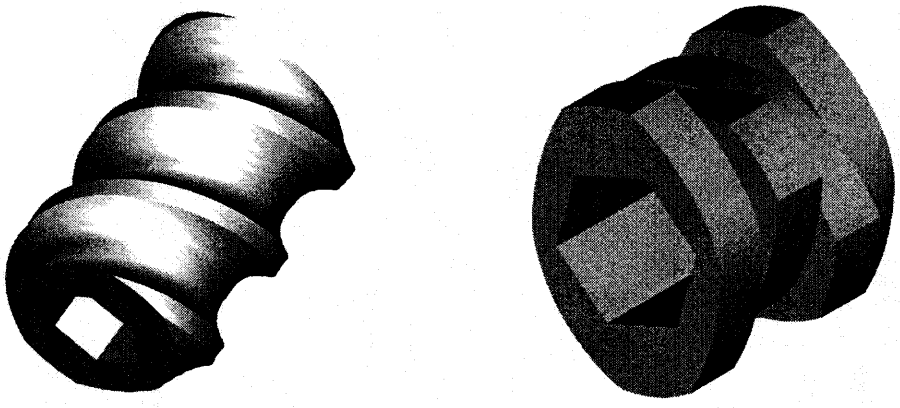

(a) (b)

Figure 1.3 Geometry of screw elements (a) conveying element, (b) kneading block.

For conveying elements, the screw pitch is an important parameter. Elements with high pitch have large drag flow capacity, but low ability to build pressure along the axial length. Consequently, high pitch element might typically be used in feeding or devolatilization zones of extruders, and narrow pitch elements in areas where compaction of materials and 100% fill are desired (10).

Kneading blocks are generally characterized with total length, number of discs, and stagger angle. The conveying capacity of kneading blocks depends on the stagger angle and width of kneading disc. When the stagger angle is less than 90° (i.e. forward kneading block), the elements have a positive conveying capacity. The conveying capacity becomes zero at a stagger angle of 90° (i.e. neutral kneading block), and

becomes negative when the stagger angle is larger than 90° (i.e. reversed kneading block). Due to the discontinuity of the geometry, kneading blocks have larger leaking flow than conveying elements. Accordingly, the conveying capacity in kneading blocks is usually lower than conveying elements. However, the mixing capacity of kneading blocks is enhanced due to the leaking flow.

The modular design of screws is achieved by mounting the screw elements, say, conveying elements and kneading blocks, on a shaft (Figure 1.1). Because various screw elements have different conveying and mixing capacities, the change of the sequence of elements along the axial length might result in a totally different flow behavior of polymers in the extruder. Consequently, in twin-screw extrusion, a specific process should use a unique screw configuration, in order to enhance the quality and reduce the cost of the product.

1.2 Reactive Extrusion

In a reactive extrusion, the synthesis or modification of a polymeric material takes place simultaneously with the processing and shaping of a final product. This is an efficient method for continuous polymerization of monomers and chemical modification of existing polymers, and is viewed as a complex reaction engineering process that combines the traditionally separated operations, i.e., polymer chemistry (polymerization or chemical modification) and extrusion (blending, compounding, structuring, devolatilization, and eventually shaping), into a single process in a screw extruder (1-3, 15). Chemical reactions, such as bulk polymerization, graft reaction, inter-chain copolymer formation, coupling/crosslinking reactions, controlled degradation,

functionalization, and reactive blending, have been performed successfully with reactive extrusion (1-3, 13-14).

Extruders have been found very attractive for many reactive processing applications because of several inherent features. Compared with other chemical reactors, say, a continuous stirred tank reactor (CSTR), a twin-screw extruder reactor has the following advantages (2, 7, 9, 15-16):

- Bulk reactions involving both low and high viscous reactants.
- Staging of sequential unit operations.
- Removal of unreacted monomers and by-product.
- Modular screw and barrel design and self-wiping structure.
- Control over residence time distribution.
- Excellent dispersive and distributive mixing.
- Continuous processing.
- A flexible process for low-tonnage trial or production.
- Reaction under pressure and temperature control.

However, the inherent feature of extruders also brings limitations to reaction processing, such as difficulty in handling large heat from reaction, and high cost for long reaction time. Furthermore, in reactive extrusion, a unique screw and barrel configuration (or design) is required for a specific reaction. In contrast, the same continuous stirred tank reactor can be used for a wide range of chemical reactions in solution. This suggests that it is of great value to investigate the effect of screw configurations, operating conditions and machine size on reactive processing.

1.3 Literature Review of Simulation of Reactive Extrusion in Twin-screw Extruders

Computer-aided simulation of polymer flow in extruders not only constitutes a key aid in improving the quality of products by optimizing the processing conditions, but also offers an effective way to reduce the cost. Furthermore, it gives access to data and information relevant to the process which is difficult to get, or indeed not available at all, by experiments.

So far, there are very limited literatures on the simulation of reactive extrusion due to the complex nature of the twin-screw extruder and reaction process, although the modeling of reactive extrusion has been investigated since the 1970s. However, the papers published in the 1970s (17-22) generally focused on the flow in a "flooding fed" single screw extruder with constant screw design along the axial length. This is different from the case of co-rotating twin-screw extruders, in which the screw channel is not necessarily fully filled, and the screw is built with elements in different geometries.

The mechanisms of reactive extrusion can be generally combined into three main groups, such as flow and mixing behavior, heat generation and transfer, and reaction (23). These factors interact with each other, as shown in Figure 1.4. The flow behavior of polymer melt in the extruder determines the degree of fill in screw channels, mixing intensity in melt, and residence time (or residence time distribution), thus affecting the heat transfer behavior and reaction rate. On the other hand, reaction and heat transfer influence the flow of melt in the screw channel, because the thermal and chemical conditions of the melt determine the rheological properties and flow characteristics. Furthermore, heat transfer and reaction interact with each other; the reaction rate and reaction equilibrium depend on temperature, whereas the dissipation heat, and reaction

heat, change the thermal state of the reaction system. As a whole, these factors determine the performance of the extruder and the quality of the products.

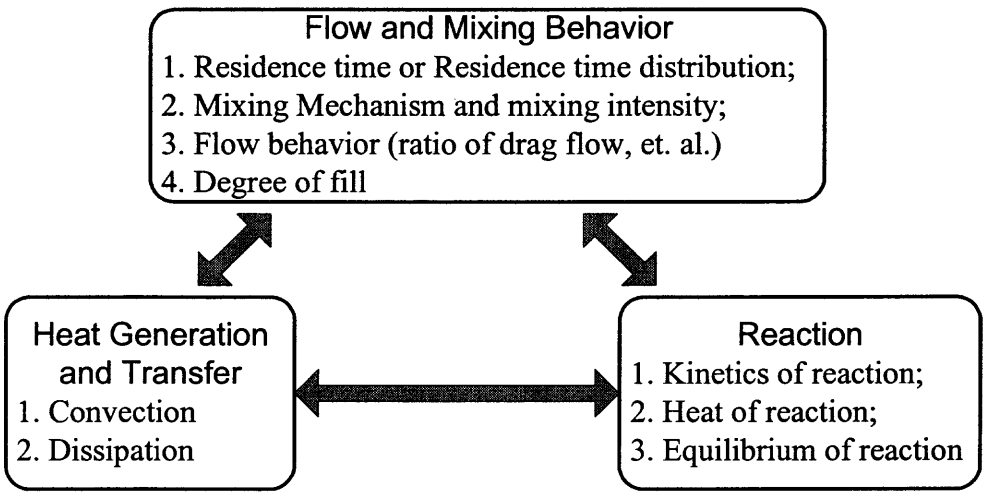

Figure 1.4 Factors in reactive extrusion (23).

Basically, the numerical simulation of reactive extrusion should at least include the following three parts:

- Solver for Continuity equation and Momentum equation;
- Solver for Energy equation;
- Solver for Kinetic equations of reaction;

Another important step in the numerical simulation is how to cope with the complex geometry of twin-screw extruders. Currently, a variety of modeling methods have been developed, in which different techniques are employed to solve the differential equations, and to describe the screw geometries.

1.3.1 General Procedure for Simulation of Reactive Extrusion

It is known that twin-screw extruders are operated with starve feeding. That is, the screw channel in twin-screw extruders is not essentially fully filled. Accordingly, the degree of fill is introduced to evaluate the distribution of materials along the screw channels in twin-screw extruders:

$$\varepsilon = \frac{Q}{Q_{d\max}} \tag{1.3}$$

in which ε represents the degree of fill. Q is the volumetric flow rate (m^3/s), and Q_{dmax} the maximum drag flow capacity of the screw element. When the channel is fully filled, ε equals 1.

Generally, a reversed procedure, i.e. from the die to the feeding port (see Figure 1.1), is used to predict the flow characteristics of polymer melt inside the extruder, because the degree of fill along the screw length is unknown a priori. In the simulation, the die and the reversed screw elements are always assumed to be fully filled. Thus, the pressure gradient at the upstream of these elements can be determined. The general procedures for the simulation of reaction in twin-screw extruders are summarized as follows:

1. The pressure at the die entrance is first calculated after assuming a melt temperature at the die exit, because it is always fully filled.
2. Next, an isothermal approximation is used to determine the location of fill and starvation along the screw axis, from the die to the feeding port. The mean residence time is calculated based on the degree of fill.
3. A non-isothermal calculation is carried out to obtain the temperature rise forwardly along the screw length (from the feeding port to the die).

4. The reaction in each screw element is calculated forwardly, based on the temperature rise and residence time. The viscosity of melt might be adjusted due to the variations in the degree of reaction, temperature, and shear rate.
5. At the die exit, a new melt temperature is calculated. If this new temperature is different from the presumed one, an iterative procedure is applied, i.e. repeating the previous three steps. The iteration stops when convergence is achieved.

1.3.2 Simulation Techniques in Reactive Extrusion

In the literatures, various techniques have been introduced to get the velocity and pressure profiles, to calculate the temperature rise, and to solve the kinetics equation, which are described as follows.

1.3.2.1 Calculation of Velocity and Pressure Profiles. Currently, three techniques are employed in the calculation of velocity and pressure profiles along the screw:

1. Unwrapped screw channel model, in work of Michaeli, et al.(23-24)

The model developed for the conventional single screw extruder is used for describing the flow in co-rotating twin-screw extruders.

2. 1-D channel model, in work of Vergnes, et al. (25-28)

A cylindrical coordinate is used in the analysis of the flow in screw channels, in which the channel section is perpendicular to the screw flights. The screw channel is considered as a succession of C-shaped chambers and the intermeshing area.

3. 2-D FAN method, in work of Fukuoka (29-30) *and White* (31-35)

The FAN method has been employed to analyze a two-dimensional flow field in conveying elements and kneading blocks of co-rotating twin-screw extruders, after

unwinding the screw channels into a flat plane. Accordingly, the pressure and velocity profiles are determined.

1.3.2.2 Modeling of Temperature Profile. In the literature, one-dimensional method (i.e. 1-D model) has been used in calculating the temperature rise along the screw channel (23-35). The temperature is assumed to have a uniform distribution at the axial cross section, and varies along the axial length only. The average shear rate is applied in the calculation of viscous dissipation. The heat transfer between polymer melt and walls (barrel and screw surfaces) is given as:

$$q = h_b(\overline{T}_f - T_b) + h_s(\overline{T}_f - T_s) \tag{1.4}$$

in which h_b and h_s are heat transfer coefficients at barrel and screw surfaces. $\overline{T}_f$ is the mean temperature of polymer melt; T_b and T_s are barrel and screw temperatures, respectively. Considering the fact that the reaction is very sensitive to temperature, modeling of temperature based on the 1-D model might not give correct results in the simulation of reaction extrusion. This is discussed in detail in Chapter 2.

1.3.2.3 Solution of Kinetics Equations of Reaction. Chemical reaction is usually characterized with kinetics equation, which describes the relationship between reaction rate, temperature and time. In the extruder, the degree of reaction differs from location to location along the screw channel, and can be given as:

$$r_r = f(X, Y, Z) \tag{1.5}$$

in which r_r stands for the degree of reaction, X, Y and Z are x-, y- and z-coordinates of the location in the screw channel. In the literature, the kinetics equation of reaction in twin-screw extruders is usually solved by four methods:

1. Ideal mixing model (23-33, 35)

It is assumed that ideal mixing (complete mixing) is achieved in the cross sections (perpendicular to the flow direction). That is, the degree of reaction is identical at any locations in the cross section. Consequently, the degree of reaction changes only along the flow direction, and Equation 1.5 is simplified to be:

$$r_r = f(Z) \tag{1.6}$$

Equation 1.6 indicates that 1-D model could be introduced when ideal mixing is achieved at the cross sections. Obviously, 1-D model would largely simplify the calculation procedure in the simulation. This method is the most commonly used approach in the simulation of reactive extrusion, such as in the studies of Michaeli (23-24), Vergnes (25-28), Fukuoka (29-30) and White (31-33, 35).

2. Residence time distribution model (23, 36-37)

The calculation of the degree of reaction is based on the residence time distribution in the extruder. In this model, the residence time distribution during extrusion is first obtained by experiments or simulation. Then, reactions in the extruder are modeled as a series of reactors, for example, a series of continuous stirred tank reactors (CSTRs). In the work of Michaeli et al. (23), polymerizations of nylon 6 and polystyrene in twin-screw extruders were simulated with the model of cascade of CSTRs and the pipe model (i.e. 1-D model), respectively. It was found that the pipe model gave much higher conversion than those from experiments, whereas the conversion based on the model of cascade of CSTRs could be close to the experimental data. However, the simulation results depend on the number of tank reactors in the model of cascade of CSTRs.

3. Composite reactor model (35)

In the studies of White et al. (35), different reactor models were used to describe the transesterification of ethylene vinyl acetate copolymer in various screw elements of a co-rotating twin-screw extruder. That is, the conveying section was regarded as drag flow reactors (DFRs), the kneading blocks as continuous stirred tank reactors (CSTRs), and the die as plug flow reactors (i.e. 1-D model). Furthermore, the starved flow and fully-filled flow were distinguished in the modeling. In our previous studies (38-39), the polymerization of ε-caprolactone in a screw channel was simulated with a 2-D channel model, and the effects of radial mixing on reaction were considered. It was found that the simulation method, 1-D model or 2-D model, has a significant effect on the simulation results. With increasing radial mixing in the channel, the results from 2-D model approach those from the 1-D model.

4. 3-D model for degradation of polypropylene (40-41)

Recently, Tzoganakis et al. (40-41) used a commercial fluid dynamic analysis package (FIDAP) to investigate the degradation of polypropylene in conveying elements of a co-rotating twin-screw extruder, and in channels of a single screw extruder. It was found that effects of both screw speed and peroxide distribution on reaction are negligible, but the pressure-to-drag flow ratio has a significant influence on degradation. Their work also suggests that it is feasible to carry out the simulation of reaction in extruders with a 3-D model.

1.4 Conclusions

Reactive extrusion is an efficient method for continuous polymerization of monomers and chemical modification of existing polymers. Co-rotating twin-screw extruders have been found suitable for reactive extrusions due to their inherent advantages. The flow of polymer melt in twin-screw extruders is very complex, due to the complex geometries of the extruder, variable properties of polymer melt and complex reaction kinetics. Computer-aided simulation is an important method in optimizing the reaction progression in extruders. Because the reaction is sensitive to temperature and residence time (or residence time distribution), simulation techniques in modeling of reactive extrusion affect the simulation results. Currently, 1-D model is commonly used in predicting the temperature rise and degree of reaction along the screw length in the simulation of reactive extrusion. However, 1-D model is a simplified method, which does not represent the realistic situation in extruders. Some work should be carried out to improve these techniques. This was the motivation and starting point of the current study.

CHAPTER 2

MOTIVATION AND OBJECTIVES

As discussed in Chapter 1, 1-D model is currently the main method used in predicting the temperature profile and reaction progression in the simulation of reactive extrusion. The main advantage of 1-D model is that it makes the simulation simple and easy. However, the phenomena described by 1-D model are different from the realistic conditions in reactive extrusion. In this chapter, the motivation and objectives of the current study are presented following the discussion on the characteristics of 1-D model and its disadvantages.

2.1 One-Dimensional Channel Model

The most important feature of a 1-D channel model is that the temperature and the degree of reaction in extruders change only along the screw length. At any locations in the axial cross section (Plane X-Y in Figure 2.1), temperature of polymeric liquid is uniform, so is the degree of reaction. Consequently, the temperature and degree of reaction in extruders is given as:

$$T = f_1(Z) \tag{2.1}$$

$$C = f_2(Z) \tag{2.2}$$

where T and C stand for temperature and degree of reaction, respectively. Z is the axial distance along the screw length, as shown in Figure 2.1.

It is known that the channel depth is not uniform along the inner periphery of the barrel surface, as shown with symbol h in Figure 2.2. Accordingly, the shear rate in

molten polymer induced by the rotating screws will differ from location to location in the axial cross section, which would result in different viscous dissipation. On the other hand, in twin-screw extruders, most of the over-heated energy in polymer melt is transferred out through the barrel surface. The variation in channel depths would cause non-uniform temperature gradients in the melt.

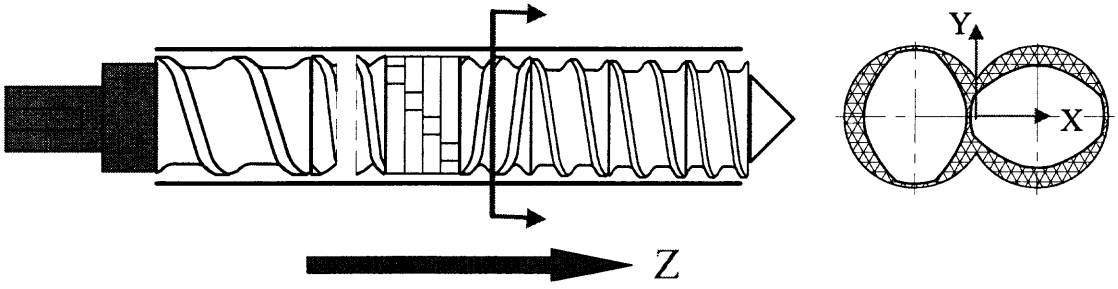

Figure 2.1 Schematic diagram for 1-D model (a) side view and (b) cross sectional view.

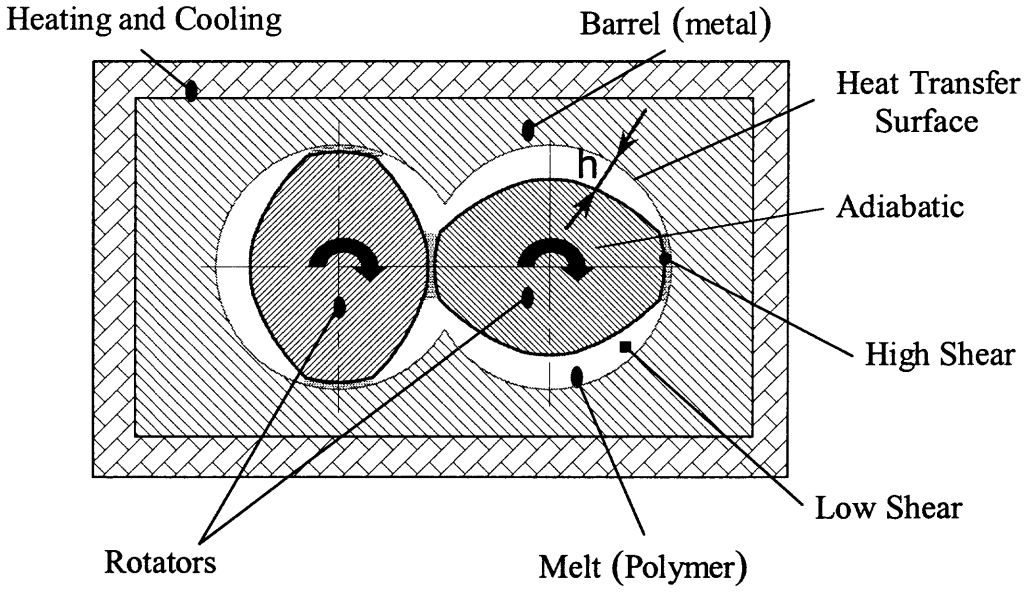

Figure 2.2 Non-uniformities in energy and shear at an axial cross section of a twin-screw extruder.

When the dimension of the machine is considered, the non-uniformity of temperature in the axial cross section would become much pronounced in the large machines. The reasons are two-fold. Firstly, the depth of screw channel rises with increasing machine size, and as discussed in the preceding paragraph, the non-uniformities in shear rates and temperature gradients would increase. Secondly, the ratio of the surface area of barrel to the channel volume decreases when the dimension of the screw is increased, which makes it difficult to release the dissipated energy (due to viscous heating) through the barrel surface.

In order to discuss the effect of temperature distribution on reaction, the energy balance during polymerization in extruders is summarized in Figure 2.3. It shows that an increase in temperature would lead to three possible scenarios (shown as 1 through 3):

1. A rise in temperature raises the degree of polymerization, which releases large exothermal heat from reaction, causing an increase in temperature;
2. The enhancement in the degree of polymerization means the increase in molecular weight and viscosity, which could reduce the heat loss through the wall surface (by convection); consequently, the temperature of the reaction system rises;
3. The increase in system viscosity raises the viscous dissipation, which, in turn, increases the temperature.

The above scenarios suggest that, in a fluid element, a small initial increase in temperature might lead to a large temperature increase, because of the increase in exothermal heat from reaction and viscous dissipation, and the decrease in heat loss through the wall. This implies that the degree of reaction cannot be homogeneous at the axial cross sections of the extruder because the temperature is not uniform there.

Furthermore, the non-uniformity in the degree of reaction could be more significant than that in temperature (As described in the next chapter, the degree of reaction is an exponential function of temperature). This suggests that 1-D model does not represent the realistic conditions in reactive extrusion, and the simulation results based on the latter would be different from the real situations, especially when the reaction heat is large, or the viscosity of the reaction system is high, or the machine size is large.

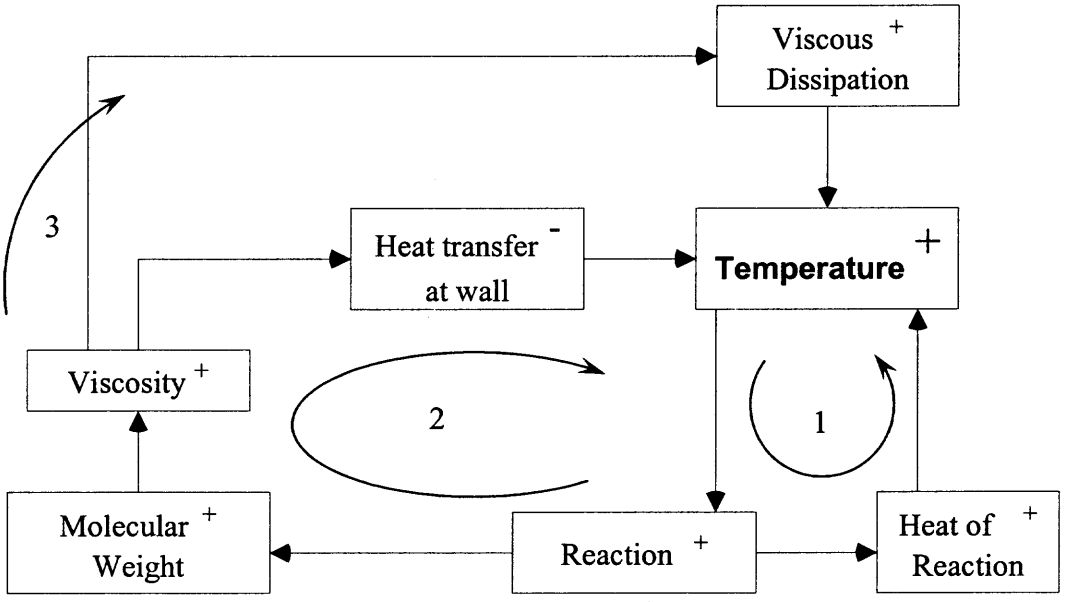

Figure 2.3 Energy relationships in reactive extrusion.

Moreover, in 1-D model, the temperature rise along the axial length (i.e. Z direction in Figure 2.1) can be given as:

$$\rho C_p Q \frac{\Delta T}{\Delta Z} = h_b (T_b - \overline{T}_f) S_b + Q_{vis} + Q_r \tag{2.3}$$

when the screw surface is assumed to have an adiabatic heat transfer condition. h_b is the heat transfer coefficient at the barrel surface. T_b and $\overline{T}_f$ are barrel temperature and averaged fluid temperature. S_b is the barrel surface area, and Q the volumetric flow rate.

ρ and C_p are density and specific heat of the reaction system. Q_{vis} and Q_r are viscous dissipation and reaction heat, respectively. Obviously, the value of the heat transfer coefficient at barrel surfaces, h_b, has a significant effect on temperature rise, and, thus, on the degree of reaction in the simulation.

It is known that the heat transfer in twin-screw extruders is a very complex problem. Although a comprehensive study of this problem was carried out by Todd more than ten years ago (42), there are very few recent studies done in this area (43-45). For a non-reaction system, most of the reported studies used Todd's empirical equation to calculate the temperature rise along the screw length. For reactive extrusion, there are no good criteria for the selection of the heat transfer coefficient, and no numerical simulation has been carried out yet in this area. Michaeli's investigation (23) shows that the melt temperatures calculated based on the heat transfer coefficient from Todd's empirical equation are lower for the synthesis of nylon and higher for the synthesizing of polystyrene than the measured values. This is interpreted by the authors (23) in terms of the heat supplied to the system. More specifically, the heat supply for the thermally initiated caprolactam polymerization and the heat removal for the highly exothermic styrene polymerization are not exactly described by Todd's equation. This suggests that heat transfer in the reactive system is different from that in the non-reaction system. For this reason, it is necessary to carry out some studies to investigate the heat transfer mechanisms in a reactive extrusion process.

2.2 Objectives of the Study

In light of the above discussed issues related to 1-D and 2-D models for simulation of reactive extrusion, the following objectives have been set out:

1. To develop a 3-D model for the simulation of polymerization in fully-filled screw elements of co-rotating twin-screw extruders, in which the kinetics equation of polymerization is coupled with continuity equation, momentum equation and energy equation.

2. To investigate the effects of geometries of screw elements, operation conditions, screw diameters, and initiator concentrations of the reactive system upon polymerization parametrically, based on the 3-D model, in order to find out the dominant factors in reactive extrusion;

3. To study the effect of scale-up on reaction with the 3-D model;

4. To explore the heat transfer mechanisms in reactive extrusion;

5. To propose a method to predict the reaction in partially-filled screw channels, on the basis of the simulation results from 3-D model in the fully-filled zones;

6. To predict the global progression of polymerization in a co-rotating twin-screw extruder; and to compare the numerical simulation results with experimental data from literatures.

CHAPTER 3

THEORETICAL MODEL AND COMPUTATIONAL TECHNIQUES

This chapter focuses on the theories and computational techniques used in the current study, which includes three sections. The first two sections describe the model system and the governing equations employed in the simulation; the last section presents the computational techniques in the numerical simulation.

3.1 Model System

Poly-caprolactone is a biodegradable thermoplastic polymer, which has good water, oil, solvent and chlorine resistance, low melting point and low viscosity. It is widely used in adhesives, building and construction, films, automotive industry, and medical applications. In this study, polymerization of ε-caprolactone was selected as a model system. The information required in the numerical simulation of polymerization of ε-caprolactone, such as kinetic equation of polymerization, rheological model, and heat generation from reaction, as presented in this section, was obtained from the experimental studies of Gimenez (46) and Vergnes (25).

3.1.1 Kinetics Equation for Polymerization of ε-caprolactone (46)

Several studies have been carried out focusing on the polymerization of ε-caprolactone in bulk or in solution. A living mechanism is observed when the polymerization is initiated and catalyzed by titanium tetrapropoxide, a family member of organo-metallic compounds (25, 46-51). The polymerization is described as a two-step "coordination-

insertion" mechanism, in which lactone first forms a complex with the initiator, and then inserts itself into the titanium-alkoxide bond, as shown in Figure 3.1.

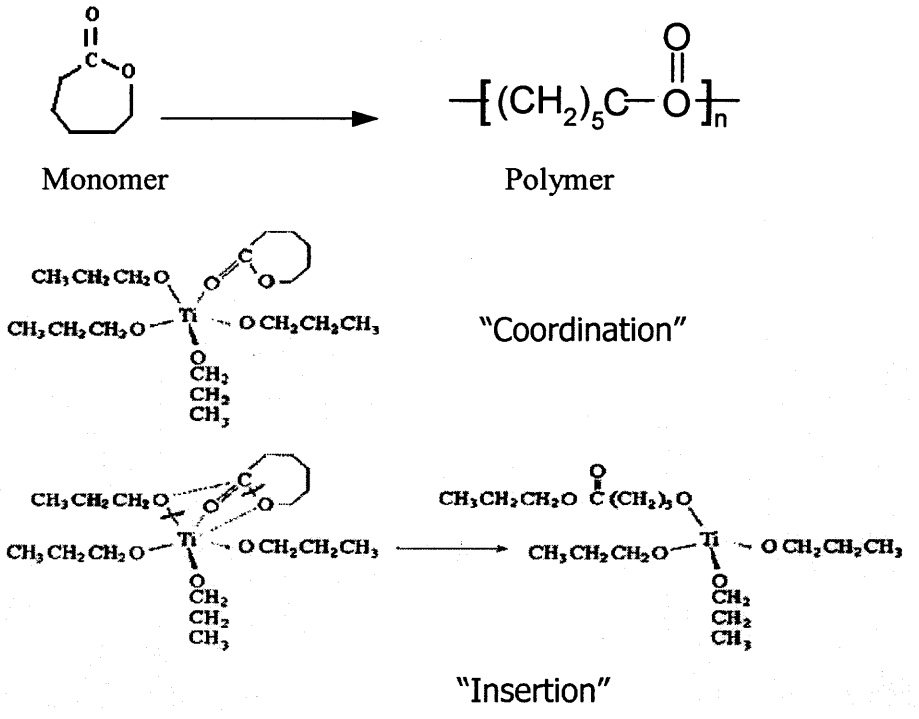

Figure 3.1 Coordination-insertion mechanisms in polymerization of ε-caprolactone (46).

In Gimenez's experimental studies (46), polymerization of ε-caprolactone was carried out in a Rheometrics RMS 800 rheometer with parallel plate geometry, at temperatures in a range of 100 – 160 °C. During the polymerization, the samples were taken manually from the rheometer and dipped into a solvent; the molecular weight distribution, and conversion ratio (degree of reaction), were then analyzed by size exclusion chromatography (SEC), and ^{1}H nuclear magnetic resonance (NMR), respectively. It was found that the variations of the monomer concentration could be described by the first order equation:

$$\frac{d[M]}{dt} = -K[M] \tag{3.1a}$$

$$K = 1.2 \times 10^{16} \times [I]_0^{\alpha} \times \exp(-E_a / RT) \tag{3.1b}$$

where, α, the partial order related to the initiator, is 3.25; E_a, the activation energy, is 9.26 kJ/mol. [M] and $[I]_0$ are monomer and initiator concentration, respectively. R is the universal gas constant, and t the reaction time. Vergnes's work (25) showed that the partial order, α, would depend on the reaction temperature. Typically, α is 2.74 at 100°C, and 3.25 at 140 °C.

The value of $[M]/[I]_o$ quantifies the concentration of the initiator, $[I]_o$, because the polymerization is carried out without solvent. The initiator concentration $[I]_o$ (mol/l) can be calculated from:

$$[I]_o = \frac{1}{r \times (m_m / \rho_m) + (m_I / \rho_I)} \quad \left(\text{mol} \cdot \text{L}^{-1}\right) \tag{3.2}$$

where m_m and ρ_m are the molecular weight and density of ε-caprolactone; m_I and ρ_I are the molecular weight and density of the initiator; r is the ratio of monomer to initiator concentration ($[M]/[I]_o$). Table 3.1 lists the relationship between initiator concentration $[I]_o$ and the value of $[M]/[I]_o$, according to Equation 3.2.

Table 3.1 The Relationship Between $[M]/[I]_o$ and Initiator Concentration $[I]_o$

$[M]/[I]_o$	400	800	1000	1300
$[I]_o$ (mol/l)	0.022588	0.011294	0.0090352	0.00695

The progression of polymerization is usually characterized with the conversion ratio, C, which is defined as:

$$C = \frac{[M]_o - [M]}{[M]_o} \tag{3.3}$$

where [M] and $[M]_0$ are the monomer concentration (during polymerization) and the initial monomer concentration, respectively.

Based on Equations 3.3 and 3.1, the conversion ratio during polymerization can be given by:

$$\frac{dC}{dt} = K(1 - C) \tag{3.4}$$

After integration and rearrangement, the conversion equation takes the form:

$$C = 1 - (1 - C_o)\exp(-\mathrm{K}\,\mathrm{t}) \tag{3.5}$$

where C_0 is the initial conversion ratio, and t the reaction time. When the initial conversion ratio is zero, Equation 3.5 is simplified into:

$$C = 1 - \exp(-\mathrm{K}\,\mathrm{t}) \tag{3.6}$$

Figure 3.2 shows the relationship between conversion ratio, reaction temperature and time, based on Equation 3.6, when $\alpha = 3.25$ (as in Equation 3.1b). The solid curves represent the increase in conversion ratio versus reaction time at constant temperatures during reaction (isothermal curves). It shows that with increasing temperature, conversion ratio has a fast increase; the time to complete polymerization drops significantly at high temperature. The dashed curve demonstrates the conversion ratio profile, assuming that the temperature has a linear increase with time from 80 to 130°C during polymerization. It is seen that the trend of conversion ratio vs. time under a non-isothermal condition differs significantly from that under isothermal conditions. Considering the fact that large exothermic reaction heat is released during the polymerization of ε-caprolactone, the

increase in conversion ratio in a processing device, say, a twin-screw extruder, can not be described by an isothermal equation.

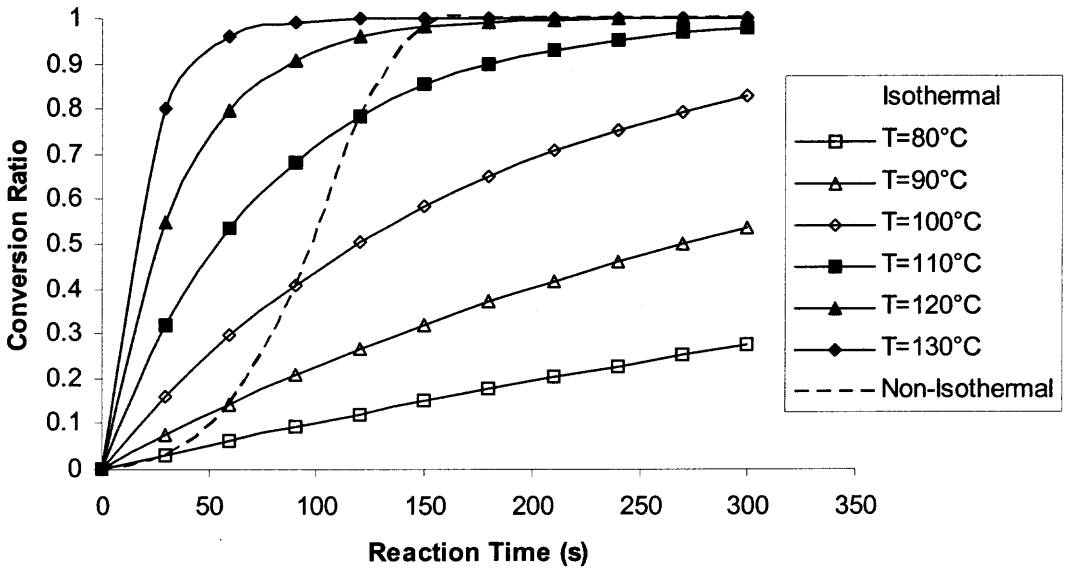

Figure 3.2 Increase of conversion ratio at different temperatures.

Another important factor for the polymerization is the shearing and premixing conditions of the reaction mixtures before they are fed into the extruder, which was also studied by Vergnes et. al (25). In their experiments, two samples of the reaction mixture were collected: one from the bottle containing the reactive mixture, the other from the injection pipe (connected to extruder) after the pump. Rheological characteristics of these two samples during polymerization were investigated at 100°C and 140°C, respectively, as shown in Figure 3.3. These data indicate that the effect of premixing on polymerization is small, although it becomes more significant at 100°C than at 140°C. This suggests that it is acceptable to assume an ideal mixing between monomer and initiator in the numerical simulation.

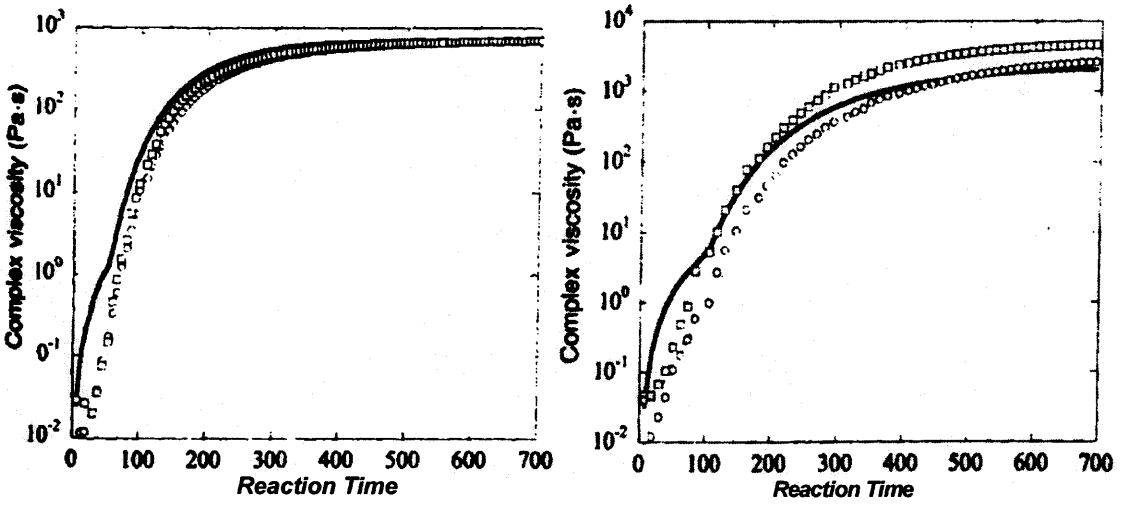

(a) (b)

Figure 3.3 Evolution of complex viscosity versus time at (a) 140°C and (b) 100°C from studies of Vergnes (25), (o), bottle sample, (□) Pipe sample, (-) Rheological law.

3.1.2 Molecular Weight During Polymerization

Experimental data (46) show that the length of polymer chain depends directly upon the ratio $[I]_o/[M]$. High ratio would result in large weight averaged molecular weight. When $[M]/[I]_o$ is in a range of 100-1500, a global linear equation can be used to describe the relationship between weight averaged molecular weight and conversion ratio:

$$\overline{M}_w(t) = K_{[M]/[I]_o} C(t) + M_o \quad \text{(g)} \tag{3.7}$$

where M_o is the molecular weight of ε-caprolactone; $K_{[M]/[I]_o}$ depends only on $[M]/[I]_o$ when the temperature is in a range from 100°C to 160 °C, and may be expressed in the from:

$$K_{[M]/[I]_o} = 3.86 \times 10^{-1} [M]/[I]_o \quad \text{(g)} \tag{3.8}$$

3.1.3 The Viscosity Model

The numerical simulation of reactive extrusion requires a rheological model, which predicts the evolution of the rheological behavior of the reaction system at any reaction time and processing conditions, such as temperature, initiator concentration, and shear rate. In the polymerization of ε-caprolactone, the viscosity model should include two parts: a rheological model for bulk poly-ε-caprolactone with different conversion ratios, and a dilution effect of monomer upon the viscosity of the reaction system. The latter should be considered because the monomer remains in the reactive system until the polymerization is complete. Such a monomer dilution effect strongly modifies the viscoelastic behavior of the reaction system.

1. Viscosity model for bulk poly-ε-caprolactone

Based on the experimental results (46), the viscosity of bulk poly-ε-caprolactone at different temperatures, shear rates and conversion ratios can be modeled with the generalized Yasuda-Carreau equation (52-53):

$$\eta(\dot{\gamma}) = \frac{\eta_0}{\left[1+(\tau\dot{\gamma})^a\right]^{(1-n)/a}} \tag{3.9}$$

where n = 0.52, and a = 1.05. τ characterizes the shear-stress level at which η is in the transition between Newtonian and shear thinning behavior, given by:

$$\tau = 1.7\times10^{-20}\times M_w^{4.1}\times\exp\left[\frac{E_b}{R}\left(\frac{1}{T}-\frac{1}{T_o}\right)\right] \tag{3.10}$$

where E_b is the flow activation energy (40.0 kJ/mol), T_o is the reference temperature (140°C). $\overline{M}_w$ is the weight averaged molecular weight, expressed by Equation 3.7.

The zero shear viscosity η_o of poly-ε-caprolactone samples in the power law zone ($M_w \geq M_c$) were determined to be (46):

$$\eta_o = 1.35\times10^{-17} \times M_w^{4.4} \times \exp\left[\frac{E_b}{R}\left(\frac{1}{T}-\frac{1}{T_o}\right)\right] \tag{3.11}$$

In the Rouse regime ($M_w < M_c$), η_o is described by:

$$\eta_o = 2.24\times10^{-5} \times M_w^{1.2} \times \exp\left[\frac{E_b}{R}\left(\frac{1}{T}-\frac{1}{T_o}\right)\right] \tag{3.12}$$

where the critical molecular weight, M_c, is about 6000g/mol.

2. Dilution effect

Considering the presence of monomer in the reaction system, the critical molecular weight, M_c, and the entanglement molecular weight, M_e, would depend on the concentration of polymer in solution, φ (54-55):

$$(M_c)_{solution} = 2(M_e)_{solution} = (M_c)_{bulk}\,\varphi^{1.25} \tag{3.13}$$

The viscoelastic parameters of the reaction system are modified with respect to the parameters of the bulk polymer (56). For instance, the intrinsic viscosity of the reaction system, η_{0S}, is changed to be:

In Rouse regime,

$$M_w < (M_c)_{bulk}\,\varphi^{1.25},\ \eta_{0S} = (\eta_0)_{bulk}\,\varphi \tag{3.14}$$

In entangled regime:

$$M_w \geq (M_c)_{bulk}\,\varphi^{1.25},\ \eta_{0S} = (\eta_0)_{bulk}\,\varphi^4 \tag{3.15}$$

According to Bistrup and Macosko (57), the monomer friction factor, i.e. the free volume, changes with the degree of polymerization due to the evolution of the glass

transition temperature. This should be taken into account in the polymerization of ε-caprolactone. Thus, the viscosity of the reaction system after considering the free volume correction takes the following form:

$$(\eta_0)_{solution} = \eta_{0s} \cdot a_\varphi \tag{3.16}$$

in which η_{0S} refers to Equations 3.14 and 3.15. The free volume correction during polymerization of ε-caprolactone would be:

$$a_\varphi = \exp\left(-\frac{1}{RT}(E_b - E_s)\right) \tag{3.17}$$

where E_b and E_s are the flow activation energy for the bulk and solution systems, respectively. If assuming an additive law of the free volume (46), E_s can be related to E_b as:

$$\frac{1}{E_s} = \frac{\varphi}{E_b} + \frac{1-\varphi}{E_{monomer}} \tag{3.18}$$

in which the flow activation energy of the monomer, $E_{monomer}$, is about 29 kJ/mol. In this study, the concentration of polymer, φ, is assumed to be equal to the conversion ratio, C, with the assumption that the density of the reaction system does not have a significant change during the polymerization. Furthermore, heat capacity, heat conductivity, and heat of reaction were also assumed to remain constant during polymerization. Thus, the zero viscosity η_o of poly-ε-caprolactone during polymerization is expressed as:

In the power law zone ($M_w \geq M_c$):

$$\eta_o = 1.35 \times 10^{-17} \times M_w^{4.4} \times \exp\left[\frac{E_b}{R}\left(\frac{1}{T} - \frac{1}{T_o}\right)\right] \times C^4 \times a_\varphi \tag{3.19}$$

In the Rouse regime ($M_w < M_c$):

$$\eta_o = 2.24\times10^{-5}\times M_w^{1.2}\times\exp\left[\frac{E_b}{R}\left(\frac{1}{T}-\frac{1}{T_o}\right)\right]\times C\times a_\varphi \tag{3.20}$$

3.2 Governing Equation for Reactive Extrusion

3.2.1 Equations of Fluid Mechanics

The governing equations of fluid mechanics are:

Mass conservation equation (or continuity equation),

$$\nabla\cdot V = 0 \tag{3.21}$$

Momentum conservation equation,

$$-\nabla P + \nabla\cdot\tau = 0 \tag{3.22a}$$

$$\tau = \eta\left[(\nabla V)+(\nabla V)^T\right] \tag{3.22b}$$

where the viscosity, η, is calculated based on Equations 3.9, 3.19 and 3.20, and

Energy conservation equation,

$$\rho C_P V\cdot\nabla T = k\nabla^2 T + \tau:\nabla V + Q_R \tag{3.23}$$

where, k is the thermal conductivity and Q_R is the reaction heat generation:

$$Q_R = \rho\Delta H\frac{dC}{dt} \tag{3.24}$$

where ΔH is the reaction heat, 250 KJ/kg (25).

3.2.2 Equations for Reaction

Equation 3.4 gives the relationship between conversion ratio, temperature and reaction time. In order to apply the kinetics equation into the simulation domain, Equation 3.4 is rearranged as:

$$U\frac{\partial C}{\partial x}+V\frac{\partial C}{\partial y}+W\frac{\partial C}{\partial z}=K(1-C) \tag{3.25}$$

because $\frac{d}{dt}=\vec{V}\cdot\frac{\partial}{\partial X_i}=U\frac{\partial}{\partial x}+V\frac{\partial}{\partial y}+W\frac{\partial}{\partial z}$, in which U, V, and W stand for the x-, y-, and z-components of velocity in a three dimensional Cartesian system.

In Equation 3.25, C stands for the conversion ratio of ε-caprolactone. K is calculated based on Equation 3.1b, which was obtained from the experimental data in the polymerization of ε-caprolactone with a parallel rheometer. It is known that the flow in the parallel rheometer is a shear flow. However, in co-rotating twin-screw extruders, the flow field is not a simple shear flow, but a combination of shear flow and elongational flow. Furthermore, the fluid elements in the extruders could be re-oriented, stretched and folded. This suggests that the kinetics equation of reaction from the experiments in parallel rheometer may diverge from that in the extruder, due to the different flow behaviors in these two devices. Some studies have been done to investigate the effects of flow on reaction (58) and the influence of mixing mechanisms on multi-component reactions in counter-rotating twin-screw extruders (59).

Numerical simulation of mixing in kneading blocks (60-61) show that the shear flow occupies a large portion of flow in twin-screw extruders. Furthermore, as shown in Figure 3.3, the initial mixing between monomer and initiator does not have significant effects on polymerization, and the effect of flow behavior on reaction is insignificant when the reaction is completed in a relatively short time (58). This suggests that the kinetics equation for the polymerization of ε-caprolactone based on the parallel rheometer can be an approximation of that in the co-rotating twin-screw extruder. Thus, in the present investigation, two assumptions were made in the simulation:

1. The monomer and initiator are uniformly mixed (ideal mixing) and
2. The kinetic equation from the parallel rheometer can be used in the twin-screw extruders.

3.3 Computational Techniques

Generally, Finite Element Method (FEM) is employed in the simulation of flow behavior of polymer melt in twin-screw extrusions (40-41, 60-76). Two commercial Finite Element Analysis software, i.e. FIDAP and POLYFLOW, have been used in some studies (40-41, 60-64). Recently, Hrymak et al. (77) used FLUENT, a commercial Computational Fluid Dynamics (CFD) software based on Finite Volume Method, to predict the flow patterns in kneading blocks of an intermeshing co-rotating twin screw extruder. The velocity contours from the simulation agree well with the experimental data from Particle Image Velocimetry (PIV). This indicates that it is feasible to employ FLUENT in the simulation of processes involving twin-screw extruders. Because FLUENT is based on Finite Volume Method, it requires lower computation cost, if compared with Finite Element Method. In this study, FLUENT 6.0 was employed to solve the governing equations of reactive extrusion.

However, like most of the current numerical simulation packages, FLUENT can not deal with partially-filled channel flow. This means that it is not possible to employ FLUENT directly in the simulation of reactive extrusion in twin-screw extruders, because the screw channel in twin-screw extruders is either fully-filled or partially-filled (as described in Chapter 1). Consequently, in this investigation, the simulation of the polymerization of ε-caprolactone in twin-screw extruders was divided into four steps:

- Use FLUENT to carry out 3-D simulation of polymerization of ε-caprolactone in fully-filled screw elements under various temperatures, screw rotational speeds, and initiator concentrations;

- Compare the simulation results based on 3-D model and those from 1-D channel model, and to find out the dominant factors for the polymerization;

- Propose a model to predict the reaction in the partially-filled channels, based on the simulation results in the fully-filled channels from the 3-D model, and features of flow in the partially-filled channels (discussed in Chapter 7);

- Calculate the polymerization progressing globally in the extruder, based on the models for the partially-filled and fully-filled channel model;

It is known that FLUENT is a general program for fluid mechanics. When it is applied to a specific case, such as the simulation of reactive extrusion, three additional steps should be followed:

1. Generate 3-D mesh for different screw elements of twin-screw extruders.
2. Define a User Defined Scalar (UDS) to solve the reaction equation, as in Equation 3.25.
3. Define User Defined Functions (UDFs) for the viscosity model during polymerization, the heat from reaction, and the source term for the UDS.

Each of these steps will now be described in detail.

1. Generate 3-D mesh for different screw elements of twin-screw extruders.

Generation of 3-D mesh is a tedious task because of the complex geometry of screw elements in twin-screw extruders. In the current study, a C++ program was used to generate the 3-D mesh for FLUENT.

In twin-screw extrusion, the flow domain changes with screw rotation. Currently, in the simulation of flow in twin-screw extruders, the dynamic motion of screw is treated as a number of quasi-steady state analyses of the sequence geometries. For instance, Figure 3.4 shows that a quarter of a complete cycle of a kneading block can be described with 8 quasi-steady states (70).

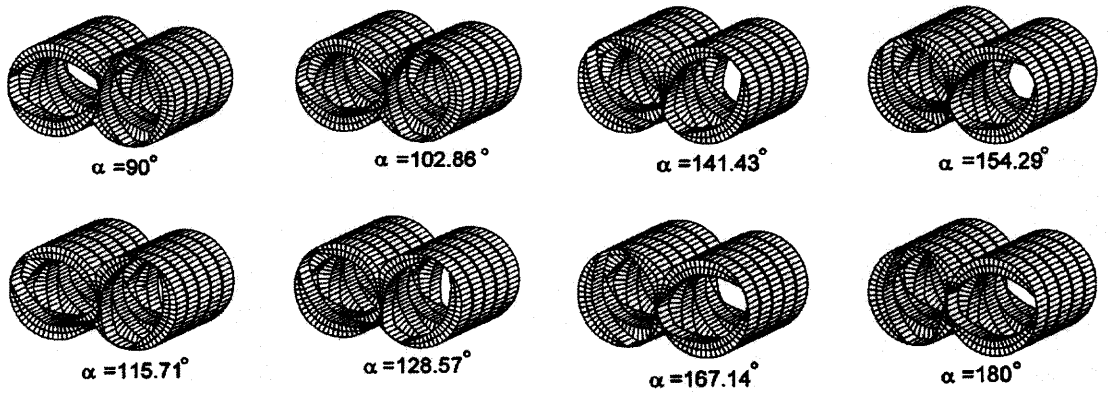

Figure 3.4 Mesh design for a quarter rotating cycle of a kneading block (70).

2. *Define a User Defined Scalar (UDS) to solve the reaction equation, as in Equation 3.25.*

In FLUENT, the transport equation can be solved as an arbitrary, user-defined scalar (UDS). Usually, the transport equation has the form:

$$\frac{\partial \rho\phi_k}{\partial t}+\frac{\partial}{\partial x_i}\left(\rho u_i\phi_k-\Gamma_k\frac{\partial \phi_k}{\partial x_i}\right)=S_{\phi_k}\text{, i = 1, 2, ...N} \tag{3.26}$$

where, φ_k is an arbitrary scalar, Γ_k and $S_{\varphi k}$ are the diffusion coefficient and source term supplied for each of the N scalar equations. For the steady-state case, FLUENT solves Equation 3.27 instead of Equation 3.26 when the diffusion coefficient, Γ_k, is zero:

$$\frac{\partial}{\partial x_i}(\rho u_i\phi_k)=S_{\phi_k} \tag{3.27}$$

The comparison between Equations 3.25 and 3.27 shows that a user-defined scalar can be defined to solve for the conversion ratio, C, in the simulation domain:

$$\frac{\partial}{\partial x_i}(\rho u_i C)=S_C \tag{3.28}$$

in which the source term is:

$$S_C=\rho K(1-C) \tag{3.29}$$

3. *Define User Defined Functions (UDFs) for the viscosity model during polymerization, the heat from reaction, the source term for the User-Defined Scalar.*

A user-defined function (UDF) is a function programmed by users that can be dynamically linked with the FLUENT solver to enhance the standard features of the code. UDFs can be used for a variety of applications, such as customization of boundary conditions, material property definitions, surface and volume reaction rates, diffusivity functions, source terms in FLUENT transport equations or in user-defined scalar (UDS) transport equations. As discussed in the preceding sections, the viscosity of the reaction system (Equation 3.9), heat from reaction (Equation 3.24) and the source term for UDS (Equation 3.29) are not constant during polymerization; they could be functions of conversion ratio, temperature and/or shear rate. Accordingly, three User Defined Functions should be defined.

The procedure followed in the application of FLUENT in reactive extrusion is summarized in Figure 3.5. It consists of three steps, *preprocessing*, *solver*, and *post-processing*. In the *preprocessing*, the 3-D mesh for the simulation domain is generated; the boundary conditions for temperature, velocity, pressure, and User-Defined Scalar are applied; the parameters for the reactive system, such as density, heat capacity and heat conductivity, are initialized; the solution method for equations is selected. In this study, the equations are solved with a segregated procedure. In the *solver*, all of the equations are solved with the segregated approach, in which the energy source term from reaction heat and the viscosity of the system are calculated by User Defined Functions. The solution is completed once it reaches convergence. In the *post-processing*, FLUENT not only gives the contour plots of parameters (including temperature, velocity, pressure, viscosity, and so on), but also offers some functions for the calculation of the parameters,

such as area weight averaged operation for the parameter at a predefined surface. Furthermore, FLUENT permits exportation of some data files for further analysis.

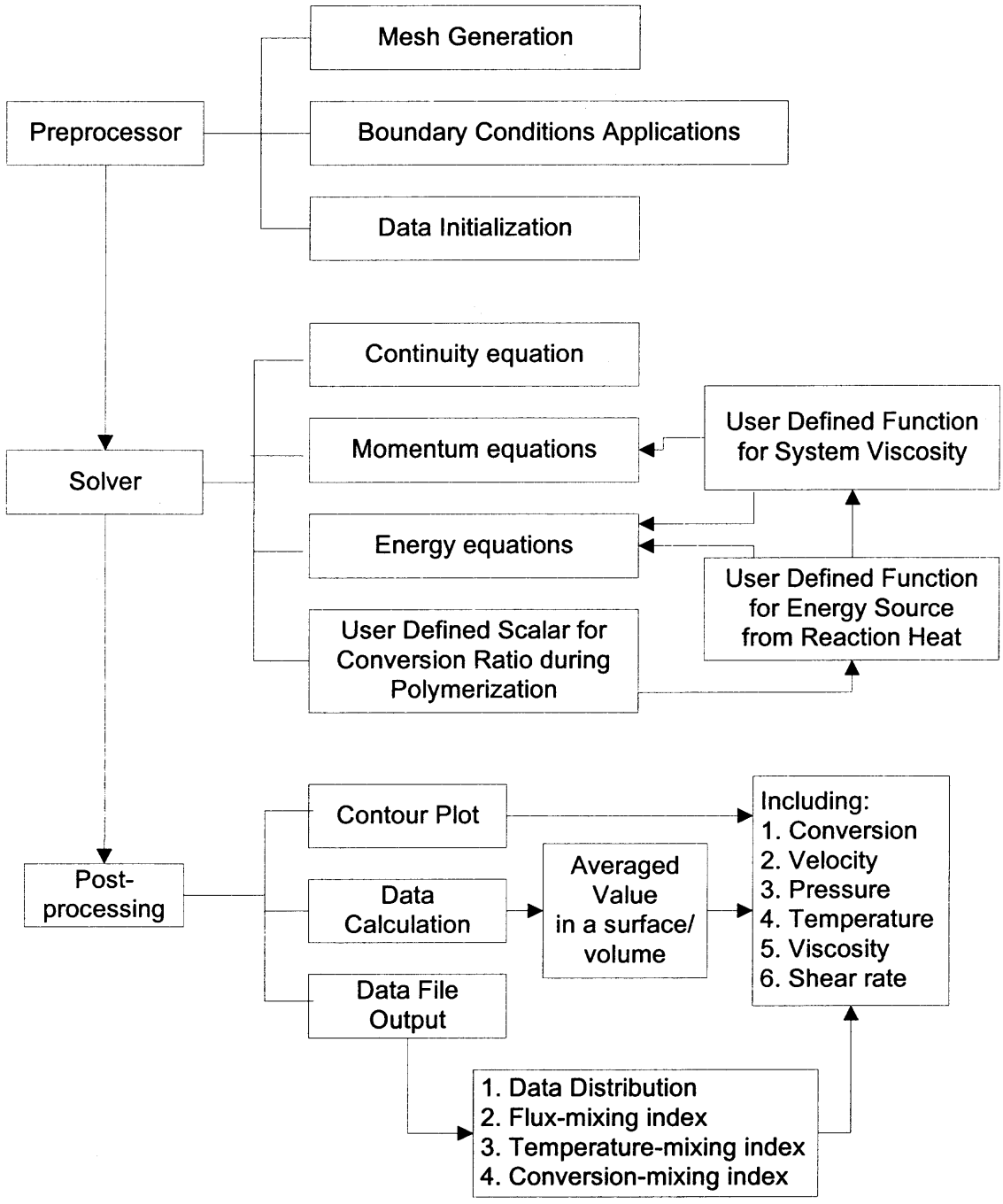

Figure 3.5 Procedure of FLUENT in reactive extrusion.

3.4 Conclusions

In the numerical simulation of reactive extrusion, continuous equation, energy equation and kinetics equations for reactions were solved, coupled with the non-Newtonian characteristic of the reaction system. In this study, polymerization of ε-caprolactone was selected as a model system. The information required in the numerical simulation of polymerization was obtained from studies of Gimenez and Vergnes.

The polymerization of ε-caprolactone in co-rotating twin-screw extruders was modeled with Finite Volume Method, using a commercial CFD package FLUENT. A C++ code was used to develop data files to generate 3-D mesh of the simulation domain. The kinetics equation for polymerization was reformatted so that it can be incorporated into FLUENT with a User Defined Scalar. The rheological model of reaction system, the source term for reaction heat and the source term for the kinetics equation were incorporated into FLUENT with User Defined Functions.

In the simulation with FLUENT, some calculation results can be exported as data files. This makes it possible to carry out further analysis about the polymerization kinetics in twin-screw extruders, as discussed in Chapters 5 and 6.

CHAPTER 4

VALIDATION OF NUMERICAL SIMULATION OF POLYMERIZATION WITH FLUENT

As presented in the previous chapter, in FLUENT, User Defined Scalar was introduced to solve the kinetics equation for the polymerization of ε-caprolactone, and User Defined Functions were used to include the viscous model, source term for the reaction heat in the energy equation and source term for the kinetics equation. On the other hand, FLUENT cannot deal with the continuous rotating of screws in the twin-screw extruders, and thus a quasi-steady state simulation was carried out. This chapter is comprised of two sections. The first one validated the simulation method for the polymerization of ε-caprolactone based on FLUENT, and the second section investigated the effect of channel geometries with different initial angles upon the simulation results in the steady state analysis.

4.1 Validation of Simulation with FLUENT

In this section, the simulation method for the reaction based on FLUENT was validated with the polymerization of ε-caprolactone in a pipe flow (Figure 4.1). The polymerization progression in a pipe is predicted with FLUENT, and the simulation results are then compared with the data based on the kinetics equation (see Equation 3.6). The reason for selecting pipe flow as a validation model is that the flow in the pipe channel is so simple that the kinetics equation can be easily applied.

As shown in Figure 4.1, the pipe channel has a length of 80 mm and a width of 4 mm. Two cases have been studied, isothermal and adiabatic, as shown in Table 4.1. In the isothermal case, the temperature of the reaction system is assumed to remain constant

during the polymerization. In the adiabatic case, there is no heat loss through the walls. All of the heat from reaction is kept in the reaction system, which raises the system temperature rapidly. The ratio of monomer to initiator concentration is 400.

In order to simplify the simulation, it was assumed that the reaction system is a Newtonian fluid. The velocity at the inlet was fully developed and had a parabolic distribution. The viscous dissipation in the system was neglected. It is known that the streamlines in the pipe flow are straight lines (from inlet to outlet), which suggests that there is no mass exchanged transversely. In order to exclude the energy exchange in the transverse direction, the heat conductivity of the material was set to be zero (1×10^{-12} in the simulation). Thus, the conversion ratio increase along a streamline can be easily calculated based on the kinetics equation (Equation 3.6), with either isothermal or adiabatic conditions.

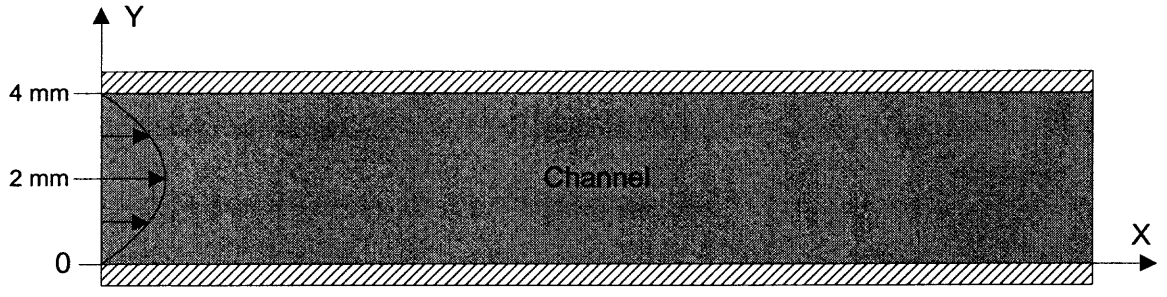

Figure 4.1 Channel model for polymerization.

Table 4.1 Conditions for Simulation of Polymerization in Pipe Flow

Case	Flow Rate	Temperature at Inlet	Conversion at Inlet
Isothermal	67.6 kg/hr	420 K	0
Adiabatic	360 kg/hr	420 K	0

In order to validate the simulation results from FLUENT, the profiles of conversion ratio along the streamlines with Y = 0.2 mm, 0.4 mm, 0.6 mm and 2 mm in

the channel (see Figure 4.1) were compared with the data from the kinetics equation, as shown in Figures 4.2 and 4.3.

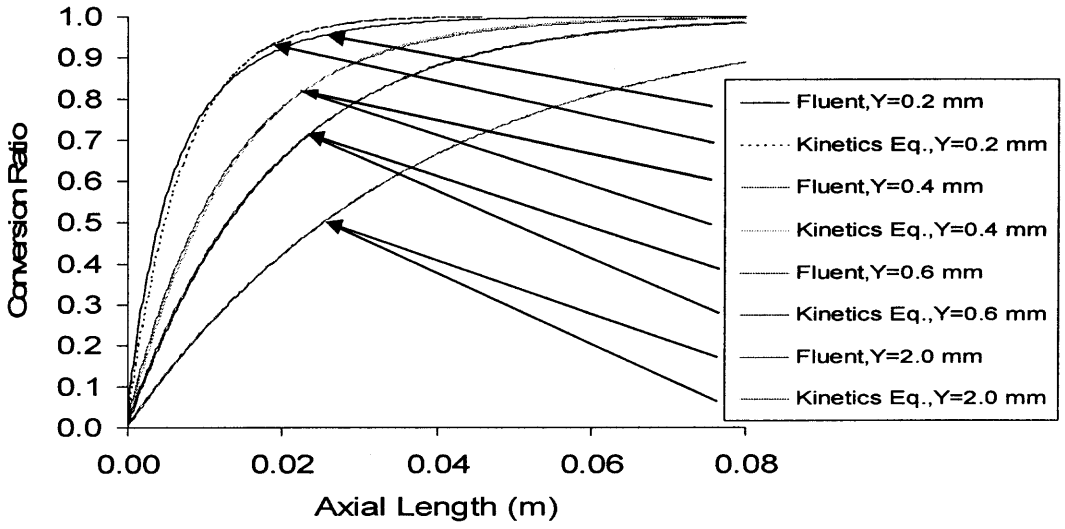

Figure 4.2 Comparison of conversion ratio based on FLUENT and kinetics equation at isothermal conditions.

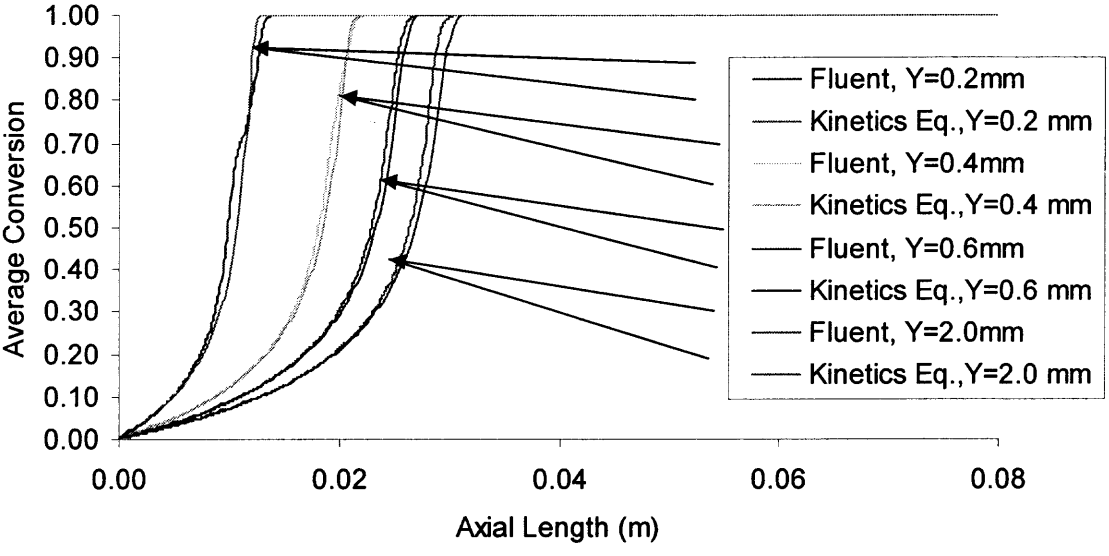

Figure 4.3 Comparison of conversion ratio based on FLUENT and kinetics equation at adiabatic conditions.

Figures 4.2 and 4.3 show that the trends of conversion ratio along the streamlines at isothermal conditions are entirely different from those based on the adiabatic conditions. On the other hand, the profiles of conversion ratio along the axial length based on FLUENT agree very well with those calculated directly from the kinetics equation. This suggests that the simulation method for the polymerization based FLUENT is reliable, and the program for the User Defined Scalar (UDS) and User Defined Functions (UDFs) are correct.

4.2 Steady State Simulation Method in Reactive Extrusion

As discussed in the preceding chapter, in the modeling of flow in twin-screw extruders, the dynamic motion of screws is treated as a number of quasi-steady state analyses with series of geometries. The geometries of screw channels in the steady state analyses are determined by the surfaces of screws and barrels. Because the barrel is fixed and the screws may have an angle in a range of 0~360° (see Figure 4.5), a sequence of channel geometries is obtained. This section investigated the effects of channel geometries upon the polymerization progression of ε-caprolactone in conveying screw elements.

4.2.1 Boundary Conditions for Simulation

The conveying screw element investigated in this section is shown in Figure 4.4. The geometry specifications of the elements are as follows: barrel diameter = 34 mm; screw tip diameter = 33.4 mm; centerline distance = 30 mm; screw root diameter = 26 mm; screw tip number = 2; screw pitch = 60 mm. This is a right hand conveying element, having an axial length of 120 mm. A pair of kneading discs with a length of 20 mm,

which has identical axial cross section as the conveying element, is attached at the end of the conveying element, to ensure good convergences in the simulation.

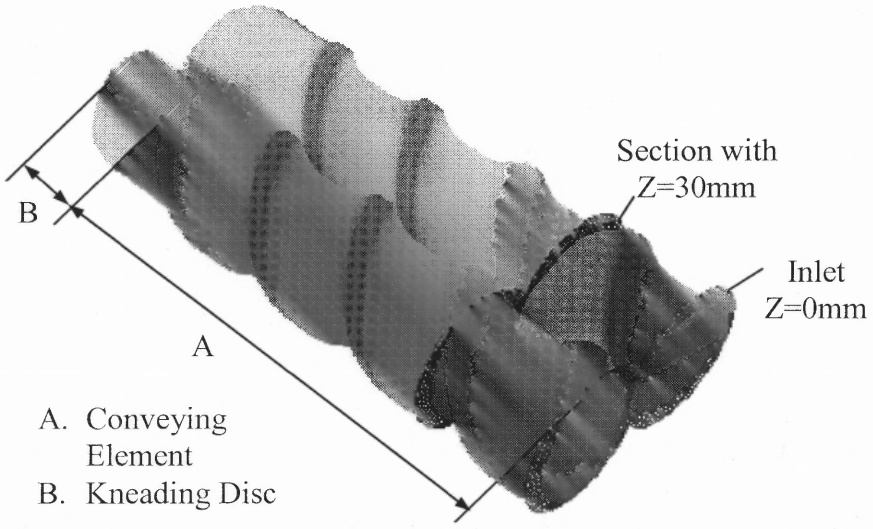

Figure 4.4 Geometry of conveying screw element.

It is assumed that temperatures at the inlet and barrel surface are 420 K, and the screw surface has an adiabatic condition. The conversion ratio at the inlet is 0.6 and the flow rate is 3.15 kg/hr. The ratio of monomer to initiator concentration is 800, and the screw rotates at 287 rpm. The flow is fully developed at the exit of the simulation domain. The gradient of the conversion ratio is assumed to be zero at barrel and screw surfaces.

As shown in Figure 4.5, the rotation of screws can be described with angle θ. Here, θ is the initial angle of lobes at the inlet. In a quarter of a rotation cycle, θ increases from 0° to 90°. In this study, the moving of screws in a quarter of a complete cycle was treated with ten quasi-steady state analyses, in which the step for the angle increase is

10°. Accordingly, ten 3-D meshes were generated in the analyses. As an example, Figure 4.6 shows the geometry of the channel and the mesh at the inlet of the simulation domain in the steady state simulation, with θ at 0°, 30°, 60° and 90°, respectively.

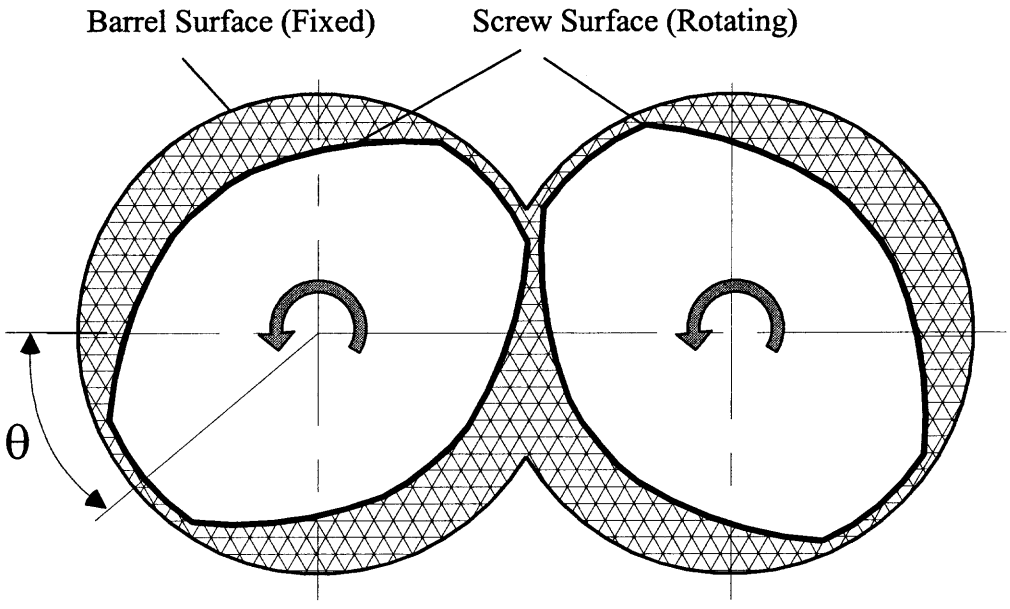

Figure 4.5 Dynamic rotation of screws.

The velocity distribution at the inlet of the simulation domain is an important boundary condition in the numerical simulation. In this study, the axial velocity profile at the inlet was calculated as follows. First, a simulation of Newtonian and isothermal flow in the screw element was carried out, in which the fluid viscosity was calculated based on the temperature and conversion ratio at the inlet, and the axial velocity at the inlet was assumed to have a uniform distribution (calculated according to the flow rate). After the simulation, the velocity distribution in the simulation domain was obtained. Because the screw tip number of the element is 2 and the pitch is 60 mm, the cross section at Z = 30 mm has the same geometry as the inlet (as shown in Fig. 4.4). Hence, the calculated axial

velocity profile at Z = 30 mm (i.e. the axial cross section with an axial location of a half pitch) with Newtonian and isothermal conditions was used as the axial velocity boundary condition at the inlet in the simulation of reactive extrusion.

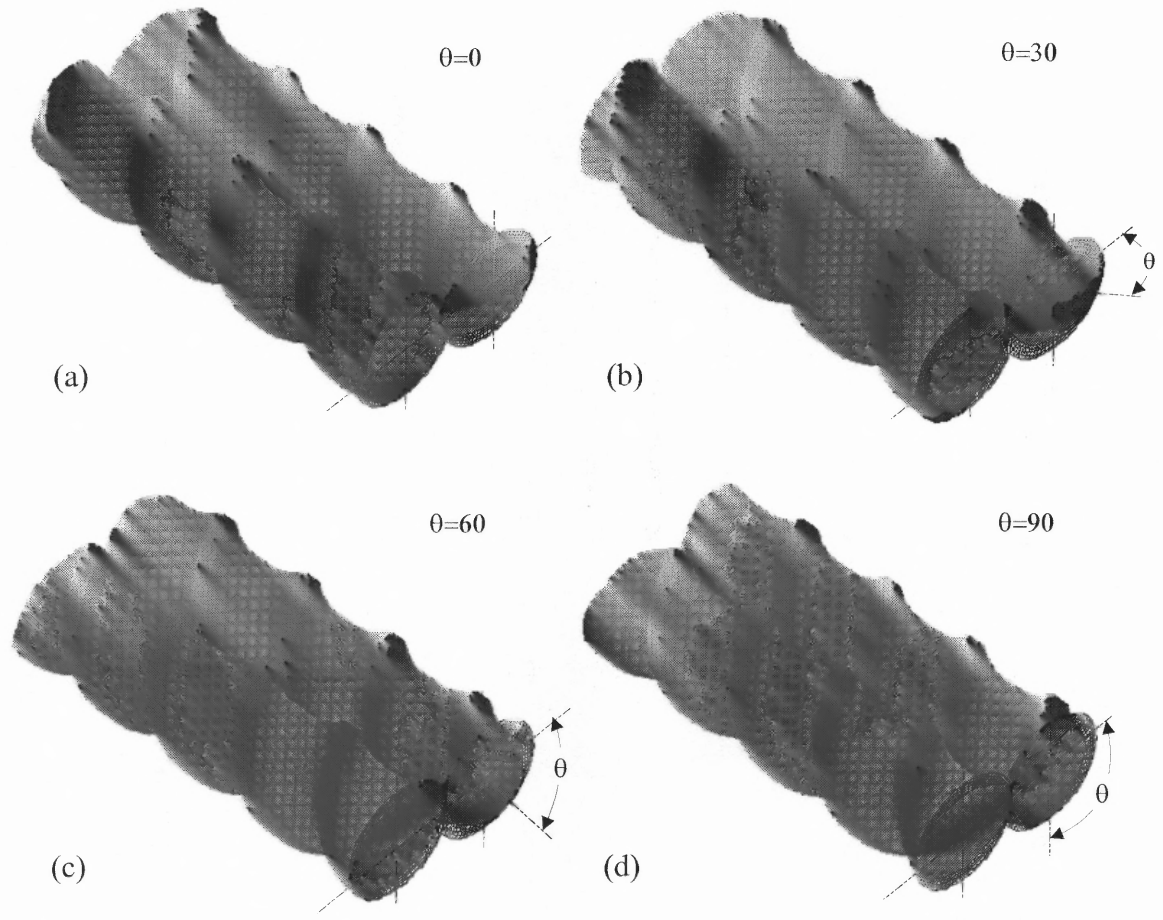

Figure 4.6 Geometries of screw channel for the steady state simulation with (a) θ = 0°, (b) θ = 30°, (c) θ =60°, and (d) θ = 90°.

4.2.2 Simulation Results for Polymerization of ε-Caprolactone in Different Channel Geometries

Numerical simulation of polymerization of ε-caprolactone in ten channel geometries with different initial angles was carried out with FLUENT. Figure 4.7 summarizes the conversion ratio profiles at the surfaces of screws with initial angles at 0°, 30° and 60°,

respectively. These pictures show that the magnitudes of the conversion ratios at an identical axial position are similar in different screw geometries. This suggests that the effect of initial angle of screws on polymerization progression is very small. Figure 4.8 illustrates the calculated results of the distributions of conversion ratio at the axial cross section with Z = 0.06 m in screw elements with different initial angles. It is seen that the shape of the distribution curves depends on the initial angle, but not large.

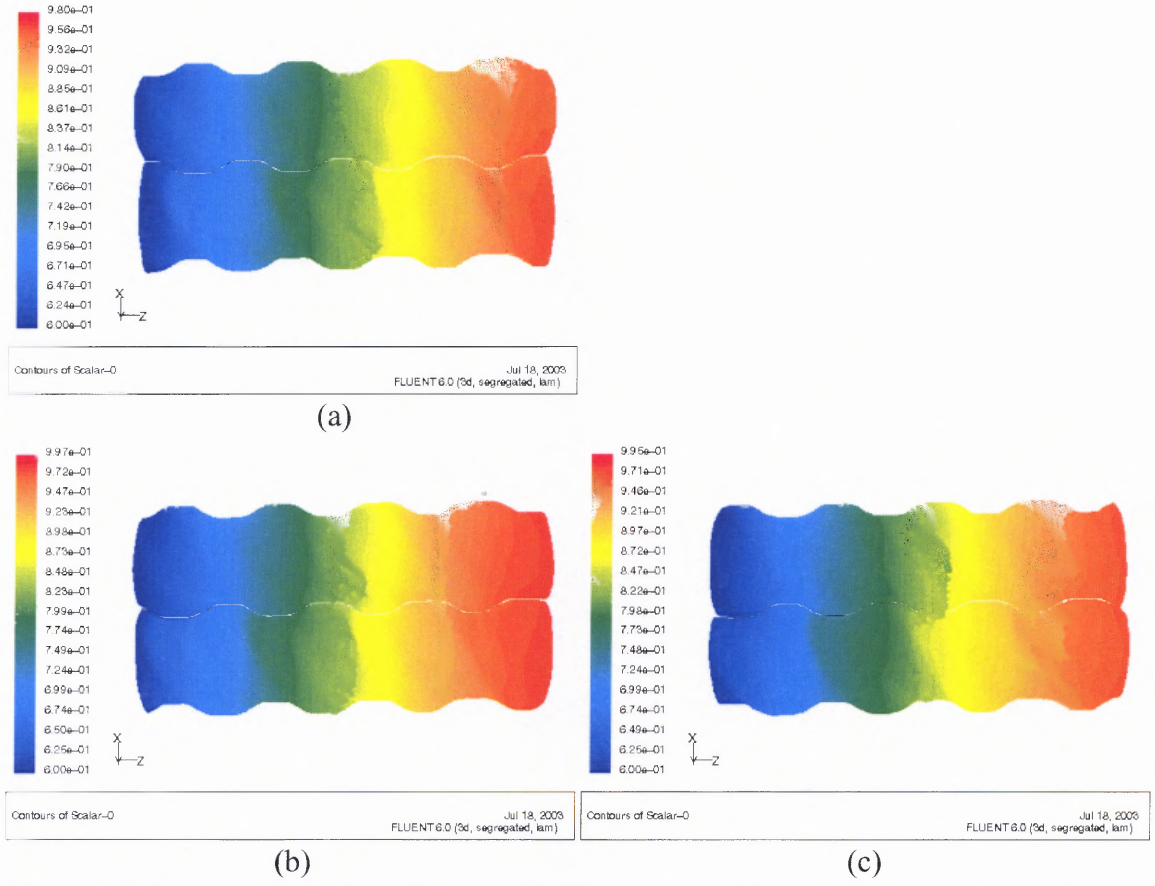

Figure 4.7 Top view of conversion ratio profile at screw surfaces. (a) $\theta = 0°$, (b) $\theta = 30°$, (c) $\theta = 60°$.

In order to evaluate the polymerization in different geometries, the area weighted average conversion ratio, temperature, viscosity, pressure and shear rate along the axial length were calculated (see Equation 5.2), and shown in Figure 4.9. These plots show that

each of the averaged parameters along the axial length is almost independent of the initial angle of the screws. This suggests that for each screw configuration, it is not necessary to carry out numerical simulation based on a series of channel geometries with different initial angles. Instead, it is reasonable to perform a simulation based on a certain screw initial angle, which would reduce the calculation cost significantly.

Based on the above results, from now on, the screw configuration with an initial angle of 0° will be used as the model geometry in the numerical simulation of polymerization of ε-caprolactone in fully-filled screw elements.

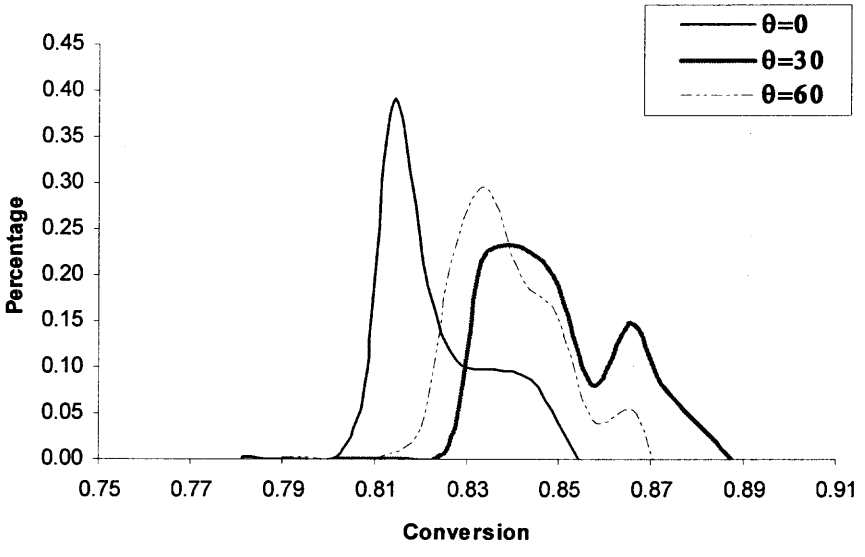

Figure 4.8 Distribution of conversion ratio at cross sections with Z = 0.06 m at different initial angles.

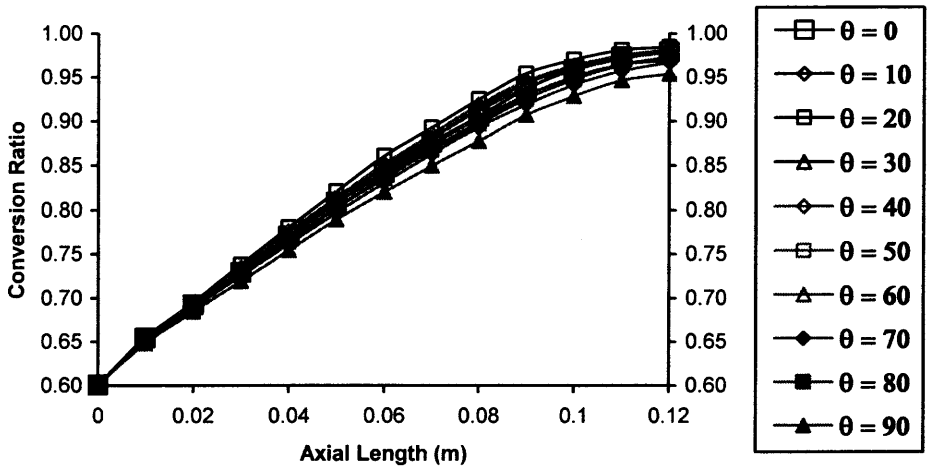

(a)

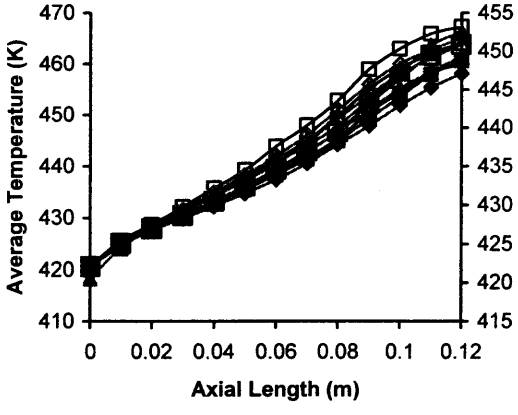

(b)

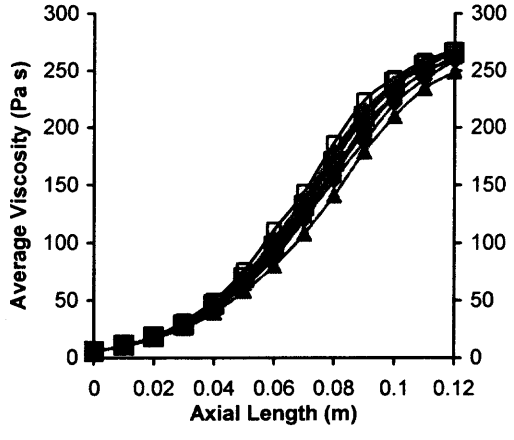

(c)

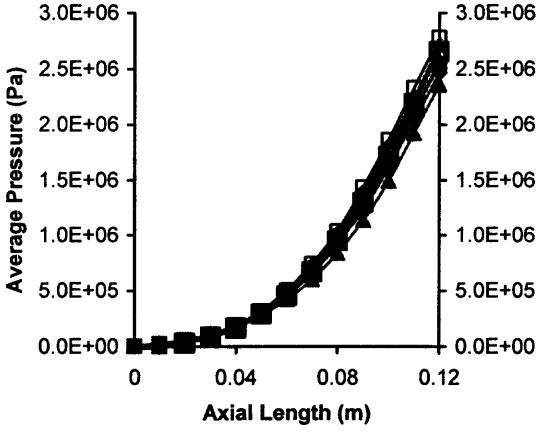

(d)

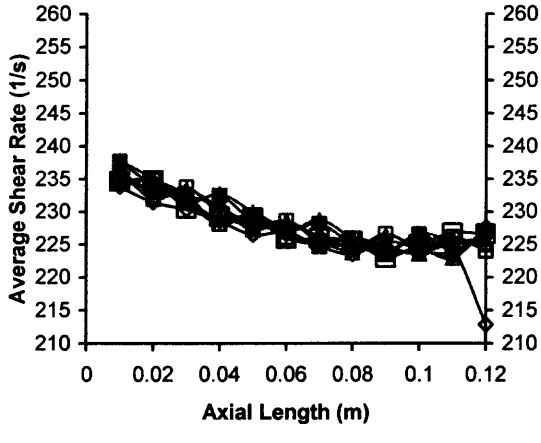

(e)

Figure 4.9 Averaged parameters along the axial length. (a) conversion ratio, (b) temperature, (c) viscosity, (d) pressure and (e) shear rate. (symbols in plots b-e are the same as those in plot a).

4.3 Conclusions

In this chapter, the simulation method for polymerization based on FLUENT was validated with a pipe flow. It is seen that the simulation results predicted with FLUENT agree well with those calculated directly from the kinetics equation, indicating that the application of FLUENT in predicting polymerization progress is reliable.

The polymerization progressions of ε-caprolactone in conveying screw elements with different initial angles were calculated with quasi-steady state simulation method. The simulation results show that the effect of the initial angle of conveying elements upon polymerization progression is small. This suggests that in the reactive extrusion, it is reasonable to carry out the steady-state numerical simulation based on the screw channel with a certain initial angle, instead of series of channel geometries with different initial angles. This would reduce the calculation cost significantly.

CHAPTER 5

POLYMERIZATION OF ε-CAPROLACTONE IN FULLY-FILLED CONVEYING ELEMENTS: SIMULATION RESULTS AND DISCUSSION

As mentioned in Chapter 1, conveying elements and kneading blocks are two commercially available screw elements in co-rotating twin-screw extruders. During processing, conveying elements could be either fully-filled, or partially-filled. In this chapter, the conveying elements are assumed to be fully-filled and modeled by a 3-D simulation method. The simulation of reaction in the partially-filled screw elements is discussed in Chapter 7. This chapter consists of two sections. The first one investigated the effects of screw geometry, operational condition, initiator concentration of reactive system and screw dimension on reaction, based on the 3-D simulation method. The second section compared the simulation results between 3-D model and 1-D model.

5.1 Simulation of Polymerization of ε-Caprolactone in Conveying Elements with 3-D Model

In conveying elements, screw pitch and helical direction (forward or reversed) are two important parameters, because they determine the conveying and mixing mechanism of polymer melt in the elements. In this section, two systems were studied, in which system No. 1 has a screw diameter of 34 mm and system No. 2 has a diameter of 68 mm, as listed in Table 5.1. For system No. 1, four elements were investigated, and for system No. 2, two elements were studied (Table 5.2).

In order to ensure that the iteration reaches convergence easily in the simulation, an extensional disc, which has identical end view as the screw element, was added at the

end of the screw element. The dimensions of the screw element and the extensional disc are listed in Table 5.1 and shown in Figure 5.1.

Table 5.1 Dimension of Simulation Domain

	System No. 1	System No. 2
Barrel diameter (mm)	34.0	68.0
Screw tip diameter (mm)	33.4	66.8
Centerline distance (mm)	30.0	60.0
Screw root diameter (mm)	26.0	52.0
Screw tip number	2	2
Length of screw element (mm)*	120	240
Length of extensional disc (mm)	20	40

*The length of SE20R is 20mm, and its extensional disc is 7.5 mm long.

Table 5.2 Description of Conveying Screw Elements

	Conveying elements	Description
System No.1	SE20F, SE20R SE40F SE60F	Conveying elements with pitch 20 mm, 40 mm and 60 mm, respectively; F stands that the element has Forward helical direction, R represents Reversed direction.
System No.2	SE40F, SE120F	Conveying screw elements with pitch 20 mm and 120 mm respectively;

Three-dimensional mesh of the simulation domain was generated with 8-node, brick elements, as shown in Figure 5.2. As discussed in the preceding chapter, the screw with an initial angle of 0° was used as the model geometry in the simulation, instead of a sequence of screw geometries. The number of elements for the conveying screw element is 179,200, and it is 22,400 for the extensional disc domain. The length of the reversed element SE20R is 20 mm, which is composed of 67,200 brick elements; its extensional disc is 7.5 mm long, and has 22,400 brick elements.

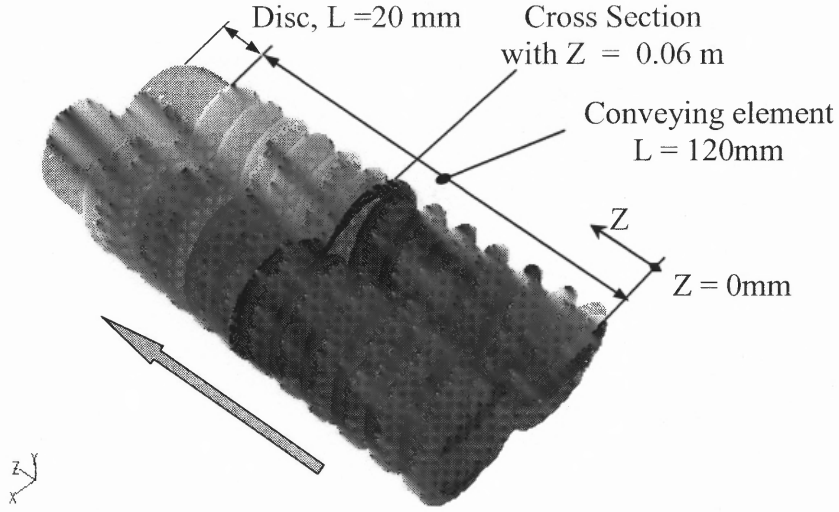

(a)

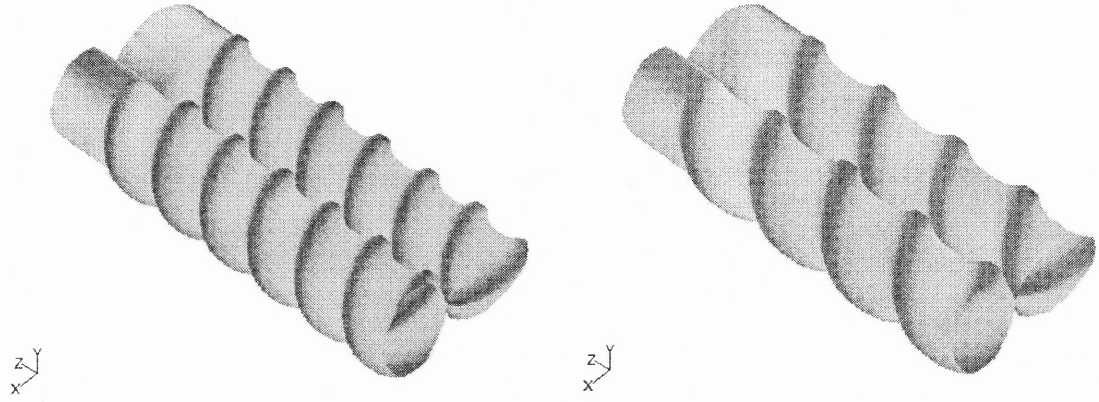

(b) (c)

Figure 5.1 Geometry of conveying elements (a) SE20, (b) SE40, (c) SE60. (The arrow in (a) shows the flow direction of melt in screw elements).

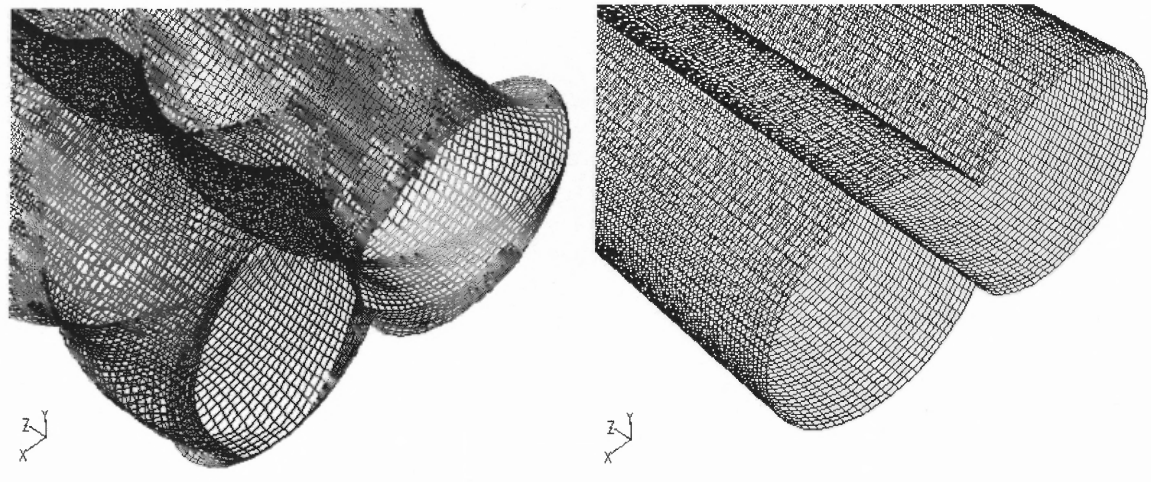

(a) (b)

Figure 5.2 Mesh of conveying screw element SE60 at (a) screw surface, and (b) barrel surface.

Table 5.3 Boundary Conditions

Ratio $[M]/[I]_o$	Flow Rate	Screw Speed	Barrel Temperature	Inlet Temperature	Inlet Conversion Ratio
Screw Diameter D = 34 mm					
400	40.55 kg/hr	287 rpm	405 K	405 K	0
400	40.55 kg/hr	48 rpm	405 K	405 K	0
800	3.15 kg/hr	287 rpm	420 K	420 K	0
800	3.15 kg/hr	48 rpm	420 K	420 K	0
800	3.15 kg/hr	287 rpm	410 K	410 K	0
800	3.15 kg/hr	48 rpm	410 K	410 K	0
800	3.15 kg/hr	287 rpm	420 K	420 K	0.6
800	3.15 kg/hr	48 rpm	420 K	420 K	0.6
Screw Diameter D = 68 mm					
800	25.2 kg/hr	287 rpm	420 K	420 K	0.6

Table 5.3 shows the boundary conditions for the simulation, in which the effects of screw rotational speed, inlet and barrel temperatures, and concentration of initiator on reaction are considered. It is assumed that the screw surface has adiabatic heat transfer conditions, and the barrel maintains constant temperature during the reaction. The gradient of the conversion ratio at barrel surface, screw surface, and outlet of simulation domain is assumed to be zero. The effect of flow rate on reaction is obvious, since decreasing in flow rate means increase in residence time. As shown in Figure 3.2, the degree of reaction rises with increase in reaction time (i.e. decrease in flow rate). The simulation results of the effects of flow rate on polymerization are not covered in this thesis; these have been reported elsewhere (78).

5.1.1 Polymerization at $[M]/[I]_o = 800$ with T = 420 K, $C_o = 0$ and D = 34 mm

5.1.1.1 Simulation Results with 3-D Model. In this section, three conveying elements, SE20F, SE40F and SE60F, were studied. Figure 5.3 summarizes the conversion ratio profiles at the top surfaces of these conveying elements, in which the reaction system is conveyed from left to right. These pictures show that the patterns of the

conversion at screw surfaces depend on screw geometries: with increasing screw pitch, the conversion ratio has a faster increase.

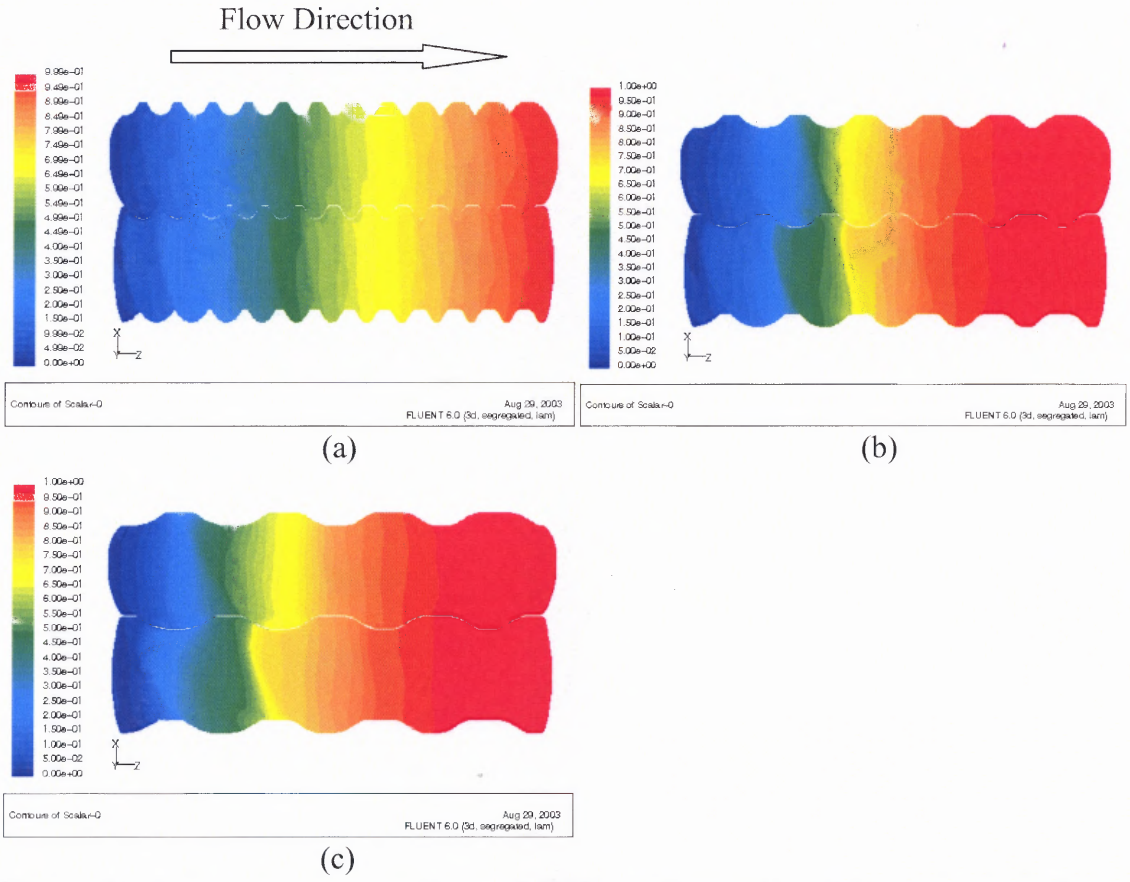

Figure 5.3 Conversion ratio profiles at $[M]/[I]_o$ = 800 and N = 287 rpm at top surfaces of elements (a) SE20F, (b) SE40F, and (c) SE60F.

Figure 5.4 shows the conversion distribution at the axial cross section with Z = 0.06 m in SE20F and SE60F (see Figure 5.1a), respectively. It is seen that the conversion ratio at the axial cross section is not uniform. The distribution of conversion ratio changes when the screw pitch is increased. In SE20F, the region with high conversion ratio is located near the barrel surface, whereas in SE60F, the maximum conversion appears in the area close to the center of the screw channel. However, in both SE20F and SE60F, the conversion ratio near the screw surfaces is lower than that in other regions. Figure 5.4

also shows that the maximum and minimum conversion ratios in SE60F are larger than those in SE20F.

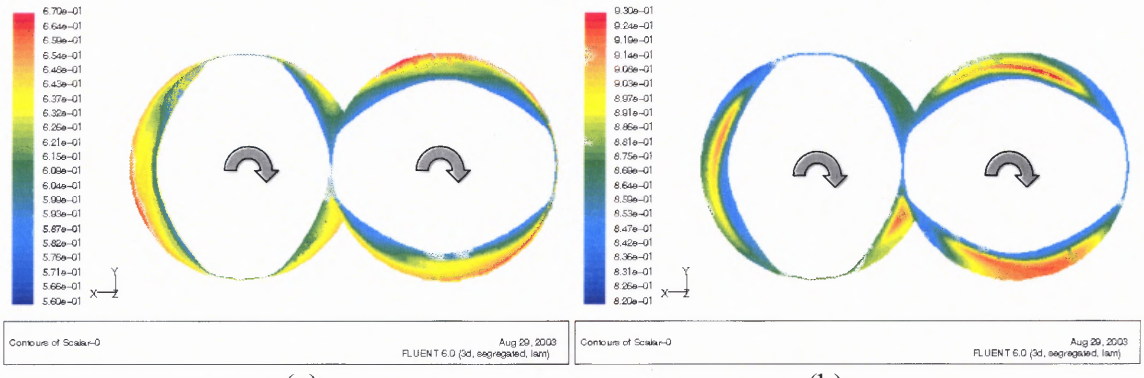

(a) (b)

Figure 5.4 Conversion profile at axial cross sections of Z = 0.06 m at $[M]/[I]_o$ = 800 and N = 287 rpm in elements (a) SE20F and (b) SE60F.

In order to evaluate the profiles of conversion ratio at the axial cross section, the area weighted distribution of conversion ratio is defined, as following:

$$d(i) = \frac{A(i)}{A} = \frac{A(i)}{\sum_{i=1}^{N} A(i)} \tag{5.1}$$

in which d(i) is the distribution; A(i) is the area with conversion ratio C(i) at an axial cross section; A is the area of the axial cross section. For example, Figure 5.5 summarizes the area weighted distributions of conversion ratio at axial cross sections with Z = 0.01 m, Z = 0.04 m and Z = 0.07 m in SE20F and SE60F. The plots in Figure 5.5 show that with increasing screw pitch from 20 mm to 60 mm, the distribution of conversion ratio becomes broader, and the average conversion ratio in SE60F is higher than that in SE20F at the cross section with identical axial location.

In order to elucidate the effect of screw pitch on polymerization, the flow of polymer melt in different conveying elements was investigated. Figure 5.6 shows the

patterns of the positive axial velocity (i.e. velocity along the downstream direction) in the cross section with Z = 0.06 m in SE20F, and SE60F, respectively. In order to make the contour clearer, the region with negative axial velocity is hatched with the grid only, and the patterns of the negative axial velocities are not displayed. Figure 5.6 reveals that in the cross section, a large fraction of fluid elements have negative axial velocity. These fluid elements move upstream, not downstream. Furthermore, the maximum positive axial velocity in SE60F is larger than that in SE20F.

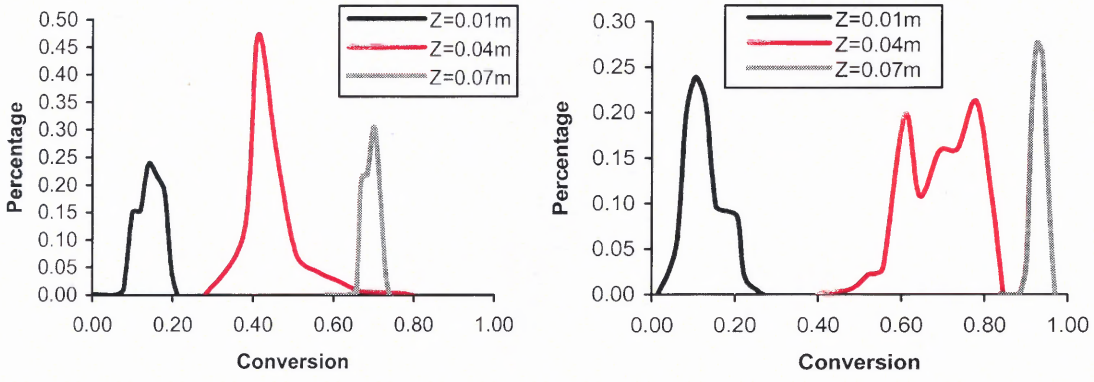

(a) (b)

Figure 5.5 Conversion distribution at different axial cross sections at $[M]/[I]_o$ = 800 and N = 287 rpm in elements (a) SE20F and (b) SE60F.

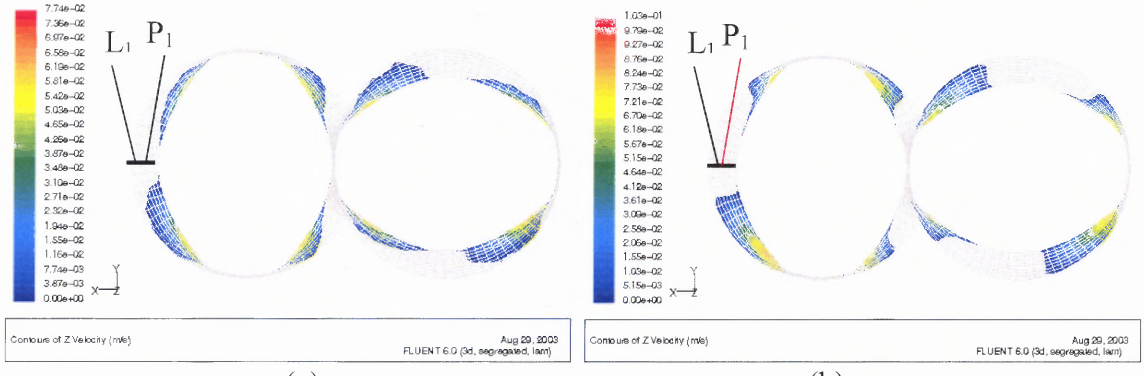

(a) (b)

Figure 5.6 Axial velocity profiles at axial cross section of Z = 0.06 m at $[M]/[I]_o$ = 800 and N = 287 rpm in elements (a) SE20F and (b) SE60F.

Analogous to the definition of the area weighted distribution of conversion ratio (Equation 5.1), the area weighted axial velocity distribution was calculated. Figure 5.7 shows the distributions of the axial velocity at the axial cross section with Z = 0.06 m in SE20F and SE60F. It is seen that the axial velocity has a much broader distribution in SE60F than in SE20F.

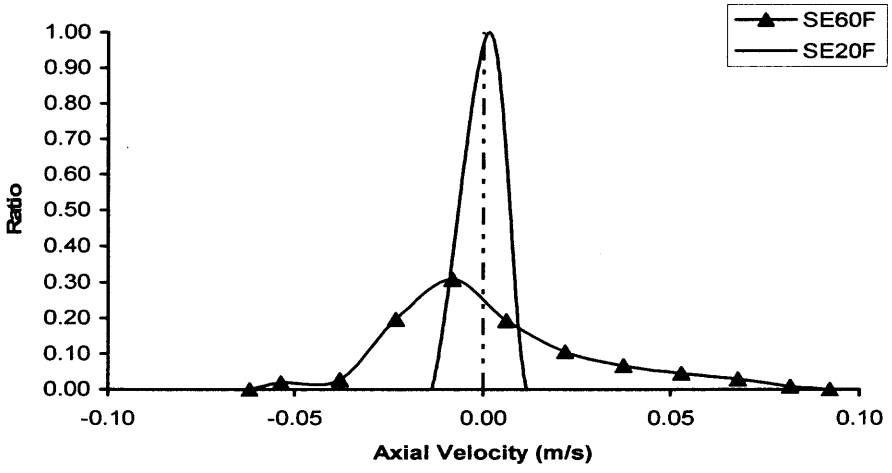

Figure 5.7 Axial velocity distribution at cross section with Z = 0.06 m in SE20F and SE60F.

The effects of velocity profiles on polymerization can be further interpreted by tracing the movement of fluid elements (i.e. streamlines) in the conveying elements. Figure 5.6 has already revealed that some fluid elements have negative axial velocities, and move toward the upstream. Figures 5.8a and b show the streamline of a fluid element initially located at (0.029, 0, 0.06), as marked by P1 in Figure 5.6. It is found that the element follows a very complex streamline in the screw channel. Globally, the element moves upstream. However, it could move downstream for a certain distance, and then move upstream. This is the mechanisms for the axial and transverse mixing. Figures 5.8b

and c show that the displacement of the fluid element along the axial length is smaller in SE20F than that in SE60F, although the lengths of the streamlines in these two cases are the same. This indicates that the axial mixing in SE20F is weaker than that in SE60F. Furthermore, the time required to move the element at a certain length along the streamline in SE20F is longer than that in SE60F (as indicated by the legend in Figure 5.8). This is because the axial velocity distribution in SE20F is narrower than in SE60F (Figure 5.7). The longer moving time of the fluid element in SE20F also suggests that the axial mixing in SE20F is weaker than in SE60F.

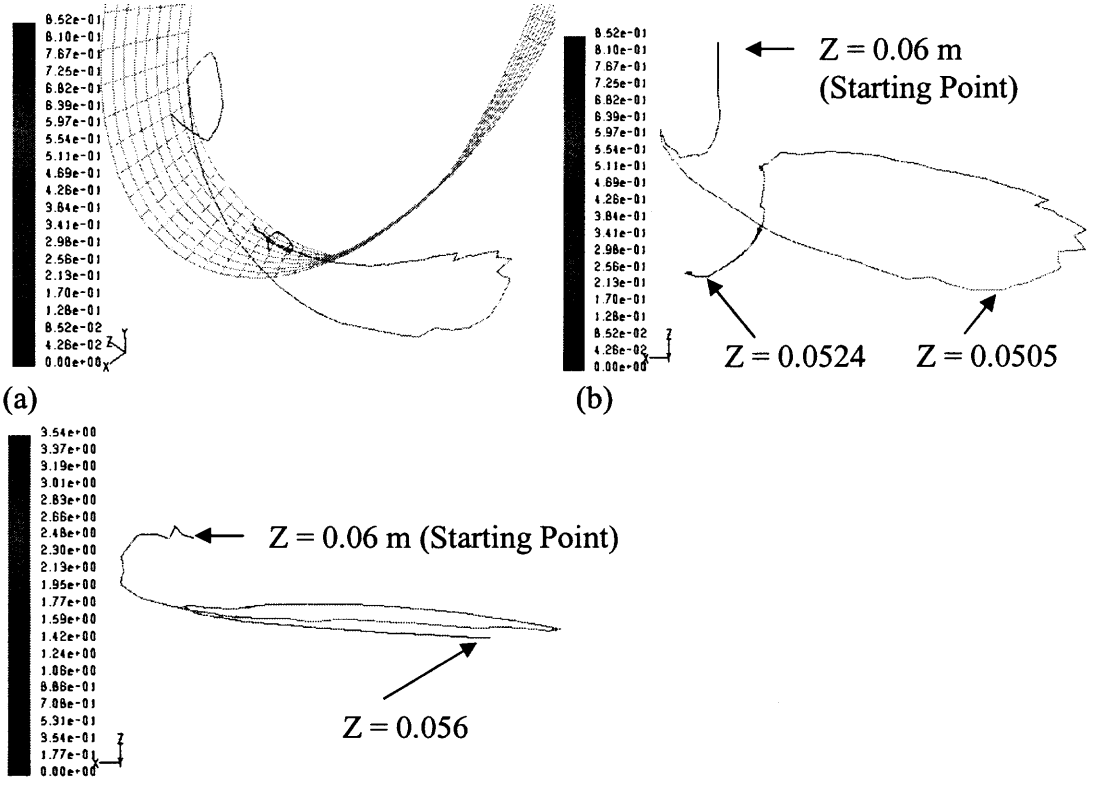

Figure 5.8 Streamlines of an element initially located at (0.029, 0, 0.06) (marked by P1 in Figure 5.6). (a) isometric view of the streamline in SE60F, (b) top view of the stream line in SE60F and (c) top view of the streamline in SE20F.

In this thesis, the fluid elements with downstream velocities are denoted as forward-flow and those with upstream velocities as back-flow. The forward-flow pushes the reaction system downstream, as the conversion ratio increases along the flow direction. The back-flow carries the fluid upstream. Because the conversion ratio in the downstream is higher than in the upstream, the back-flow helps to increase the conversion ratio at the upstream. Hence, the increase in conversion ratio in the conveying elements is a competing consequence between the forward-flow and back-flow. This implies that the conversion ratio profile depends not only on the ratio of back-flow rate to forward-flow rate, but also on the local distribution of conversion ratio.

Figure 5.9 demonstrates the calculation results of the area weighted average conversion ratio, temperature, viscosity, pressure and shear rate along the axial length in different conveying elements. Here, the area weighted average operation at an axial cross section is defined as:

$$\bar{\zeta} = \frac{\sum_{i=1}^{N} \zeta(i) A(i)}{\sum_{i=1}^{N} A(i)} \tag{5.2}$$

where A(i) and $\zeta(i)$ are the area and the calculated parameter at cell i at an axial cross section. N is the total number of cells at the cross section.

Figure 5.9a shows that, globally, the conversion ratio has a fast increase with increasing screw pitch, from 20 mm to 40 mm, and 60 mm. As discussed previously, this is due to the fact that the axial mixing is enhanced when the screw pitch is raised. It is seen that with decreasing screw rotational speed, the reaction becomes faster. This can be

attributed to the weak heat transfer at the barrel surface at low screw speed (see Figure 5.10).

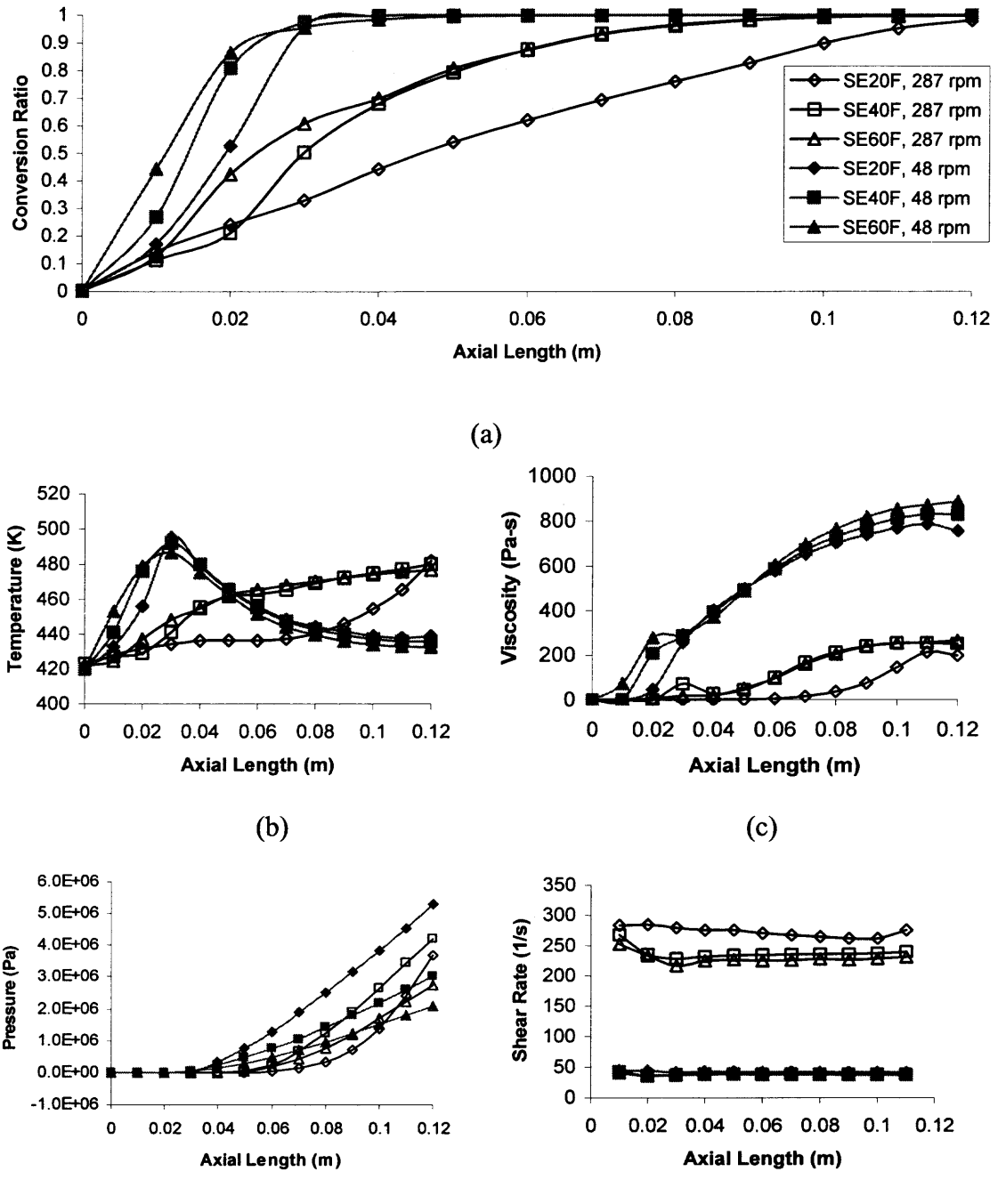

Figure 5.9 Area weighted average parameters along the axial length during polymerization at $[M]/[I]_o = 800$, N = 48 rpm or 287 rpm, T = 420 K and $C_o = 0$. (a) conversion ratio, (b) temperature, (c) viscosity, (d) pressure, and (e) shear rate (Symbols in plots b-e are the same as those in plot a).

Figure 5.9b reveals that the temperature profile along the axial length depends on the screw rotational speed. The temperature increases monotonously along the axial length, when the screw speed is 287 rpm. At 48 rpm, the temperature rises first, reaching a maximum value at a certain position close to the channel entrance, and then drops gradually. Moreover, the maximum temperature at 287 rpm is lower than that at 48 rpm. This is due to the fact that the heat from reaction, which depends on the increase in conversion ratio, is the dominant energy source. As shown in Figure 5.9a, at 48 rpm, the conversion ratio has a fast increase and jumps to about 1 in a very short axial distance along the channel, causing the appearance of the temperature peak there. The lower increase in temperature at 287 rpm near the channel inlet is due to the smaller increase in conversion ratio but the larger heat loss at the barrel surface.

The decrease in temperature at the downstream of Z = 0.03 m at 48 rpm means that the heat transfer between the reaction system and barrel surfaces plays an important role there. Because the temperature at barrel surfaces remains constant during polymerization and the screw surface has an adiabatic condition, the reaction system with high temperature would release its energy through the barrel surface. Considering the fact that the reaction is complete at an axial location about 0.03 m, the temperature profile at the downstream of Z = 0.03 m relies on the competition between viscous dissipation and heat loss at the barrel surface. Although the viscosity of the system is quite high at 48 rpm (in a range from 300 to 800 Pa-s, as shown Figure 5.6c), the shear rate is very low (about 40 s^{-1}, Figure 5.9e). However, the melt temperature is much higher than the barrel temperature, which is 400 K. This indicates that the heat loss at the barrel surface is larger than the viscous dissipation, causing the decrease in temperature along the axial

length beyond Z = 0.03 m, at 48 rpm. The monotonous increase of temperature along the channel at 287 rpm is due to the fact that the polymerization is not complete even at the channel exit, and the heat from polymerization is larger than the heat loss at the barrel.

In the simulation, the inlet pressure was set to zero. Thus, a positive pressure at the channel exit means that the element builds pressure, while a negative pressure means that the pressure is consumed in the element, i.e. the inlet has a higher pressure than the outlet. Figure 5.9d shows that the pressure rises along the axial length. For SE40F and SE60F, the pressure at the channel exit rises with increasing screw speed. However, the pressure in SE20F is lower at 287 rpm than that at 48 rpm. This is because the pressure gradient in conveying elements depends on screw speed, system viscosity, and screw geometry. In SE20F, the variation in viscosity is a more important role than the increase in screw speed. Figure 5.9e shows that the shear rate drops with decreasing screw speed. The effect of screw geometry on shear rate is very small at 48 rpm, but is significant at 287 rpm.

In order to explain the effect of screw rotational speed on the heat transfer at the walls, the velocity profile at the mid-line of the channel at Z = 0.06 m (marked line L_1 in Figure 5.6b) is calculated and demonstrated in Figure 5.10. It is seen that with decreasing screw speed, the velocity gradient near the barrel surface drops. It is known that the heat loss through the barrel surface depends on the convection near the wall, which relies on the velocity gradient. The small gradient of velocity means low convection near the wall, which leads to the decrease in the heat loss through the barrel. Consequently, more heat from reaction is retained in the reaction system at a low screw speed, resulting in a faster polymerization.

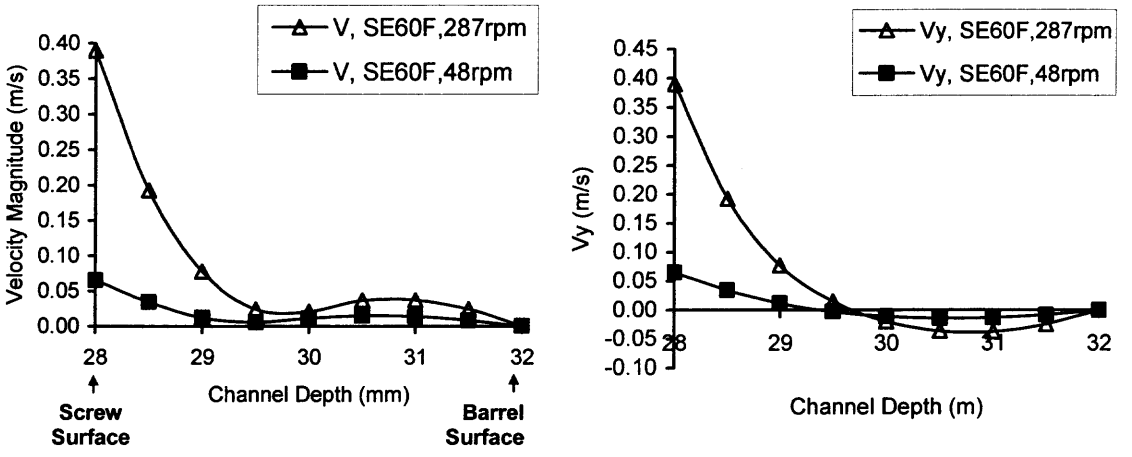

Figure 5.10 (a) Velocity magnitude and (b) velocity component at Y direction at mid-line of channel at Z = 0.06 m and Y = 0 m in SE60F.

5.1.1.2 Axial Mixing Mechanisms in Screw Elements. As discussed previously, the progression of polymerization in conveying elements not only depends on the back-mixing capacity, but also relies on the local variation in conversion ratio. The flow of polymer melt in a screw channel is usually evaluated by the pressure-to-drag flow ratio, which is defined as the ratio of pressure flow rate to drag flow rate.

As shown in Figure 5.6, in the axial cross sections of conveying elements, some fluid elements move downstream (with positive axial velocity), and others moves upstream. This indicates that the fluid elements in a cross section can be divided into two groups: the fluid with positive (downstream) velocity, and that with negative (upstream) velocity. In this study, the axial mixing in screw elements is evaluated with the flux mixing coefficient, G_F, following the definition proposed by White (6):

$$G_F = \frac{Q_B}{Q_F - Q_B} = \frac{Q_B}{Q_N} \tag{5.3}$$

where Q_B is the back flow rate; Q_F is the forward flow rate and Q_N the net flow rate.

Figure 5.11 shows the plots of the flux-mixing coefficient in SE20F and SE60F at 48 rpm and 287 rpm, respectively, as a function of axial length. It is seen that the flux-mixing coefficient is higher in SE60F than SE20F, especially at 287 rpm. As discussed previously, the conversion ratio in SE60F has a faster increase than that in SE20F, which can be correlated to the fraction of the back-flow rate, i.e. the flux-mixing coefficient. Figure 5.11 also indicates that the flux-mixing coefficient drops with decreasing screw rotational speed. However, the polymerization is faster at 48 rpm than at 287 rpm. This suggests that the flux-mixing coefficient is not sufficient in evaluating the reaction process. This is due to the fact that, in reactive process, there is not only mass exchange, but also temperature and species exchanges as well.

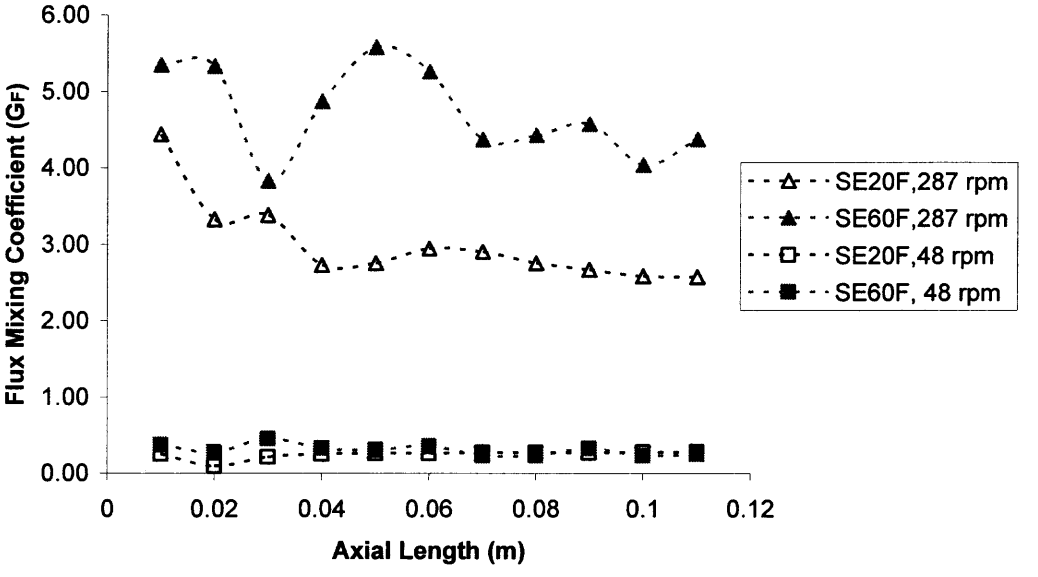

Figure 5.11 Flux-mixing coefficients in conveying elements at $[M]/[I]_o$ = 800, N = 48 rpm or 287 rpm and $C_o = 0$.

Following the definition of the flux-mixing coefficient, in the present study, two more parameters are defined to characterize the axial mixing in conveying elements during reactive extrusion:

1. Temperature mixing index, G_T

$$G_T = \frac{\sum_{i=1}^{N_B} Q_{B_i} T_{B_i}}{\sum_{j=1}^{N_F} Q_{F_j} T_{F_j}} = \frac{\sum_{i=1}^{N_B} A_{B_i} V_{B_i} T_{B_i}}{\sum_{j=1}^{N_F} A_{F_j} V_{F_j} T_{F_j}} \tag{5.4}$$

2. Conversion ratio mixing index, G_C

$$G_C = \frac{\sum_{i=1}^{N_B} Q_{B_i} C_{B_i}}{\sum_{j=1}^{N_F} Q_{F_j} C_{F_j}} = \frac{\sum_{i=1}^{N_B} A_{B_i} V_{B_i} C_{B_i}}{\sum_{j=1}^{N_F} A_{F_j} V_{F_j} C_{F_j}} \tag{5.5}$$

In Equations 5.4 and 5.5, F and B stand for the forward and back flux, respectively; Q is the flow rate. C and T are conversion ratio and temperature. N_b and N_f are the number of the cells with forward and reversed axial velocity, respectively. A and V are the area and axial velocity of a cell at an axial cross section.

The values of temperature-mixing coefficient, and conversion-mixing coefficient, represent the exchange in temperatures, and conversion ratios, respectively, among fluid elements at an axial cross section. Figure 5.12 shows the conversion ratio mixing coefficient and temperature mixing coefficient in conveying elements SE20F and SE60F at 287 rpm and 48 rpm. Globally, both the conversion mixing coefficients and temperature mixing coefficients are higher in SE60F than SE20F, and drop with decreasing screw rotational speed. This indicates that the exchange in conversion ratio and temperature between the forward flux and back flux is more intensive in SE60F than

SE20F, especially at high screw speed. Along the axial length, the conversion mixing coefficients decrease. This is because the conversion ratio in the forward flux approaches that in the back flux (both of them are approaching 1.0), with reaction proceeding. That is, the difference in conversion ratio between the forward-flow and back flow is large near the channel inlet, and drops when approaching the outlet. Figure 5.12 also shows that the trends of temperature mixing coefficients along the axial length are similar to those of conversion mixing coefficients

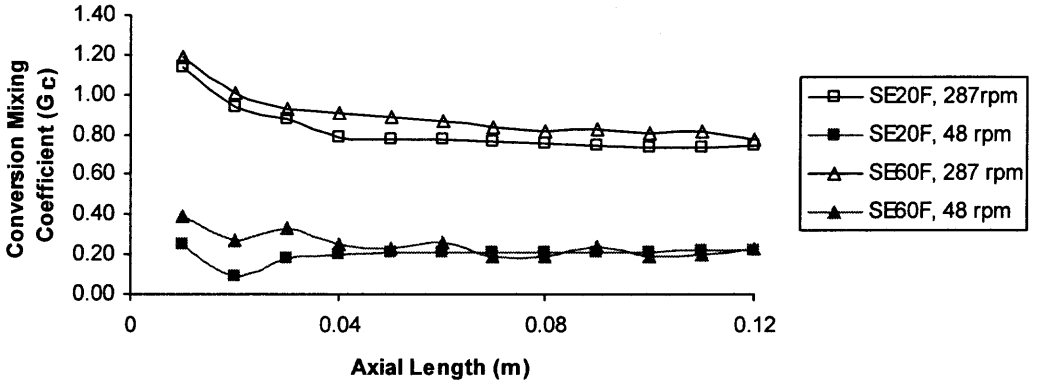

(a)

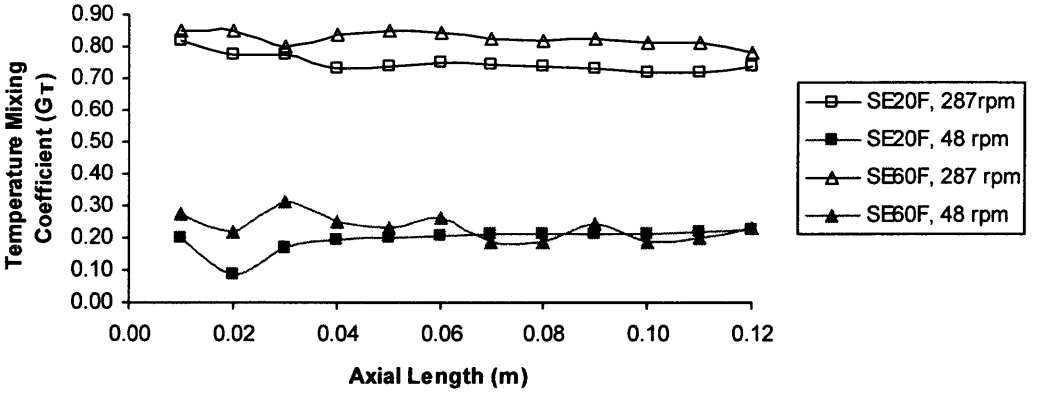

(b)

Figure 5.12 Calculated (a) conversion mixing coefficients, and (b) temperature mixing coefficients in conveying elements.

5.1.1.3 Transverse Mixing in Screw Elements. It is known that in extruders, there is not only axial mixing between the fluids in the upstream and downstream, but also the transverse mixing among fluid elements in the axial cross sections. As discussed in the preceding section, the back flow could bring the fluid with high conversion ratio upstream, in which some fluid elements would join in the forward flow due to the transverse mixing. That is, the fluid elements in the forward flow and back flow are not independent; they would exchange with each other due to the transverse mixing, as illustrated in Figure 5.13. On the other hand, the transverse mixing has a large effect on the heat transfer ability between polymer melt and the barrel surface, and heat homogenization of the polymer melt. Due to the non-isothermal nature of the polymerization, the heat transfer at walls and heat homogenization in polymer melt are very important. However, transverse mixing is not easily evaluated, due to the complicated characteristics of polymer flow.

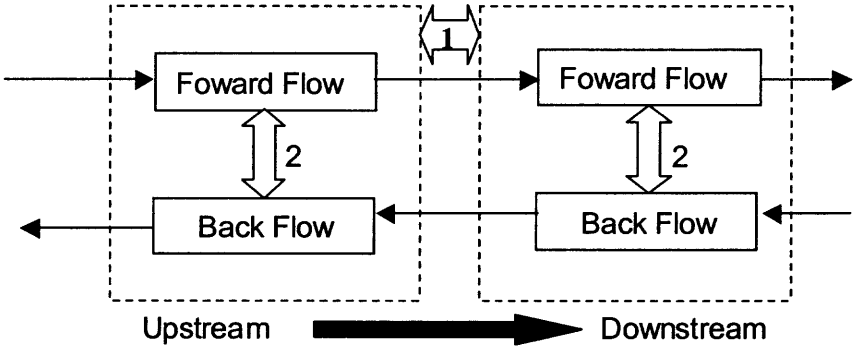

1. Axial Mixing; 2. Transverse Mixing

Figure 5.13 Schematic illustrations of the mixing mechanisms between forward flow and back flow in screw elements.

Transverse mixing of polymeric fluid in conveying elements is produced because some materials are dragged forward by the rotating screw, whereas others would be conveyed in the direction opposite to the screw rotating direction, due to the pressure gradient. Figure 5.14 shows the velocity vector of fluid elements in the cross section with Z = 0.06 m in SE60F. It is seen that near the screw surface, the materials have the velocity in the screw rotating direction. However, in the regions near the barrel surface, the fluid elements move in the direction opposite to those near the screw surface.

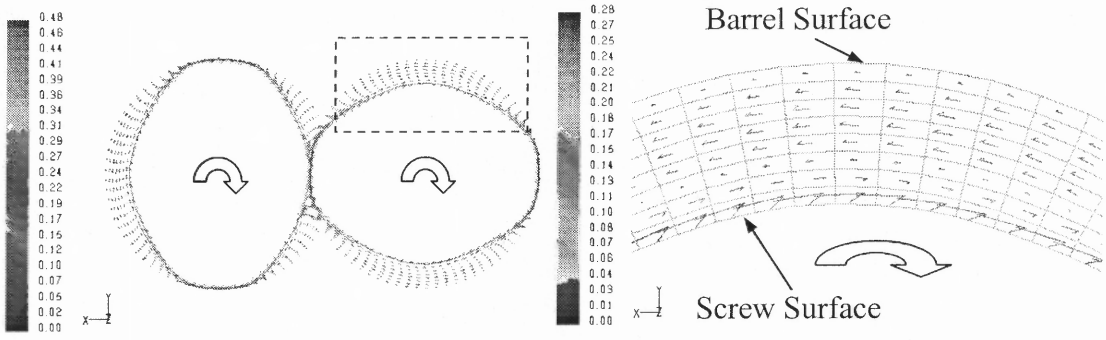

Figure 5.14 Velocity vector in (a) cross section with Z = 0.06 m in SE60F, and (b) blowing up of the rectangular region in plot a.

In the current study, the fluid elements moving in the screw rotating direction are denoted as drag flow, and the others are donated as pressure flow. Consequently, the transverse mixing is characterized as:

$$G_{TV} = \frac{Q_P}{Q_D + Q_P} \tag{5.6}$$

in which G_{TV} is the transverse mixing coefficient. Q_P and Q_D are pressure flow rate and drag flow rate in the transverse section, respectively.

Figure 5.15 summarizes the transverse mixing coefficients at the cross section of Z = 0.06 m in SE20F and SE60F, at 287 rpm and 48 rpm, respectively. This Figure shows

that the transverse mixing in SE60F is much larger than that in SE20F. This indicates that SE60F has more intensive mixing in the cross section that SE20F, which could lead to a faster increase in conversion ratio in SE60F than SE20F (see Figure 5.9a). With decreasing screw rotational speed, the transverse mixing coefficient drops slightly. As discussed previously (Figure 5.10), the heat transfer at barrel surface decreases at low screw speed. This indicates that the polymerization at low screw speed depends mainly on the heat transfer at wall, not on the transverse mixing.

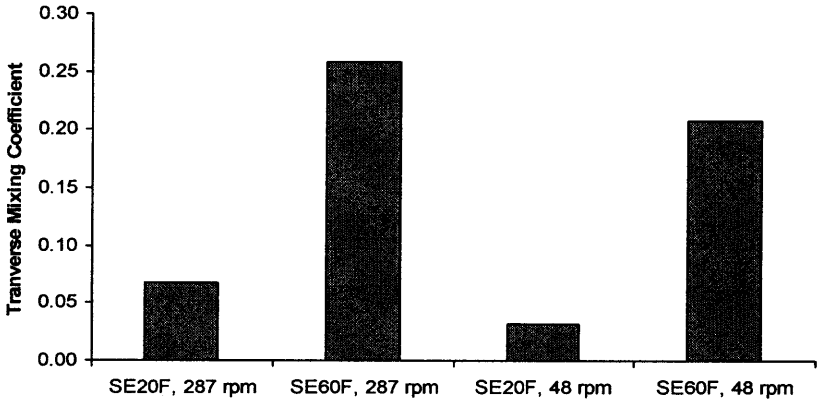

Figure 5.15 Transverse mixing coefficients at cross section of Z = 0.06 m in SE20F and SE60F.

The above discussion shows that the polymerization of ε-caprolactone in screw channels is a complex process, which depends not only on the flow and mixing behavior of the reaction system, but also on the heat generation and heat transfer in the extruder. The flux-mixing coefficient is an important index for the axial mixing, but is not sufficient in evaluating the progression of reaction, due to the non-isothermal nature of the polymerization. Accordingly, the temperature-mixing coefficient and conversion ratio mixing coefficient were defined to characterize the reaction in the conveying elements

during the reactive extrusion. On the other hand, the transverse mixing is evaluated with the ratio of pressure flow to net flow rate in the cross section. The simulation results imply that the reaction progression is determined by the competition between the intensity of mixing and the heat transfer mechanisms at the barrel surface.

5.1.2 Polymerization at $[M]/[I]_0 = 800$ with T = 410 K, $C_0 = 0$ and D = 34 mm

In this section, the temperatures at the inlet and the barrel surface were set at 410 K, instead of 420 K in the preceding section. Figure 5.16 shows the simulation results of the polymerization in conveying elements at 410 K.

Compared with the polymerization at 420 K (Figure 5.9), the conversion ratios at the channel exits at temperatures of 410 K are much lower. The increases in temperature, viscosity, and pressure are much smaller in the cases with temperatures of 410 K than those with 420 K. This is easily understood, because the reaction slows down with decreasing temperature (see Figure 3.2).

The effects of screw rotational speed on polymerization are significant. Similar to the trends in the case of the reaction with 420 K, the polymerization is accelerated at low screw speed. As shown in Figure 5.16a, the conversion ratio is about 0.4 at the element exits when the screw speed is 287 rpm, whereas it is very close to 1.0 at 48 rpm. Furthermore, the effect of screw pitch on reaction at 287 rpm is less significant than the cases at 420K (see Figure 5.9a). This is because, in the current case, the increase in conversion ratio along the axial length is small, which leads to a low system viscosity (Figure 5.16c), and a small increase in temperature (Figure 5.16b). That is, the non-uniformity in temperature is small, and the effect of screw pitch on reaction becomes negligible at 287 rpm and 410 K.

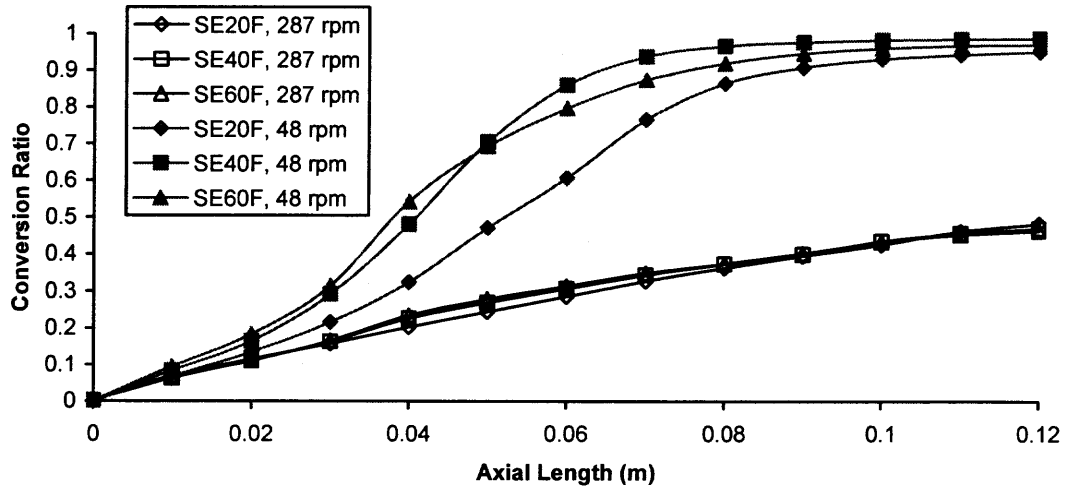

(a)

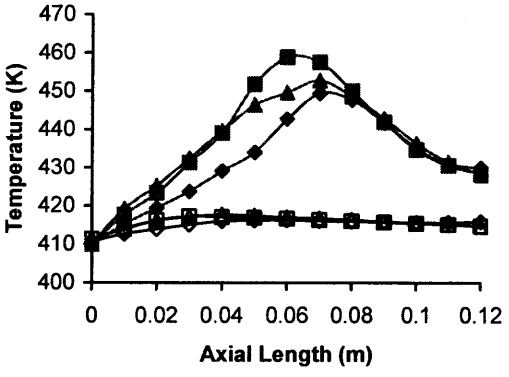

(b)

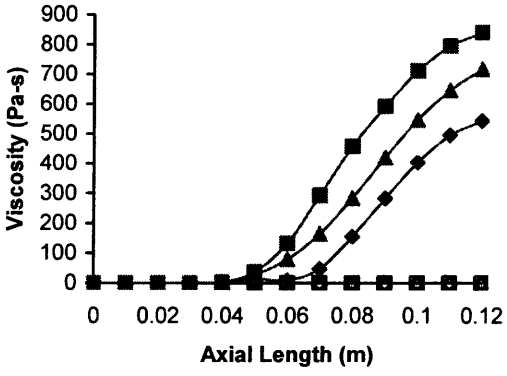

(c)

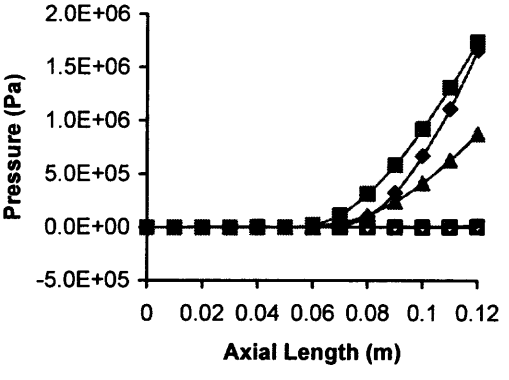

(d)

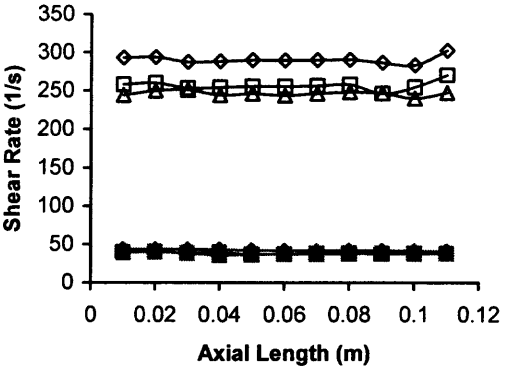

(e)

Figure 5.16 Area weighted average parameters along the axial length during polymerization at $[M]/[I]_o$ = 800, N = 48 rpm or 287 rpm, T = 410 K and C_o = 0. (a) conversion ratio, (b) temperature, (c) viscosity, (d) pressure and (e) shear rate (Symbols in plots b-e are the same as those in plot a).

5.1.3 Polymerization at $[M]/[I]_0 = 800$ with T = 420 K, $C_0 = 0.6$ and D = 34 mm

Here, the conversion ratio at the inlet of conveying elements was assumed to be 0.6, whereas it was set to 0 in the previous studies. Because the viscosity of the system is correlated to the conversion ratio, it is expected that the system viscosity near the inlet should be higher than that in the previous cases (see Figure 5.9c, 5.16c and 5.17c). Thus, the viscous dissipation could play an important role in the polymerization. On the other hand, the maximum increase in conversion ratio in the screw elements is 0.4 at an inlet conversion ratio of 0.6, whereas it is 1.0 when the inlet conversion is 0 (when the polymerization is complete, the conversion ratio is 1.0). Accordingly, the heat from reaction would be smaller in the former than that in the latter.

Figure 5.17 shows the simulation results for the polymerization with a conversion ratio of 0.6 at the channel inlet. Figure 5.17a reveals that the conversion ratio at 48 rpm is lower than that at 287 rpm. This trend is contrary to those presented in Figures 5.9a and 5.16a. The reasons are presented in the following paragraph.

The reduction in screw rotational speed would give rise to three possible results:

1. The axial mixing and transverse mixing in the conveying elements decrease at low screw speed, which would slow down the reaction progressing.
2. The convection in the reaction system near the barrel surface drops with decreasing screw speed, leading to a decrease in heat loss through the barrel surface, and resulting in an acceleration in reaction.
3. The shear rate decreases when the screw rotational speed drops, resulting in a decrease in viscous dissipation. As a consequence, the temperature might fall, and the reaction could slow down.

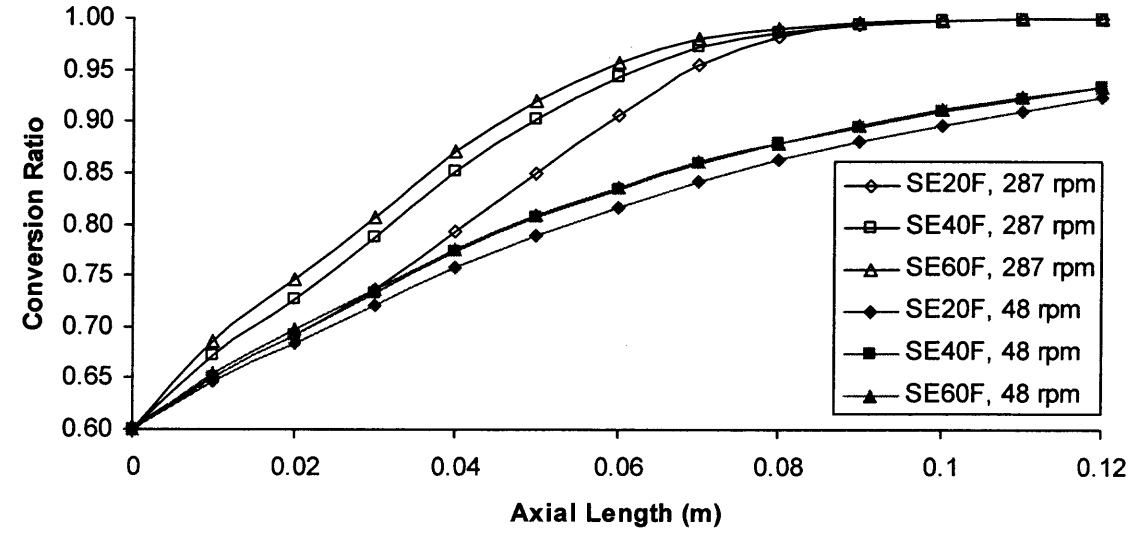

(a)

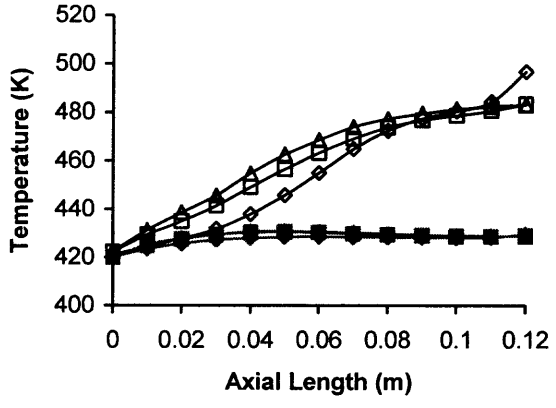

(b)

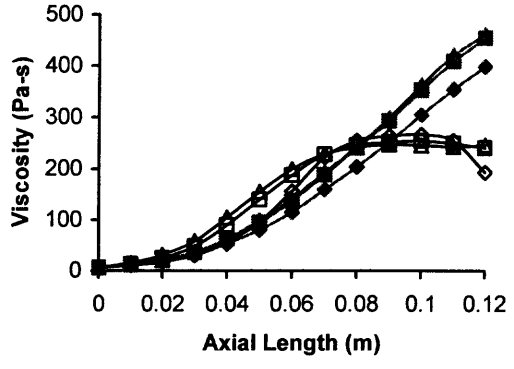

(c)

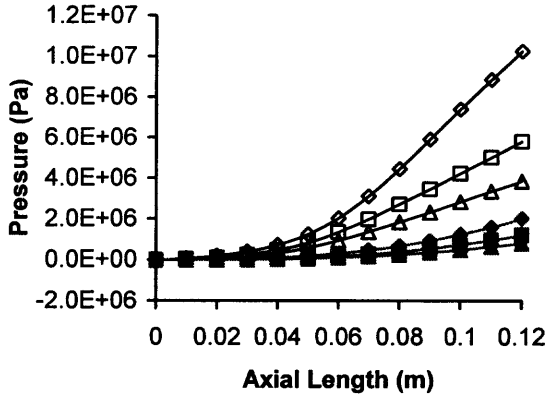

(d)

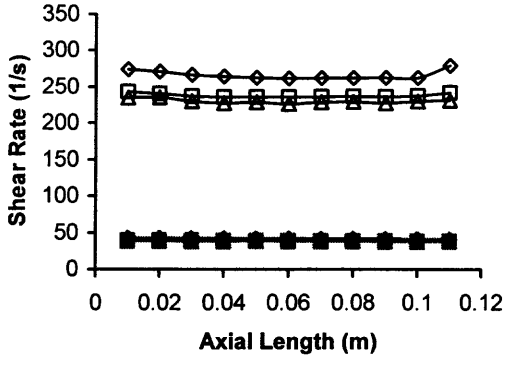

(e)

Figure 5.17 Area weighted average parameters along the axial length during polymerization at $[M]/[I]_o = 800$, N = 48 rpm or 287 rpm, T = 420 K and $C_o = 0.6$. (a) conversion ratio, (b) temperature, (c) viscosity, (d) pressure and (e) shear rate (Symbols in plots b-e are the same as those in plot a).

In order to elucidate the effects of viscous dissipation and heat transfer at walls on the reaction, three cases with different thermal conditions have been studied:

1. Adiabatic reaction, i.e. the system has no energy loss during reaction.

2. Constant temperature at barrel surface, but neglecting viscous dissipation of the reaction system, i.e. the viscous dissipation term is not included in the energy equation.

3. Constant temperature at barrel surface, and considering viscous dissipation of the reaction system, as studied in the previous cases.

Figure 5.18 demonstrates the increases in average conversion ratio along the axial length with various thermal conditions during reaction. Figure 5.18 shows that the reaction is the fastest with the adiabatic conditions and slowest in the cases when the viscous dissipation was excluded. At the adiabatic condition, the reaction is faster at 287 rpm than that at 48 rpm. This confirms that the increase in back-mixing at high screw speed favors the polymerization progression. In the case without viscous dissipation, the polymerization at 287 rpm is slower than that at 48 rpm. This can be explained by the fact that the heat loss at barrel surface is weak at low screw rotational speed. Accordingly, in the case when the viscous dissipation is included and the barrel surface maintains constant temperature during the polymerization, which is the situation investigated in the present study (Table 5.3), the reaction progression depends on the competition between the heat loss at barrel, viscous dissipation and heat from reaction. This explains why the increase of conversion ratio in the conveying elements slows down with decreasing screw speed, as shown in Figure 5.17. In this case, the viscous dissipation plays an important role to the polymerization, because the conversion ratio at the channel inlet is 0.6. With decreasing screw speed, both viscous dissipation and mixing intensity drop, leading to the decrease in temperature and conversion ratio.

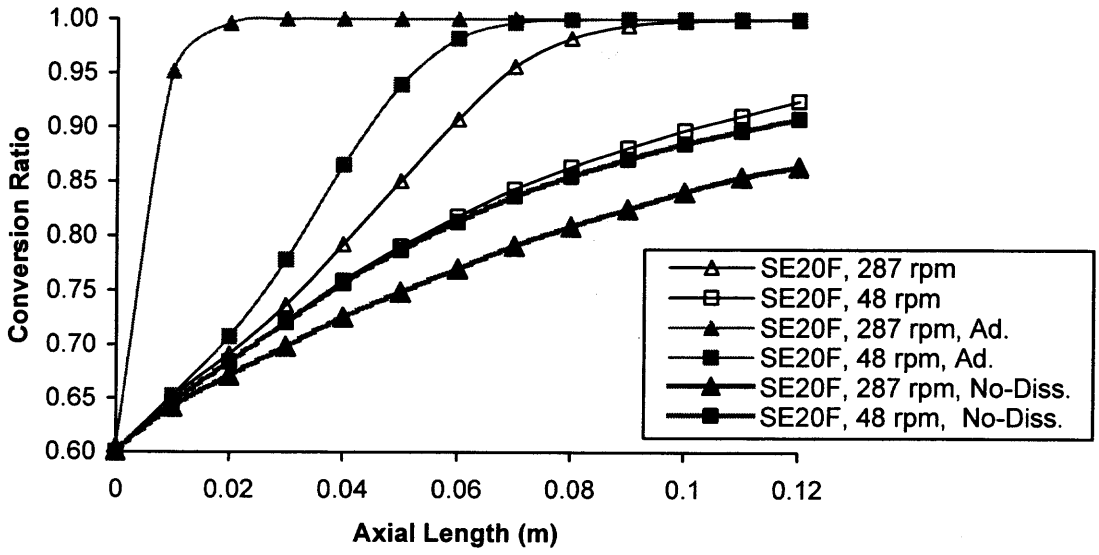

Figure 5.18 Effects of heat transfer conditions at wall on average conversion ratios at $[M]/[I]_o$ = 800, T = 420 K and C_o = 0.6. (Ad. represents adiabatic condition, No-Diss. stands for the case in which the viscous dissipation is neglected).

Similarly, the effects of mixing intensities in different screw elements on polymerization could be studied with the assumption of different thermal conditions during reactions. Figure 5.19 shows the trends of average conversion ratios along the axial length with adiabatic condition and constant temperature at the barrel (considering viscous dissipation), in SE20F and SE60F at 48 rpm. It is seen that at the adiabatic conditions, the reaction is slightly faster in SE60F than that in SE20F. This is attributable to more intensive axial and transverse mixing in SE60F (see Figures 5.11 and 5.15). On the other hand, the difference in conversion ratio between SE20F and SE60F is much larger in the cases with constant temperature at barrel surface than that at adiabatic conditions. In the former, some of the heat from reaction is released through the heat transfer at the barrel surface, whereas in the latter, there is no heat loss through the barrel. This implies that the heat transfer intensity at the barrel surface of SE20F is weaker than that of SE60F, which has a significant effect upon polymerization progression.

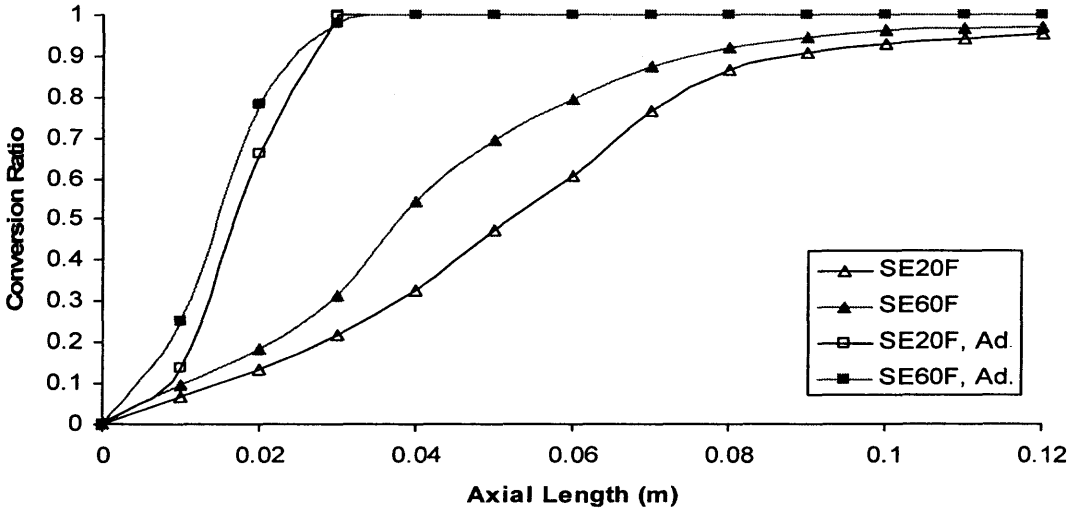

Figure 5.19 Conversion ratios in SE20F and SE60F with adiabatic condition (represented with Ad.) and constant temperature at barrels at 48 rpm.

5.1.4 Polymerization at $[M]/[I]_0 = 400$ with T = 405 K, $C_0 = 0$ and D = 34mm

The simulation results of the polymerization of ε-caprolactone with $[M]/[I]_0 = 400$ are shown in Figure 5.20. The results in Figure 5.20a reveal that with increasing pitch of conveying elements, the reaction becomes fast. Globally, the conversion ratio has a fast increase with decreasing screw speed. However, the effect of screw speed on conversion ratio is insignificant in the current case when compared with that with $[M]/[I]_0 = 800$ (see previous three sections). This is because the flow rates are very high in the current case (Table 5.3), and thus the flux-mixing coefficients are very low (see Figure 5.21). The change of screw speed has small effect on the back-mixing in the elements due to the large flow rate. On the other hand, the heat from reaction is so large that the heat transfer at the barrel is not a dominant role for the reaction.

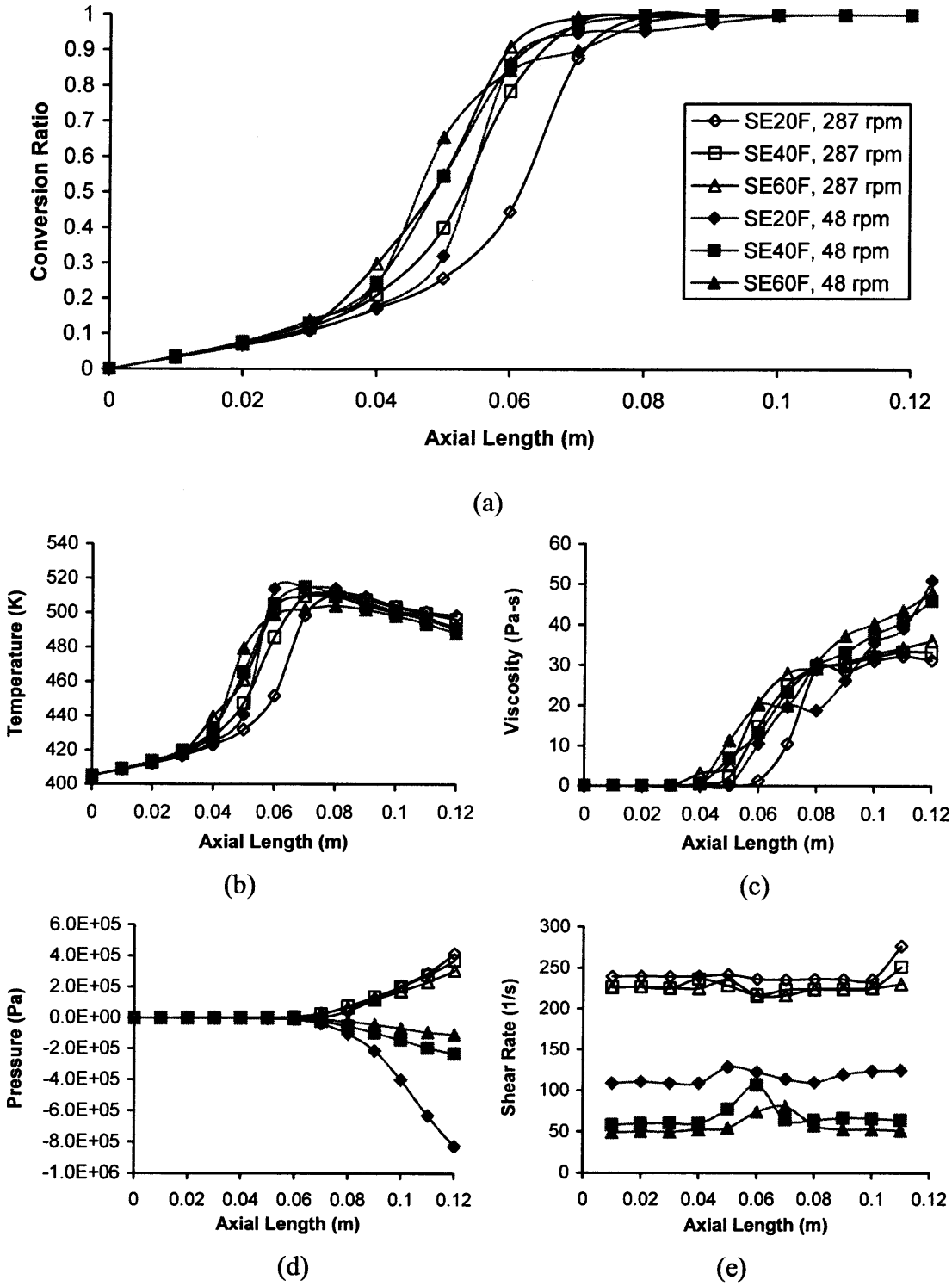

Figure 5.20 Area weighted average parameters along the axial length during polymerization at $[M]/[I]_o$ = 400, N = 48 rpm or 287 rpm, T = 405 K and C_o = 0. (a) conversion ratio, (b) temperature, (c) viscosity, (d) pressure and (e) shear rate (Symbols in plots b-e are the same as those in plot a).

Figure 5.20c shows that the viscosity is much lower than that in the previous cases (Figures 5.9c, 5.16c and 5.17c), because the initiator concentration, $[M]/[I]_o$, is 400 in the present case . With a screw speed of 48 rpm, the inlet pressure is much larger than the outlet pressure (Figure 5.20d). This is because the flow rate is larger than the drag flow capacity of the forward conveying elements at 48 rpm. Such a large flux cannot be conveyed downstream without the aid of pressure flow. In other words, the pressure at the inlet has to be larger than that at the exit. This also indicates that the flow is very close to the pressure flow, and the back-mixing is very weak.

Figure 5.21a shows that the flux-mixing coefficient at the axial cross sections of SE20F is very small: it is about 0.1 at 287 rpm and 0.04 at 48 rpm. However, in the cases presented in Figure 5.11, the flux-mixing coefficient in SE20F at 287 rpm is about 3. Furthermore, the flux-mixing coefficient fluctuates significantly along the axial length (see the peaks or valleys in Figure 5.21a), due to the large variation in viscosity with the reaction proceeding. Figure 21b shows the velocity profiles along the line from point (0.028, 0, 0.06) to point (0.032, 0, 0.06), the mid-line of the channel (marked L_1 in Figure 5.6a). It is seen that the tangential velocity components are positive at both 287 rpm and 48 rpm. This again confirms that the back-flux is negligible.

5.1.5 Scale-up Polymerization at $[M]/[I]_o = 800$ with $T = 420$ K and $C_o = 0.6$

The above discussion suggests that the reaction in conveying elements not only depends on the velocity profiles of the fluid, but also relies on the heat transfer and heat generation mechanism, and species exchanges. In this section, the effect of scale-up screw diameter on reaction is discussed.

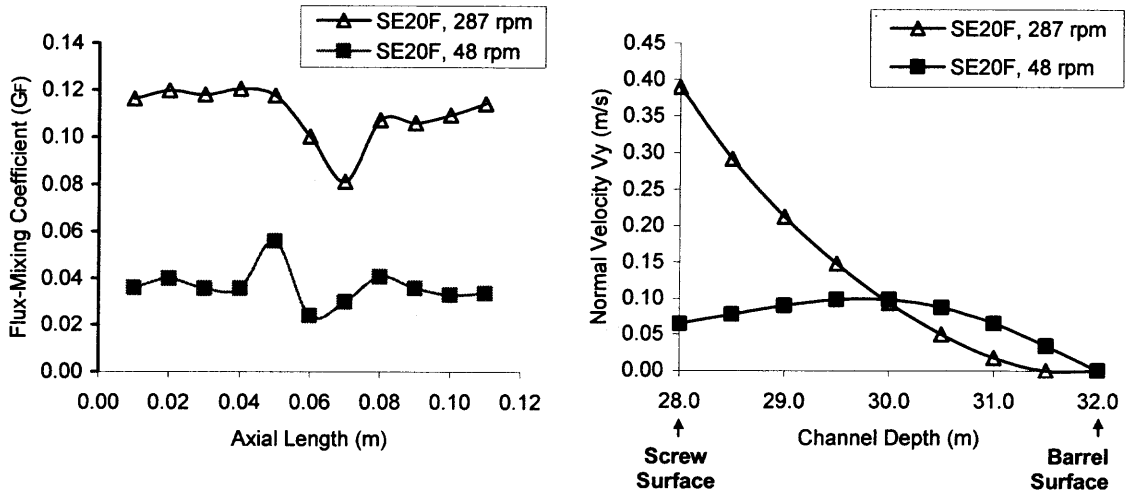

Figure 5.21 (a) Flux-mixing coefficient and (b) normal velocity at line from (0.028, 0, 0.06) to (0.032, 0, 0.06) in SE20F (marked L_1 in Figure 5.6a).

When the screw diameter is increased to 68mm from 34 mm, the cross-sectional area is quadrupled. As shown in Table 5.1, the length of the simulation domain is also doubled after the scale-up. In order to ensure that the mean residence time in the simulation domain with D = 68 mm remains identical to that with D = 34 mm, the average axial velocity at the entrance is doubled. Consequently, the flow rate with D = 68 mm is 8 times that with D = 34 mm. Figure 5.22 shows the average conversion ratio along axial length in SE40F and SE120F, with D = 68 mm (refer to Table 5.3). It is seen that the conversion ratio rises with increasing screw pitch and with increasing screw speed. These trends are consistent with those in the case at D = 34 mm, as discussed in Section 5.1.3.

Figure 5.23 presents the effect of screw diameter on polymerization. It is seen that the conversion ratio is much higher at D = 68 mm than at D = 34 mm. This can be explained by the fact that the depth of screw channel is doubled when the screw diameter is increased from 34 mm to 68 mm. In the simulation, the screw surface is assumed to be adiabatic. The over-heated energy in the reaction system can be transferred out only

through the barrel surface. Consequently, the increase in channel depth would make the release of heat from the reaction system through barrels difficult to occur. Furthermore, the ratio of the barrel surface area to the volume of the screw channel decreases with increasing screw diameter. As a result, the non-uniformity of temperature in the screw channel becomes more pronounced in large size twin-screw extruders. There are some regions with high temperature, which accelerate the polymerization.

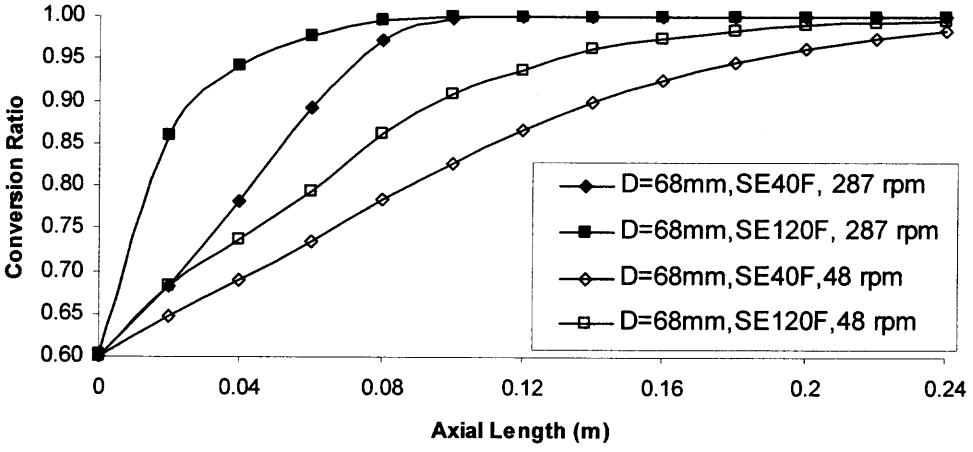

Figure 5.22 Averaged conversion ratios along the axial length at a screw diameter of 68 mm.

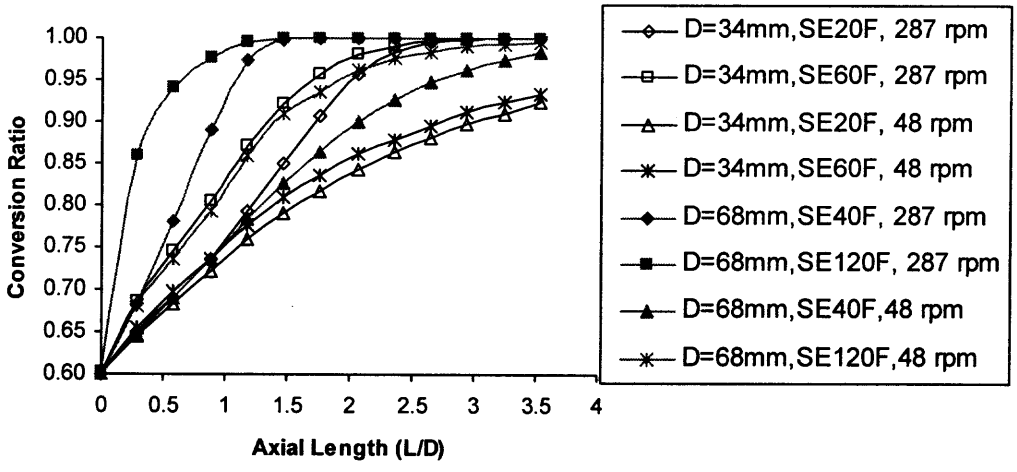

Figure 5.23 Comparison of conversion ratios between D = 34 mm and D = 68 mm.

In order to confirm the critical role of reaction heat and viscous dissipation in the scale-up of polymerization, the conversion ratios along the axial length were calculated for different thermal conditions. The results are shown in Figure 5.24. Here, two cases were studied: one considered the viscous dissipation, the other neglected it (denoted as No-Diss. in Figure 5.24). In both cases, the temperature at barrel surface remains constant, 420 K, during polymerization. The results in Figure 5.24 show that even if the viscous dissipation is neglected, the polymerization with D = 68 mm is faster than that with D = 34 mm at both 48 rpm and 287 rpm. This is due to the poorer heat transfer through the barrel surface at a larger screw diameter. Furthermore, the difference in conversion ratio with or without considering viscous dissipation is much larger in D = 68 mm than in D = 34 mm at 287 rpm, but it is not significant at 48 rpm. This suggests that the viscous dissipation plays a more important role at larger screw diameter, and at higher screw rotational speed.

5.1.6 Effect of Helical Direction of Conveying Elements on Reaction

In co-rotating twin-screw extruders, the reversed conveying elements are usually used to generate the resistance to polymer conveying along the screw length. They are always assumed to be fully-filled with the reaction system during processing. This type of conveying element generally has a short axial length and a small screw pitch. In this section, the polymerization of ε-caprolactone in the reversed conveying elements with both axial length and screw pitch of 20 mm was studied, at $[M]/[I]_0 = 800$, and T = 420 K. The difference in polymerization progression between the forward and reversed conveying elements was discussed.

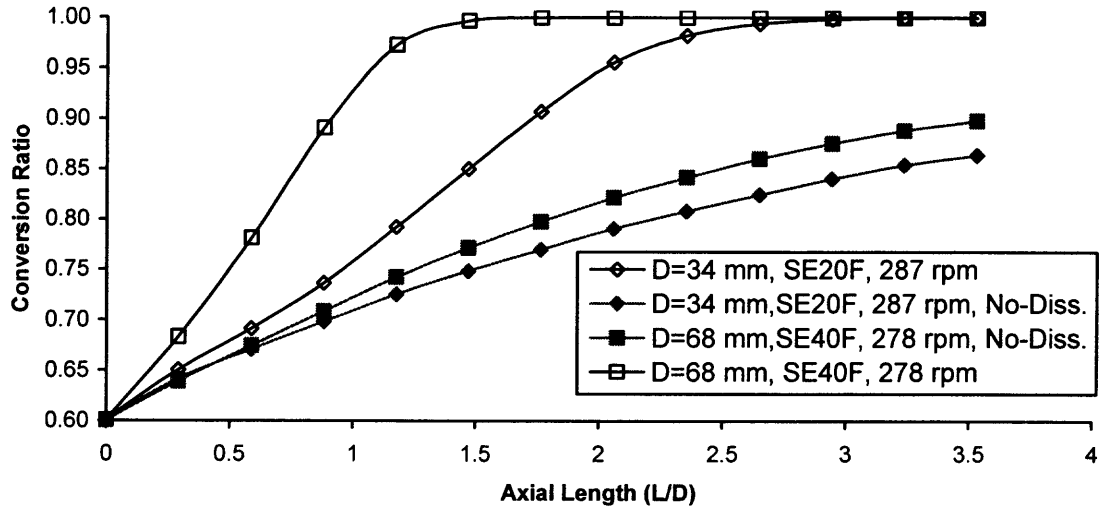

(a)

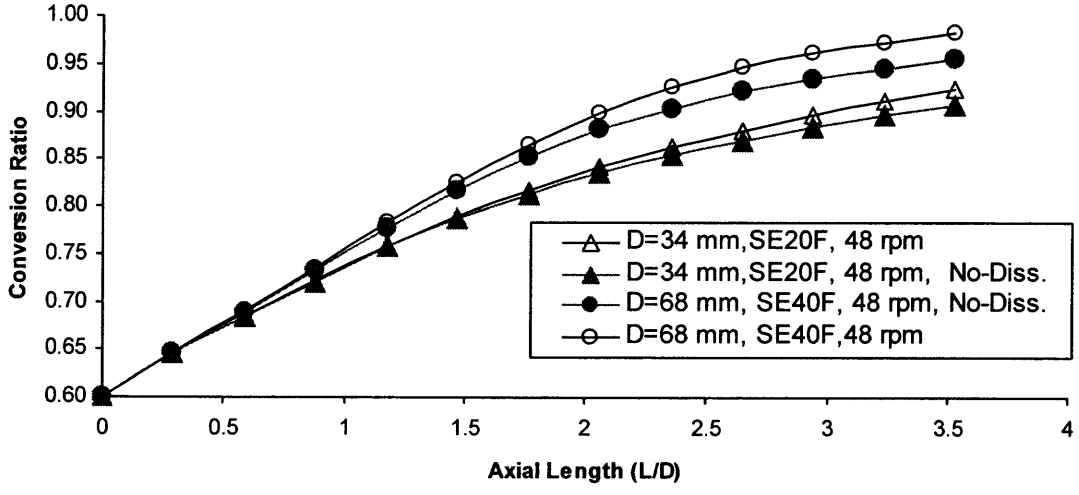

(b)

Figure 5.24 Plots of conversion ratios along the axial length as a function of screw diameter under various thermal conditions at screw speed of (a) 287 rpm and (b) 48 rpm. (No-Diss. denotes the cases in which the viscous dissipation is neglected).

Figure 5.25 summarizes the increase in conversion ratio along the axial length in the reversed conveying element SE20R (see Table 5.1), with an inlet conversion ratio of 0 or 0.6, at a screw speed of 48 rpm or 287 rpm. It is seen that the conversion ratio has a fast increase at low screw speed, and the effect of screw speed upon the increase in

conversion ratio is more significant at an inlet conversion ratio of 0 than at an inlet conversion of 0.6.

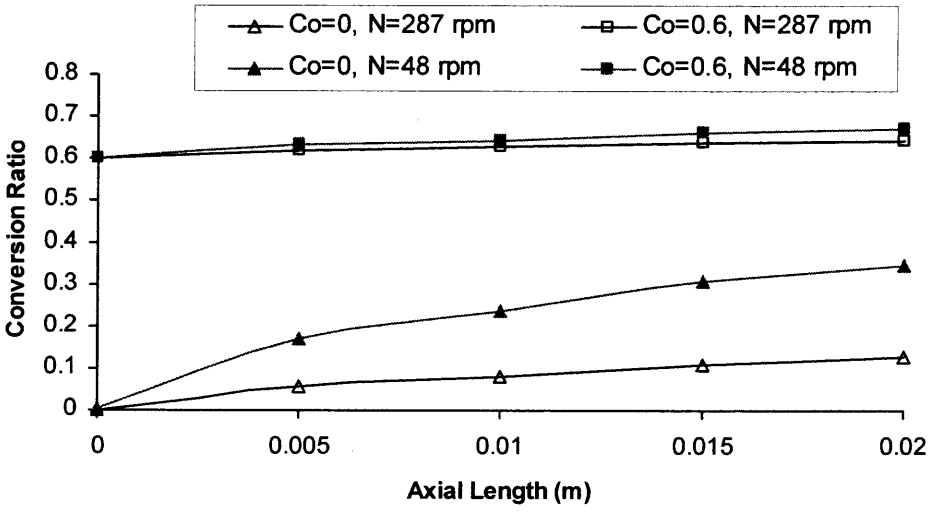

Figure 5.25 Conversion ratio along the axial length in reversed conveying element SE20R at $[M]/[I]_o = 800$, and T = 420 K.

Figure 5.26 displays the trends of conversion ratios along the axial length in the forward and reversed conveying elements. The curves in Figure 5.26 show that the conversion ratio at the exit (Z = 0.02 m) of the reversed elements (SE20R) is lower than that in the forward elements (SE20F), at an identical simulation condition. The difference in conversion ratio in the forward and reversed elements is small at an inlet conversion ratio of 0.6, but it is large when the inlet conversion ratio is zero, especially at 48 rpm. It is known that the conveying mechanisms of the reaction system in the forward elements are entirely different from those in the reversed elements. In the former, the materials are conveyed downstream by the drag flow (produced by the rotating screws), whereas the pressure flow brings the materials upstream (Usually, the forward element builds pressure, i.e. the outlet has a higher pressure than the inlet). In the latter, the reaction

system is carried downstream by the pressure flow, and is brought to the upstream by the drag flow. The variations in conveying mechanisms cause different mixing and heat transfer behavior in the forward and reversed elements, leading to different trends of conversion ratio along the axial length.

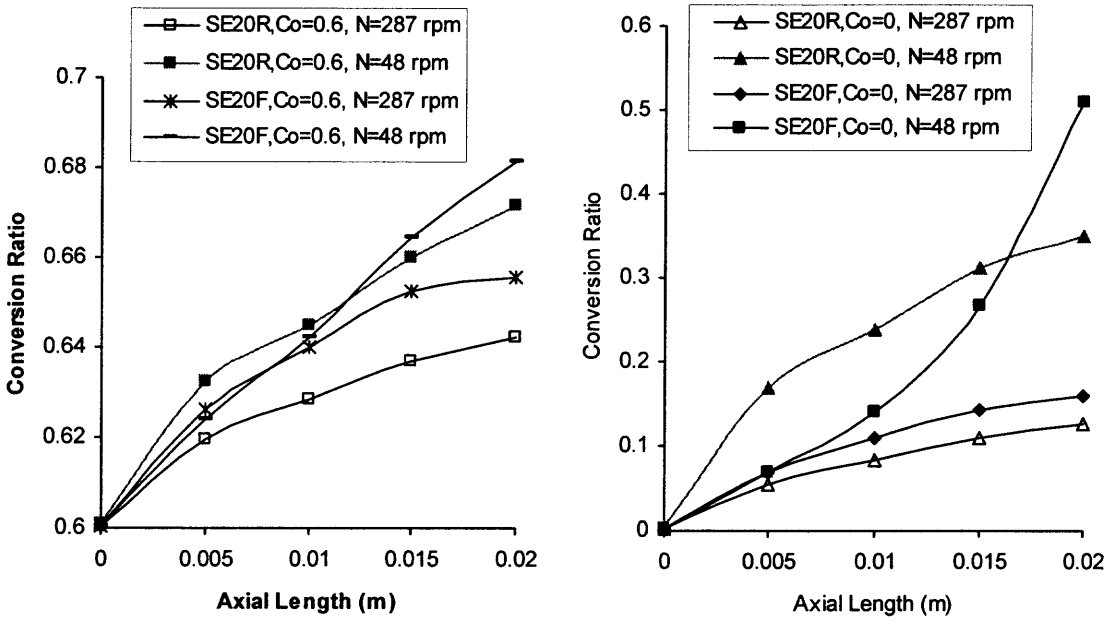

(a) (b)

Figure 5.26 Comparison of conversion ratios along the axial length in SE20F and SE20R at $[M]/[I]_0 = 800$ and $T = 420$ K. (a) $C_0 = 0.6$ and (b) $C_0 = 0$.

5.1.7 Effect of Reaction Heat on Polymerization in Conveying Elements

As discussed in the previous sections, the heat from reaction plays a critical role in the polymerization progression. In the polymerization of ε-caprolactone, one important characteristic is that the heat from reaction is quite high, about 250 kJ/kg. For example, the reaction heat for the polymerization of polyamide 6 is about 110 kJ/kg. This section focuses on the results of the effect of reaction heat on polymerization progression in conveying elements; the values of reaction heat of the model system were assumed to be

250 kJ/kg, and 100 kJ/kg, respectively. The increase of conversion ratio along the axial length with different values of reaction heat, and various operational conditions, are summarized in Figures 5.27 – 5.30.

Figure 5.27 demonstrates the trends of conversion ratio along the axial length in SE20F with different values of reaction heat at $[M]/[I]_o = 800$, $T = 420$ K, and $C_o = 0$, in which symbol "Iso" denotes isothermal conditions of reaction, i.e. the system remains at a constant temperature 420 K during the polymerization. This is very close to the case in which the heat from reaction is zero, considering that viscous dissipation in this system is small. It is seen from Figure 5.27 that the effect of the values of reaction heat on the polymerization is significant: the reaction is accelerated with increasing reaction heat. Furthermore, the variation in conversion ratio at different screw rotational speeds becomes small when the reaction heat drops.

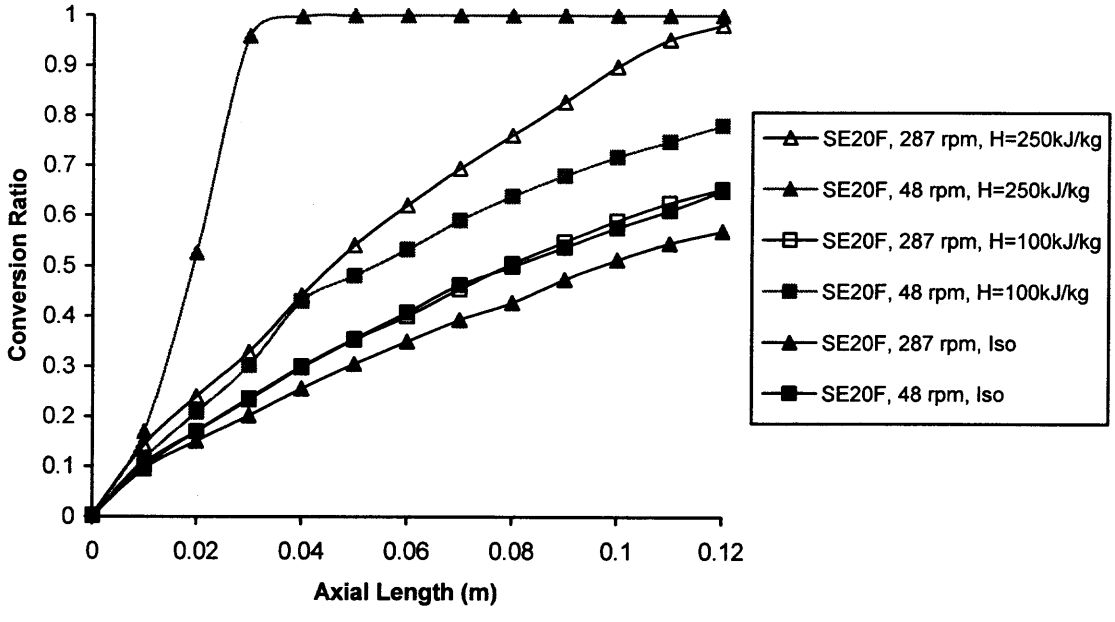

Figure 5.27 Effect of reaction heat on conversion ratio at $[M]/[I]_o = 800$, $T = 420$ K and $C_o = 0$ in SE20F.

Figure 5.28 shows that the effect of screw rotational speed on the increase in conversion ratio in SE20F is negligible when the reaction heat is 100 kJ/kg, at $[M]/[I]_o$ = 400, T = 405 K and C_o = 0, and the conversion ratio at channel exit (Z = 0.12 m) is about one third of that with a reaction heat of 250 kJ/kg.

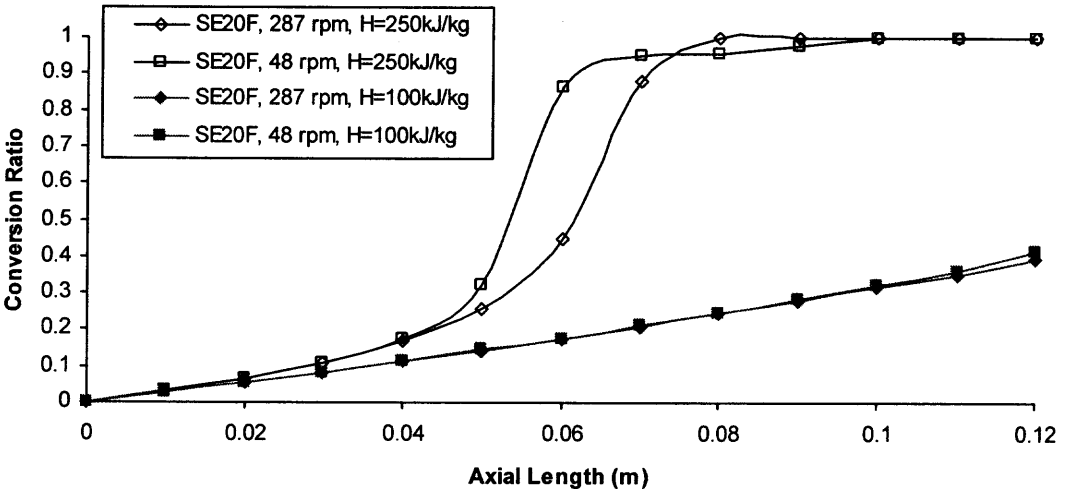

Figure 5.28 Effect of reaction heat on conversion ratio at $[M]/[I]_o$ = 400, T = 405 K and C_o = 0 in SE20F.

Figure 5.29 reveals that the polymerization with a reaction heat, H = 250 kJ/kg, is much faster than that with H = 100 kJ/kg, especially at low screw speed. However, both geometry of conveying elements (i.e. screw pitch) and screw rotational speed have insignificant effects on the polymerization at H = 100 kJ/kg.

Figure 5.30 indicates that the variation in conversion ratio with different values of reaction heat is small when the inlet conversion ratio is 0.6, which is less pronounced than that with a zero inlet conversion (Figure 5.27). This can be attributed to the fact that the reaction heat is the dominant energy source in the case with a zero inlet conversion ratio, whereas viscous dissipation plays an important role when the inlet conversion is 0.6.

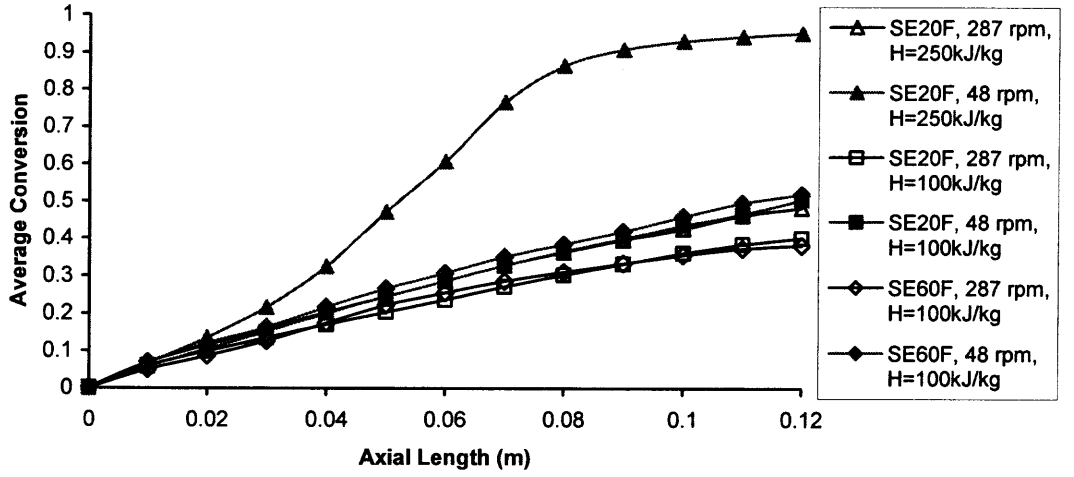

Figure 5.29 Effect of reaction heat on conversion ratio at $[M]/[I]_o = 800$, $T = 410$ K and $C_o = 0$ in SE20F and SE60F.

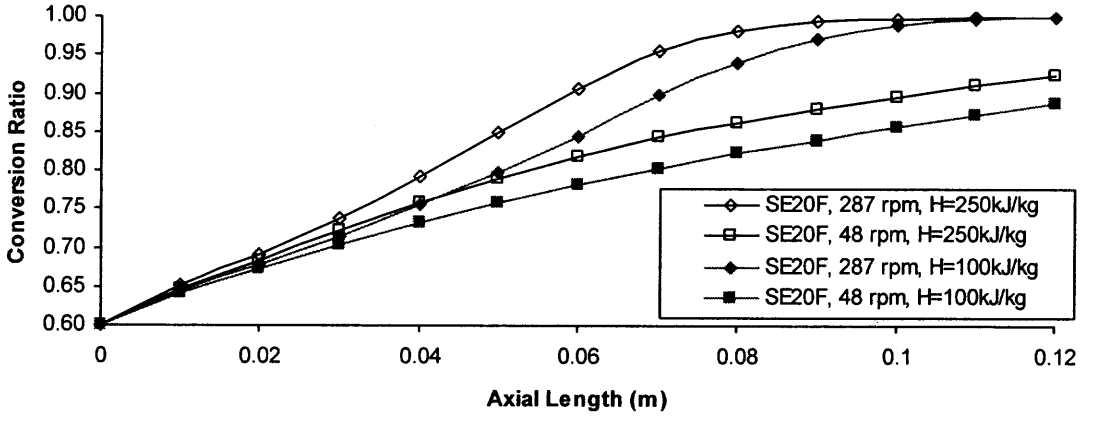

Figure 5.30 Effect of reaction heat on conversion ratio at $[M]/[I]_o = 800$, $T = 420$ K and $C_o = 0.6$ in SE20F.

The above discussion indicates that the value of reaction heat is an important factor in the polymerization. As the value of reaction heat decreases, the effect of screw pitch and screw rotational speed on the polymerization progression in conveying elements becomes less significant, particularly, at an inlet conversion ratio of zero. This implies that it is important to introduce a 3-D model in the simulation of the polymerization with a large heat from reaction, such as polymerization of ε-caprolactone.

5.2 Comparison of Simulation Results Based on 1-D and 3-D Models

In this section, the simulation results from 3-D model are compared with those based on 1-D model. As discussed in Chapter 2, the simulation results from 1-D model depend largely on the heat transfer coefficient at the wall. Hence, the effect of heat transfer coefficient on reaction progression predicted with 1-D model is also discussed.

Figure 5.31 displays the effect of simulation methods, i.e. 1-D model or 3-D model, on the increase in conversion ratio along the axial length, at $[M]/[I]_o = 400$, and T = 405 K. It is seen that the conversion ratios based on 3-D model are larger than those obtained from 1-D model, even with a heat transfer coefficient of zero at the barrel surface. That is, the reaction progression obtained from 3-D model is faster than that predicted from 1-D model with adiabatic conditions at the barrel surface. This is due to the fact that the reaction is a very fast one at $[M]/[I]_o = 400$. The large reaction heat is hardly transferred out through the barrel surface at a short time, leading to a non-uniform temperature distribution at the axial cross section. This indicates that temperature is very high in some regions, where the reaction is further accelerated. As a consequence, the polymerization based on 3-D model is faster than that from 1-D model with an adiabatic condition at walls. In the latter, the temperature at the axial cross section is assumed to be uniform.

Figure 5.31 also shows that in simulation with the 1-D model, the values of heat transfer coefficient at the barrel surface have an insignificant effect on the increase of conversion along the axial length. This is attributable to the fact that the heat from reaction is so large that the heat transfer at the wall is not an important factor in the polymerization progression.

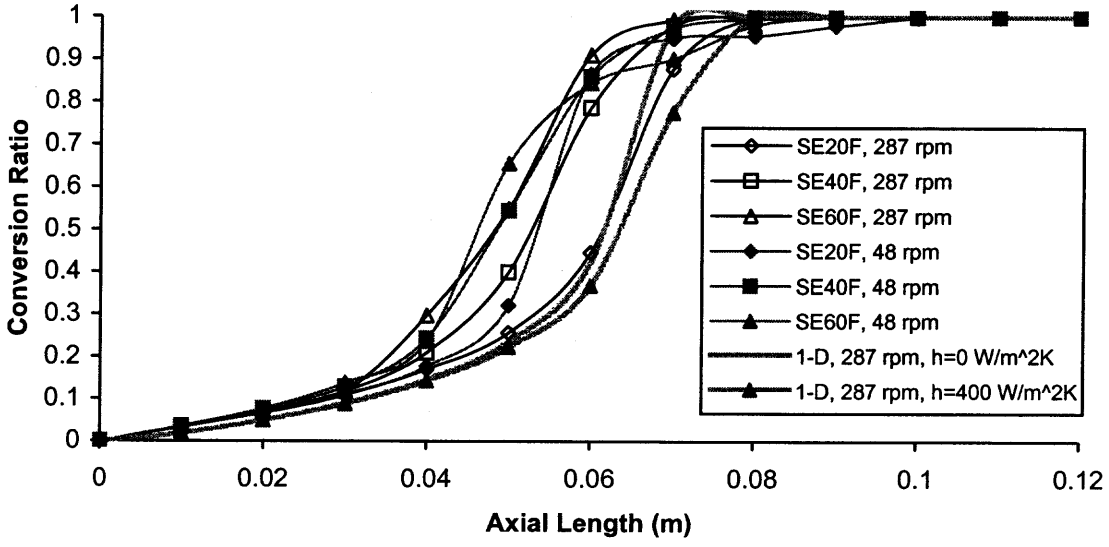

Figure 5.31 Average conversion ratio at $[M]/[I]_o = 400$, T = 405 K, and $C_o = 0$ based on 1-D and 3-D models.

Figure 5.32 shows that at 48 rpm, the conversion ratios from 3-D model are higher than those from 1-D model with adiabatic conditions at the barrel surface, at $[M]/[I]_o = 800$, T = 420 K, and $C_o = 0$. However, at 287 rpm, the conversion ratios based on 3-D simulation are much lower than those from 1-D model, even when a heat transfer coefficient of 400 W/m^2 K is used. This is because, at low screw speed, the transverse mixing is weak, which results in a poor heat transfer at the barrel surface. At high screw speed, the heat loss at the barrel surface based on the 3-D model would be larger than that in the 1-D model, as explained in the following.

As presented in Chapter 2, the heat transfer at the barrel surface in 1-D model is given by:

$$q = h(T_b - \bar{T}_f) \tag{5.7}$$

where q is the heat flux; T_b is the barrel temperature, and $\bar{T}_f$ the average temperature of fluid. h is the heat transfer coefficient at barrel surface, which depends on convection of

the fluid near the wall, and the heat conductivity of the fluid. However, in 1-D modeling, h is usually given as a constant, independent of the polymerization progression.

When 3-D model is applied, the heat flux at the barrel surface takes the form:

$$q = k\frac{dT}{dn}\bigg|_{Wall} \tag{5.8}$$

where k is the heat conductivity of the fluid; the temperature gradient is evaluated based on the fluid temperature near the barrel surface:

$$\frac{dT}{dn}\bigg|_{wall} = \frac{T_{fl} - T_b}{\Delta} \tag{5.9}$$

where T_{fl} is the fluid temperature in the layer next to the barrel surface, and Δ is the layer thickness. Due to the large reaction heat, the fluid temperature in the layer next to the barrel surface can be high. Consequently, the heat loss at the barrel surface during polymerization based on 3-D model would be larger than that in 1-D model.

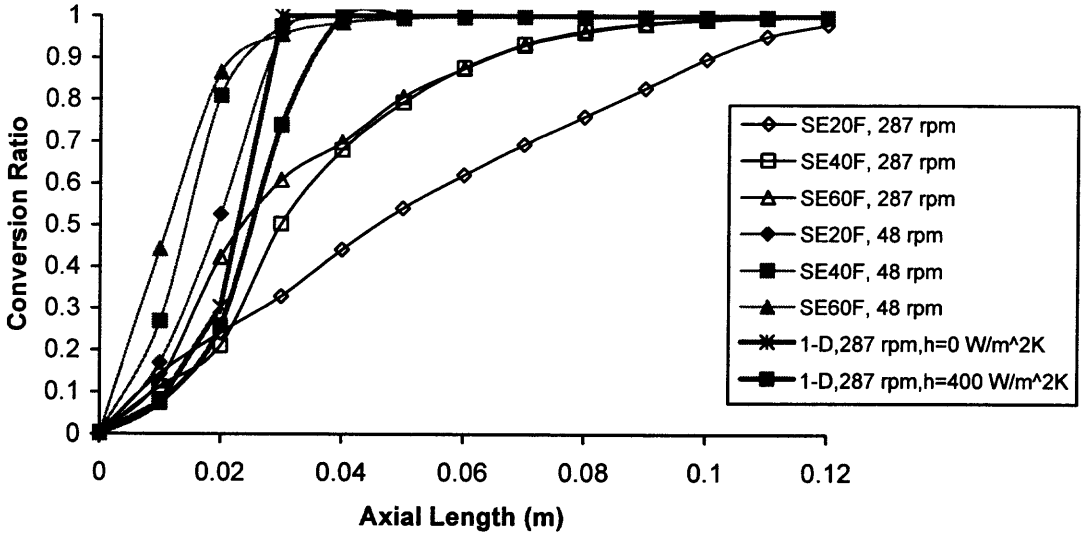

Figure 5.32 Average conversion ratio at $[M]/[I]_o$ = 800, T = 420K, and C_o = 0 based on 1-D and 3-D models.

As shown in Figure 5.33, when the temperatures at barrels and inlet are set to 410 K, and the inlet conversion ratio is 0, the conversion ratio obtained from 3-D model at 287 rpm is much lower than that from 1-D with a heat transfer coefficient, h = 400 W/m^2 K, at the barrel surface. This is similar to the trends shown in Figure 5.32. At 48 rpm, the conversion ratio from 3-D model is very close to that based on 1-D model with h = 400 W/m^2 K, but is lower than that from 1-D model with h = 0 W/m^2 K. On the other hand, Figure 5.32 already shows that the conversion ratio from 3-D model is higher than that from 1-D model with h = 0 W/m^2 K, when the inlet and barrel temperatures are 420 K. The divergent trends in these two cases indicate that the 1-D model, developed based on the assumption of uniform temperature/conversion distribution at axial cross sections of the flow channel, cannot predict the complex mechanisms of reaction and energy generation in the reactive extrusion correctly.

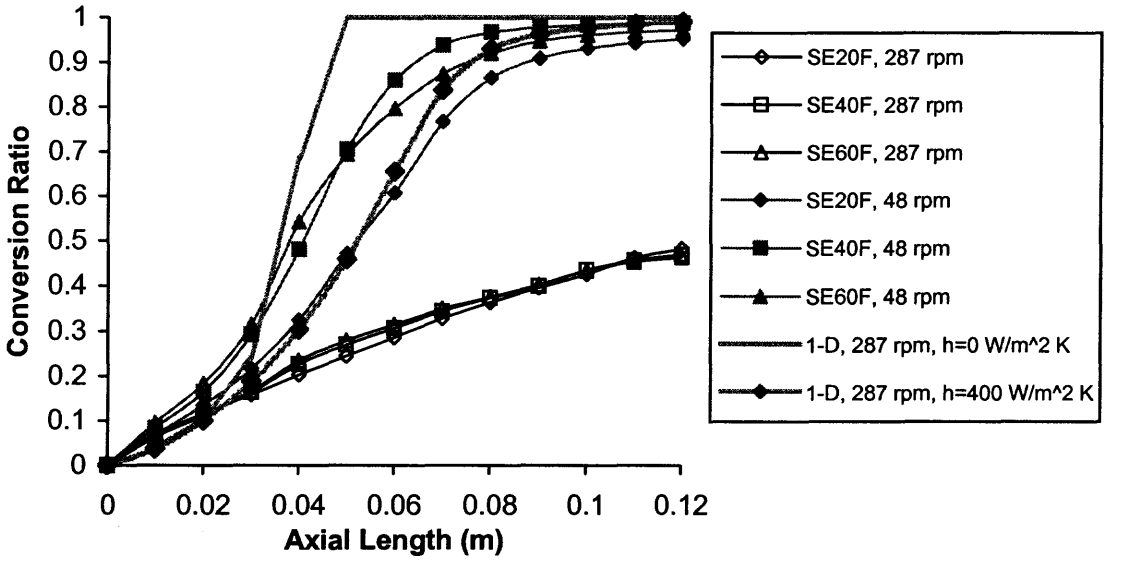

Figure 5.33 Average conversion ratio at $[M]/[I]_o$ = 800, T = 410K, and C_o = 0 based on 1-D and 3-D models.

Figure 5.34a shows that at an inlet conversion of 0.6, the conversion ratio from 3-D model at 48 rpm is very close in magnitude to that from 1-D model with a heat transfer coefficient, h = 400 W/m^2 K. At 287 rpm, the conversion ratios from 3-D model are slightly higher than those from 1-D model with an adiabatic condition (h = 0 W/m^2 K). This can be interpreted with the fact that the energy generation from viscous dissipation in 3-D model is enhanced at high screw speed. As discussed previously, viscous dissipation is an important factor for reaction when the inlet conversion ratio is 0.6.

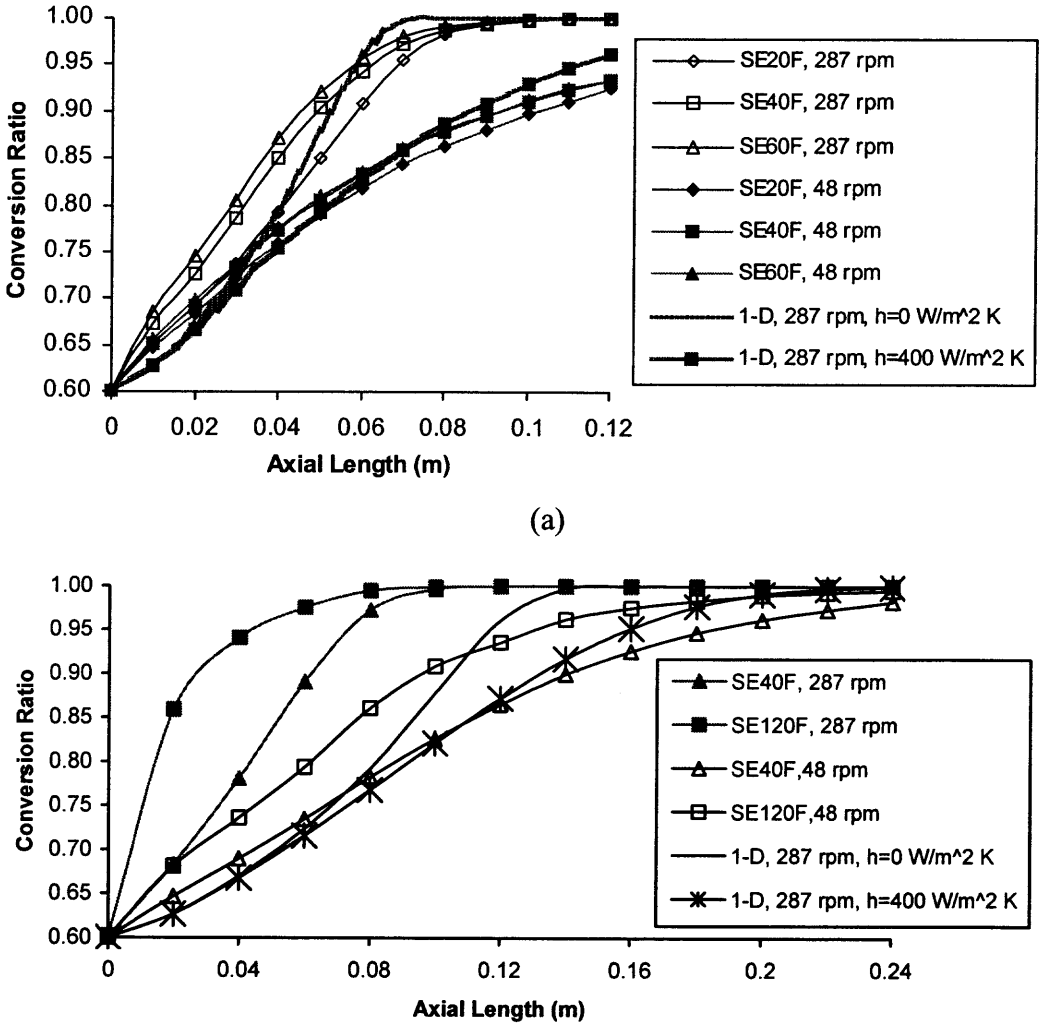

Figure 5.34 Average conversion ratio at $[M]/[I]_o$ = 800, T = 420 K, and C_o = 0.6 based on 1-D and 3-D models with (a) D = 34 mm, (b) D = 68 mm.

When the screw diameter is increased to 68 mm from 34 mm, the difference in conversion ratio at 48 rpm based on 3-D model and 1-D model with a heat transfer coefficient of 400 W/m^2 K at walls, is small. However, the difference between 3-D and 1-D results at 287 rpm is very significant. Furthermore, the variation in conversion ratio between 1-D and 3-D models at 287 rpm with D = 68 mm is much larger than that with D = 34 mm. This implies that the application of a 1-D model in the simulation of polymerization in large machines is not reliable.

The comparison of conversion ratio profiles between 1-D and 3-D models along the axial length at $[M]/[I]_o$ = 400 with a reaction heat, H, of 100 kJ/kg is presented in Figure 5.35. It is seen that that the difference in conversion ratios based on 3-D model and 1-D model at H = 100 kJ/kg is negligible, and is smaller than that with H = 250 kJ/kg (see Figure 5.31). Similarly, the variation in conversion ratios between 1-D and 3-D models at $[M]/[I]_o$ = 800, T = 420 K and C_o = 0 with H = 100 kJ/kg (Figure 5.36) is smaller than that with H = 250 kJ/kg (Figure 5.32). This can be explained by the fact that the decrease in heat from reaction slows down the increase in temperature along the axial length. As a sequence, the temperature in the axial cross section becomes much uniform with decreasing heat from reaction. Accordingly, the characteristics of the non-isothermal process in the conveying elements predicted by the 3-D model approach those obtained from the 1-D model. This suggests that it could be feasible to apply the 1-D model in predicting polymerization when the heat from reaction is low.

Figure 5.37 shows the effect of simulation methods, 1-D and 3-D models, on the average conversion ratio at $[M]/[I]_o$ = 800, T = 420 K, and C_o = 0.6, along the axial direction, with a reaction heat, H, of 100 kJ/kg, and 250 kJ/kg, respectively. At a screw

speed of 48 rpm, the difference in conversion ratio between 3-D model and 1-D model with a heat transfer coefficient of 400 W/m^2 K is smaller at H = 100 kJ/kg than that with H = 250 kJ/kg. However, the difference is very large at 287 rpm. This is due to the fact that viscous dissipation at 287 rpm is much larger than that at 48 rpm. This again confirms that viscous dissipation is a vital energy source for the polymerization at 287 rpm; the heat from reaction is important at 48 rpm, in which viscous dissipation is weak.

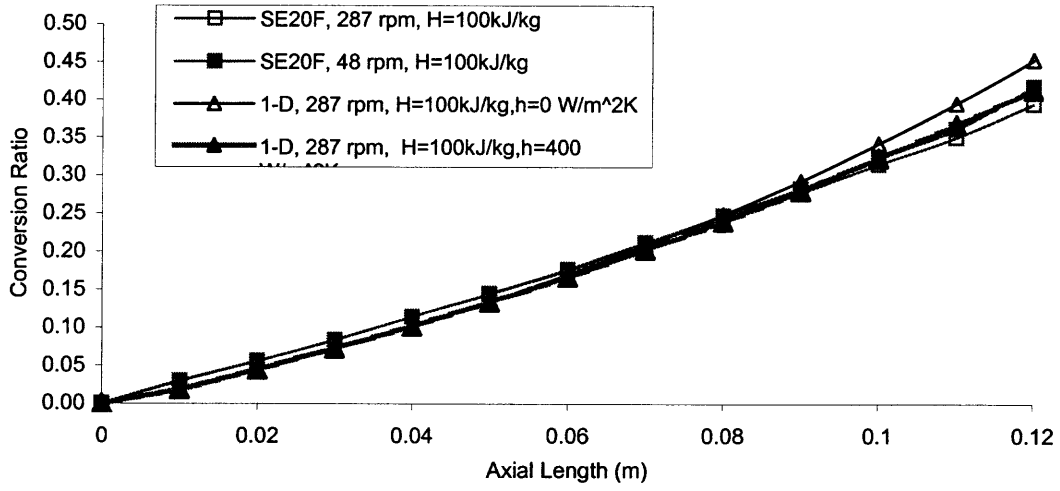

Figure 5.35 Effect of simulation method on average conversion ratio at $[M]/[I]_o$ = 400, T = 405K and C_o = 0, with H = 100 kJ/kg.

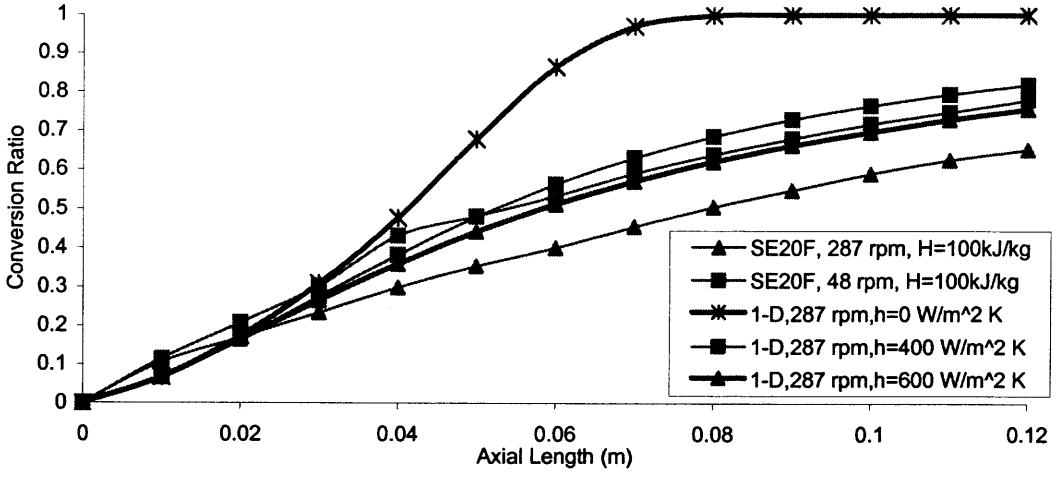

Figure 5.36 Effect of simulation method on average conversion ratio at $[M]/[I]_o$ = 800, T = 420K and C_o = 0 with H = 100 kJ/kg.

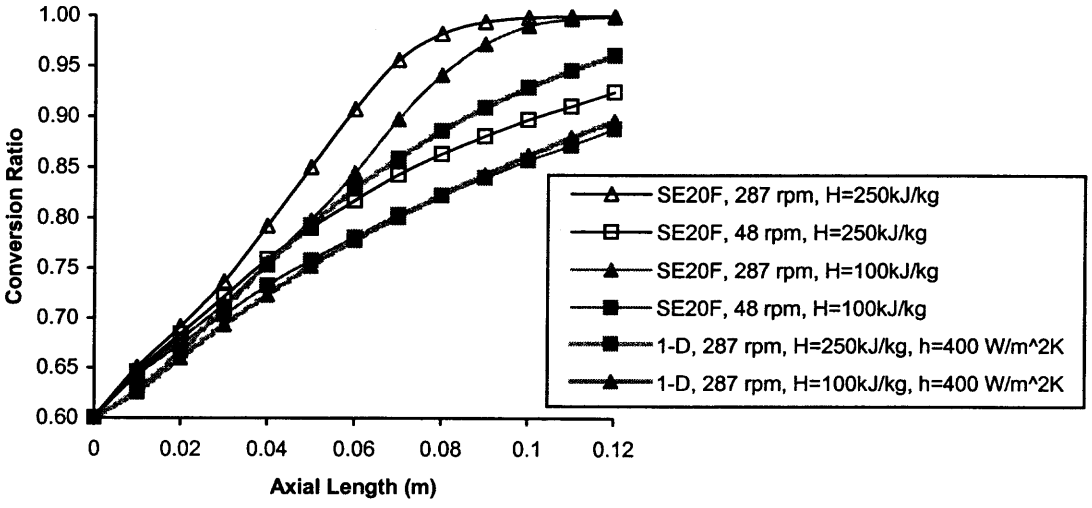

Figure 5.37 Effect of simulation method on average conversion ratio at $[M]/[I]_o = 800$, T = 420K and $C_o = 0.6$ with H = 100 kJ/kg.

5.3 Conclusions

In this chapter, the results of numerical simulation with a 3-D model of the polymerization of ε-caprolactone in fully-filled conveying elements were presented. The effects of screw geometries, screw rotational speed, and initiator concentration on polymerization kinetics were discussed. The results show that the polymerization kinetics in the conveying elements is very complex. The extent of polymerization is the result of competition among such factors as residence time, heat transfer at the barrel surface, viscous dissipation, and heat from reaction. Consequently, the flux-mixing coefficient, which represents the axial mixing of mass in the conveying element, is not sufficient to evaluate the reaction progress; the heat generation, and heat transfer mechanisms, should be incorporated into the evaluation of mixing intensity. Accordingly, two indices, temperature mixing coefficient, and conversion ratio mixing coefficient, have been introduced for the first time to describe the extent of axial mixing during reactive

extrusion. Furthermore, the transverse mixing during reactive extrusion is evaluated with the ratio of pressure flow rate to net flow rate.

The dependence of polymerization of ε-caprolactone in the conveying elements on screw rotational speed, temperatures at inlet and barrel surface, pitch of conveying elements, initiator concentration, and screw diameter, can be interpreted in terms of the energy balance during the reaction, which is illustrated in Figure 5.38.

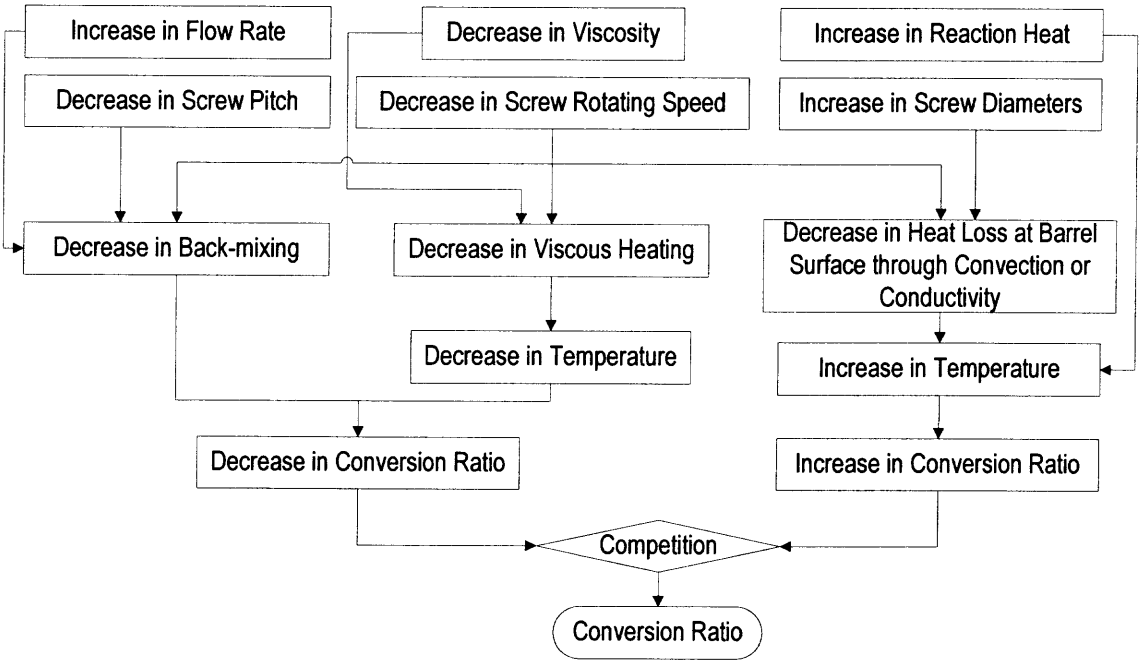

Figure 5.38 Factors affecting polymerization in conveying elements.

When the reaction system has a low viscosity (say, when the inlet conversion ratio is 0), the viscous dissipation is not a key factor in the energy balance, whereas the heat from reaction is the dominant factor. With decreasing screw speed, the heat loss at barrel surface drops, and the reaction would be accelerated. On the other hand, when the system has a high viscosity (say, when the inlet conversion ratio is 0.6), the viscous dissipation

plays an important role in the energy generation, which drops at low screw speed. Accordingly, the reaction is slow at low screw speed. When the reaction heat is low, the effect of screw speed on polymerization becomes small, especially for the system with low viscosity.

The comparisons of simulation results, based on 1-D model, and those based 3-D model, show that the reaction progress based on 3-D model at low screw speed (i.e. 48 rpm) is similar to that based on the 1-D model, however, the difference is quite significant at high screw speed (say, 287 rpm). This can be attributed to the fact that at high screw speed, the back-mixing and heat transfer at the barrel surface are very complex, factors not considered in the 1-D model. On the other hand, it is found that the value of heat from reaction is an important factor to the polymerization. The difference in simulation results between 1-D model and 3-D model becomes small when the value of heat from reaction decreases.

The polymerization would be fast when the size of the extruder is enlarged. This can be explained by that the heat transfer through the barrel surface is poor in large machines; temperature is very high in some regions, where the polymerization is accelerated. The 1-D model fails to predict the polymerization in the large machine because, unlike the 3-D model, it assumes that the temperature is uniform at the axial cross sections. The 3-D model is a valuable tool in optimizing the reactive extrusion in large extruders.

CHAPTER 6

PARAMETRIC STUDY OF POLYMERIZATION OF ε-CAPROLACTONE IN KNEADING BLOCKS

The kneading block is a mixing element in co-rotating twin-screw extruders, which offers not only excellent distributive mixing, but also good dispersive mixing, as described in Chapter 1. Unlike the conveying elements having a continuous flight, kneading blocks are configured with individual profile discs to form a geometrically discontinuous unit. The intensities of distributive mixing and dispersive mixing in kneading blocks depend on not only the individual disc width and stagger angle, but the feeding rate and screw rotational speed as well.

In this chapter, numerical simulation results based on a 3-D model of polymerization of ε-caprolactone in different kneading blocks are presented, and are compared with those in the conveying elements. The kneading blocks can be forward, reversed, or neutral, as shown in Figure 6.1, and Table 6.1. They are built with 16 pieces of kneading discs. The dimension of kneading blocks used in the simulation is listed in Table 6.2. When the diameter of kneading blocks is scaled up, i.e. from 34 mm to 68 mm, the disc width is doubled, but the stagger angle remains constant.

Similar to the treatment of the conveying elements, and described in Chapter 5, an extensional disc with a length of 20 mm is added at the end of the kneading block, in order to ensure that the iteration easily reaches convergence during the simulation. The boundary conditions for the simulation are listed in Table 6.3, in which the effects of screw rotational speed, initial conversion ratio at the inlet, and temperature on polymerization in kneading blocks are studied. The barrel surface is assumed to maintain

constant temperature during the reaction. The conversion ratios at the wall surfaces and the exit of the simulation domain are assumed to have a zero gradient, and the flow is fully developed at the exit. The 3-D mesh of the kneading blocks used in FLUENT is generated with 403,200 8-node, brick elements. For instance, Figure 6.2 shows the mesh of KB30. In the simulation, the reversed kneading blocks have the same mesh as the forward ones, but they rotate in a direction opposite to that of the forward elements.

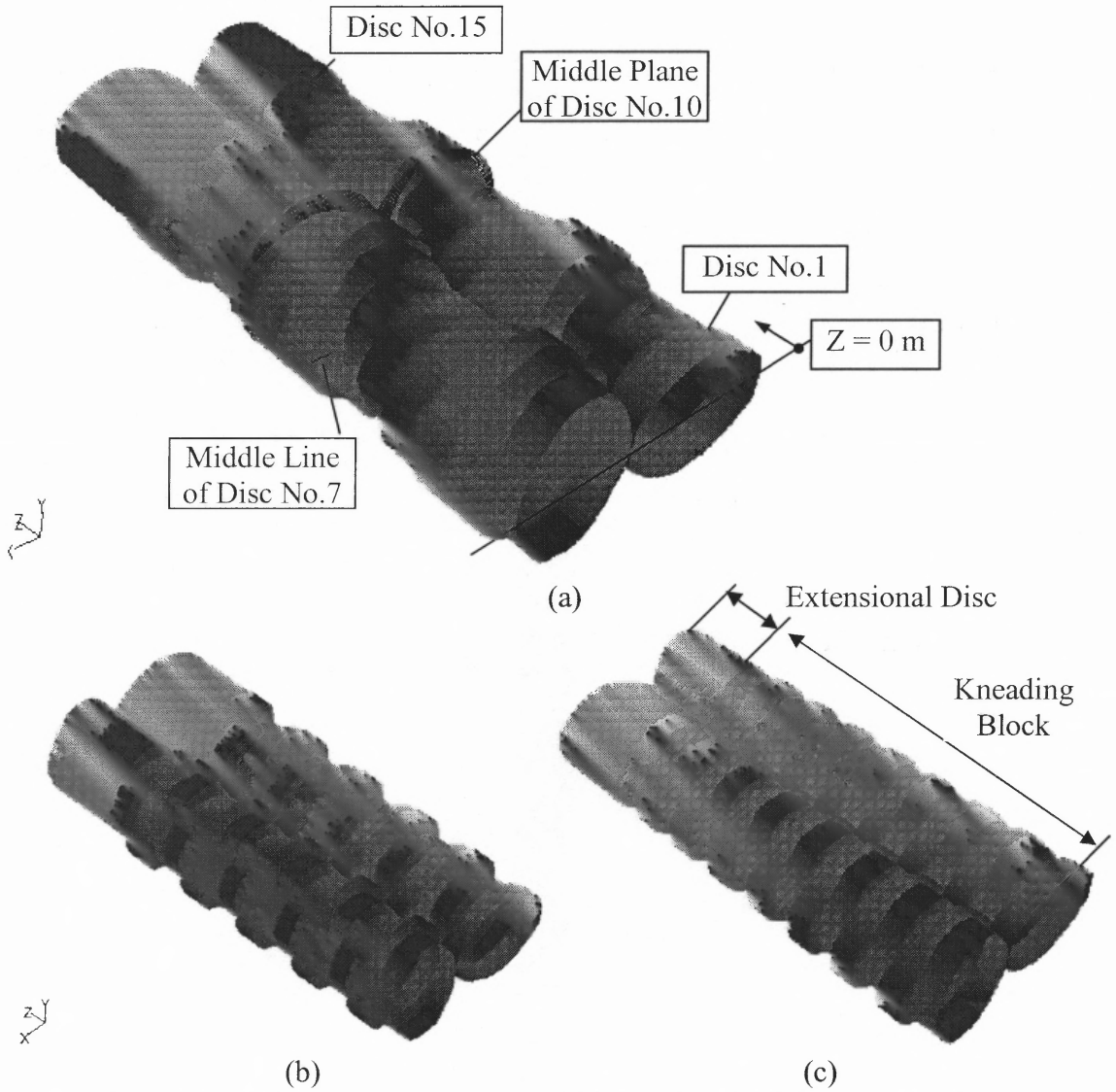

Figure 6.1 Kneading block configurations of (a) KB30, (b) KB60 and (c) KB90.

Table 6.1 Kneading Block Configurations

KB30F, KB60F, KB30R, KB60R, KB90	Kneading block configured by 16 pieces of kneading discs, each having a thickness of 7.5 mm (at D = 34 mm) or 15 mm (at D = 68 mm), with stagger angle 30°, 60° and 90°, respectively.

Table 6.2 Dimension of Kneading Blocks

	System No. 1	System No. 2
Barrel diameter (mm)	34.0	68.0
Screw tip diameter (mm)	33.4	66.8
Centerline distance (mm)	30.0	60.0
Screw root diameter (mm)	26.0	52.0
Screw tip number	2	2
Number of kneading discs	16	16
Kneading disc width (mm)	7.5	15

Table 6.3 Boundary Conditions for Simulation

$[M]/[I]_o$	800	800	800	800	800
Screw Diameter	34 mm	34 mm	34 mm	34 mm	68 mm
Flow Rate	3.15 kg/hr	3.15 kg/hr	3.15 kg/hr	3.15 kg/hr	25.2 kg/hr
Screw Speed	287 rpm	48 rpm	287 rpm	48 rpm	287 rpm
Barrel Temperature	410 K	410 K	420 K	420 K	420 K
Entrance Temperature	410 K	410 K	420 K	420 K	420 K
Initial Conversion Ratio	0	0	0.6	0.6	0.6
Screw Temperature	Adiabatic heat transfer condition				

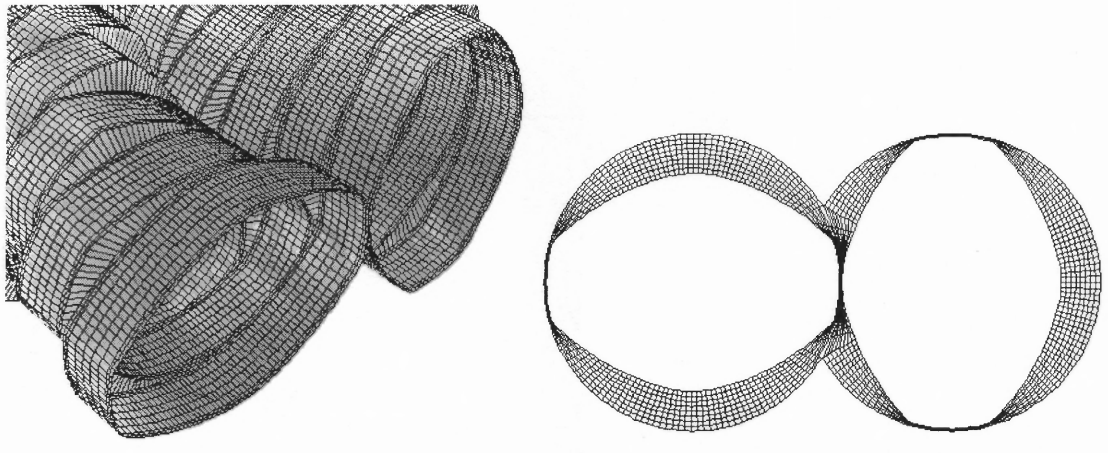

(a) (b)

Figure 6.2 Mesh for (a) kneading block surfaces and (b) axial cross sections.

6.1 Simulation Results for Polymerization in Kneading Blocks with 3-D Model

6.1.1 Polymerization at $[M]/[I]_o = 800$, T = 410 K, $C_o = 0$, and D = 34 mm

Figure 6.3 shows the top view of conversion ratio distributions at kneading block surfaces, in which the reaction system is conveyed from left to right. It is seen that the transition trend of conversion ratio from low to high value (from blue to red, in color) varies in different kneading blocks. In the regions near the inlet, KB90 has a slow increase in conversion ratio than KB30F. However, in the region close to the outlet, the conversion ratio is higher in KB90 than in KB30F.

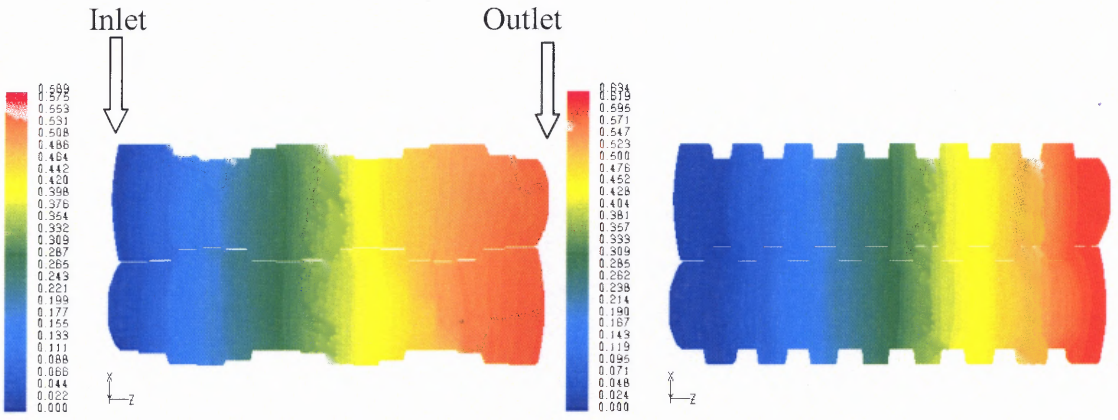

Figure 6.3 Top view of conversion ratio profiles at kneading block surfaces of (a) KB30F and (b) KB90 at $[M]/[I]_o = 800$ and N = 287 rpm.

The conversion ratio profiles at the middle plane of kneading disc No.10 in KB30F (see Figure 6.1a) and KB90 at 287 rpm are shown in Figure 6.4. The axial coordinate of the middle planes of kneading disks are listed in Table 6.4. Figure 6.4 shows that the distribution of conversion ratio is not uniform at the axial cross sections. In KB30F, the conversion ratio is higher in the middle of the channel than other regions, whereas in KB90, the high conversion is located near the barrel surface.

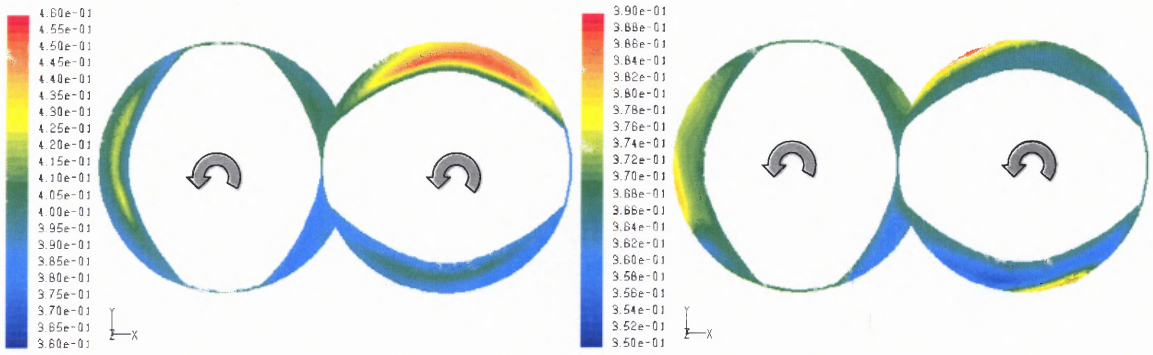

(a) (b)

Figure 6.4 Conversion profiles at middle plane of kneading disc No.10 (Z = 0.07125m) at $[M]/[I]_o = 800$ and N = 287 rpm in (a) KB30F and (b) KB90.

Table 6.4 Axial Location of Middle Plane of Kneading Discs with D = 34 mm

Kneading Disc No.	1	2	3	4	5	6	7	8
Location of middle plane (mm)	3.75	11.25	18.75	26.25	33.75	41.25	48.75	56.25
Kneading Disc No.	9	10	11	12	13	14	15	16
Location of middle plane (mm)	63.75	71.25	78.75	86.25	93.75	101.25	108.75	116.25

As discussed in Chapter 5, the distribution of conversion ratio at the axial cross section of screw elements can be characterized with the area weighted function of conversion ratio (Equation 5.1). Figure 6.5 shows the calculated area-weighted distributions of conversion ratio at the middle plane of kneading discs No.7, No.10 and No.14 in both KB30F and KB90. It is found that the distribution of conversion ratio is broader in KB30F than in KB90. Furthermore, in the axial cross sections with Z = 0.04875 m and Z = 0.07125 m, the averaged conversion ratio in KB30F is higher than that in KB90.

The broader distribution of conversion ratio in KB30F can be interpreted with the flow mechanism of the reaction system in kneading blocks. Figure 6.6 shows the positive axial velocity profiles at the middle plane of kneading disc No.10 in KB30F and KB90, in which the negative (upstream) velocity contour is not displayed in order to increase the

clarity of plots. The contour plots in Figure 6.6 reveal that the maximum positive axial velocity in KB30F is much higher than in KB90, which suggests that the residence time distribution in the former should be broader than in the latter. This indicates that the distribution of conversion ratio may be correlated to the residence time distribution.

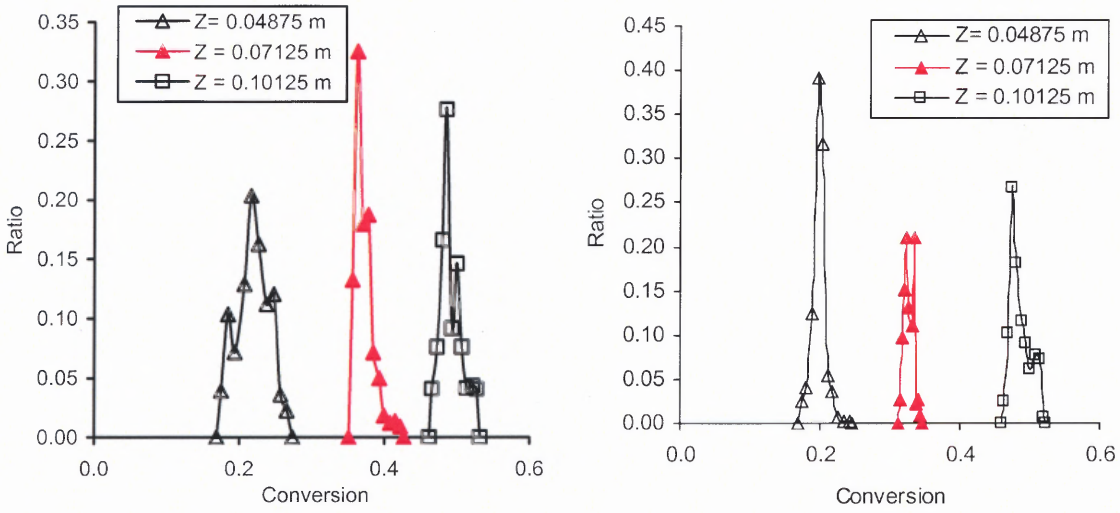

(a) (b)

Figure 6.5 Area weighted distribution of conversion ratio at middle planes of kneading disc No. 7, No. 10 and No. 14 at $[M]/[I]_o$ = 800 and N = 287 rpm in (a) KB30F and (b) KB90.

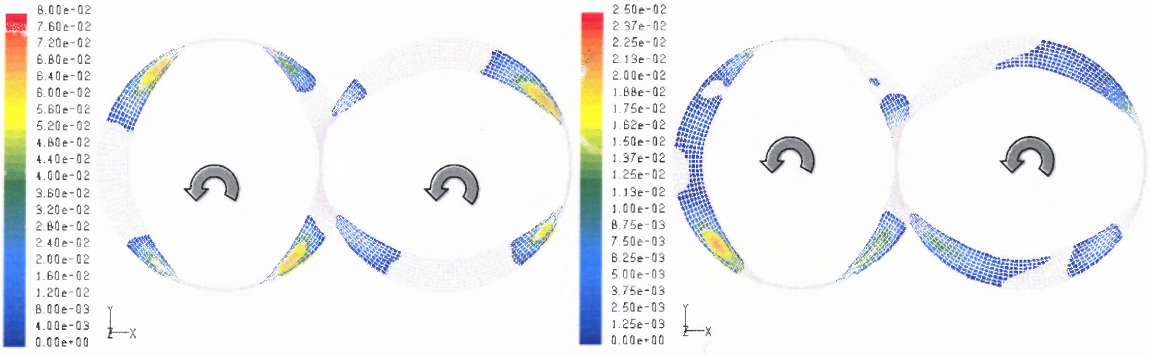

(a) (b)

Figure 6.6 Axial velocity profiles in middle plane of kneading disc No.10 at $[M]/[I]_o$ = 800 and N = 287 rpm in (a) KB30F and (b) KB90.

Figure 6.6 also shows that KB30F has a much smaller fraction of the cross sectional area with positive (i.e. downstream) velocity than KB90. Moreover, the regions with upstream velocity (i.e. the areas hatched with grid, but not filled with colors in Figure 6.6) are located in the areas with high conversion ratio (see Figure 6.4). This implies that the back-flux carries fluid elements with high conversion ratio upstream, leading to a rapid increase in conversion ratio in the upstream. This mechanism is similar to that in the conveying elements, as discussed in the preceding chapter.

Figure 6.7 summarizes the increase in conversion ratio along the axial length in kneading blocks with different configurations at 48 rpm, and 287 rpm. These curves show that the conversion ratio at 48 rpm has a faster increase than that at 287 rpm, which is consistent with the simulation results in the conveying elements (see Figure 5.16a). This confirms that the reaction relies not only on the mixing mechanisms, but also on the heat transfer and heat generation of the reaction system. Because the heat loss through the barrel surface drops with decreasing screw speed, the reaction system has a high temperature and a fast increase in conversion ratio at low screw speed.

Figure 6.7 reveals that the conversion ratio in KB30F is higher than that in KB60F. This can be interpreted in terms of the values of flux-mixing coefficient (see Equation 5.3). As shown in Figure 6.8, the flux-mixing coefficient is larger in KB30F than in KB60F. On the other hand, Figure 6.7 also shows that at 287 rpm, the trends of conversion ratio along the axial length in KB90 are different from those in KB30F and KB60F: in regions near the inlet, KB90 has the lowest conversion ratio, but it has a fast increase in the middle of the axial length. However, the flux-mixing coefficients in KB90 are much lower than those in KB30F and KB60F, as shown in Figure 6.8. This is

explained by the fact that the polymerization in kneading blocks is dominated not only by the back-flow ratio, but the heat transfer and mixing mechanisms as well.

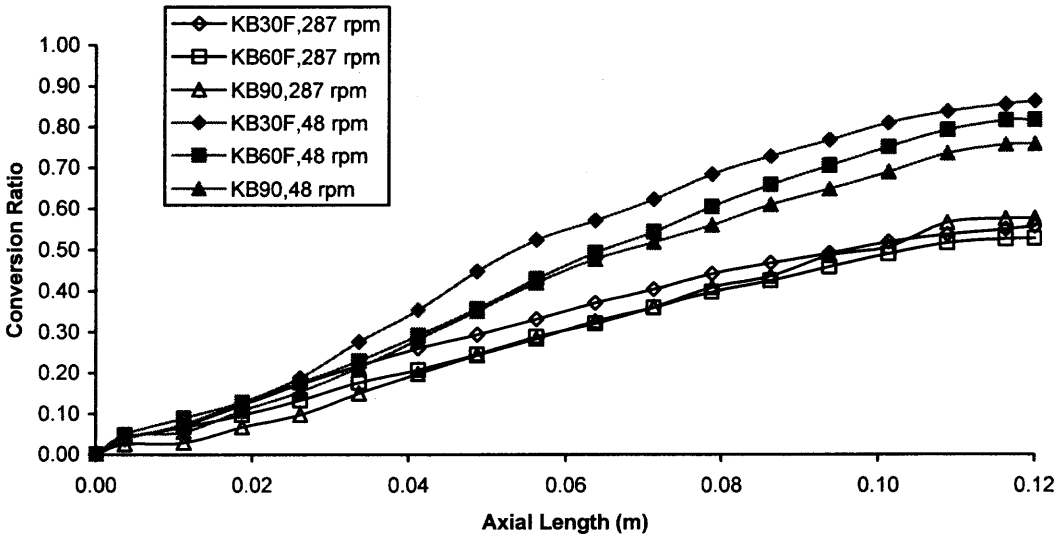

Figure 6.7 Average conversion ratios along the axial length in kneading blocks at 287 rpm and 48 rpm.

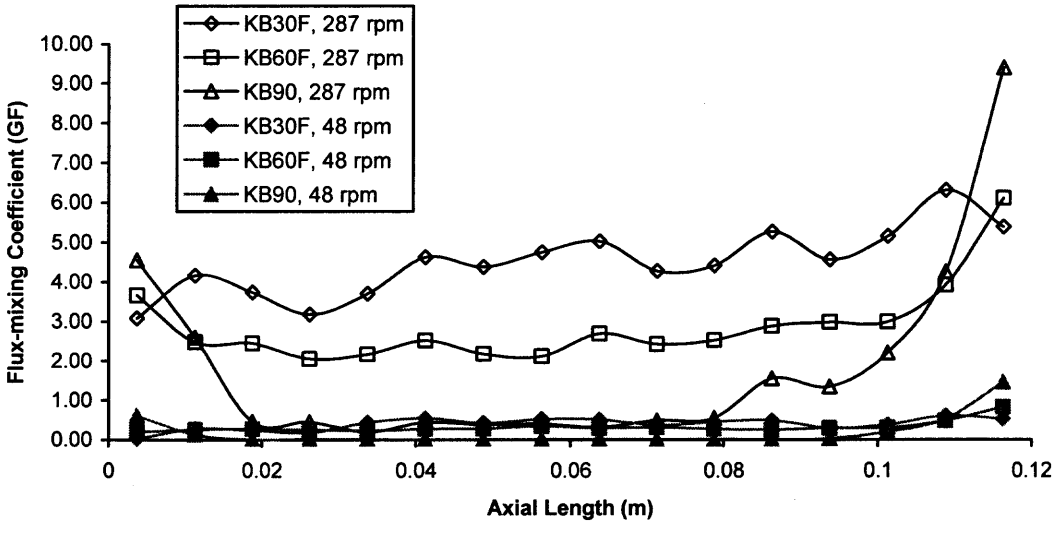

Figure 6.8 Flux-mixing coefficients in kneading blocks at 287 rpm and 48 rpm.

In order to elucidate the mechanisms of heat transfer at barrel surface and mixing in KB30F and KB90, the tangential velocity profile, and the temperature at the line with

Y = 0 m in the middle plane of Z = 0.04875 m (denoted as mid-line in disc No.7 in Figure 6.1a) at 287 rpm are plotted in Figure 6.9. As shown in Figure 6.9a, the tangential velocity could be positive or negative in KB30F. This indicates that in the axial cross section, some fluid elements move in the same direction as the screw rotation; the others move in the opposite direction to the screw rotation. However, in the cross section of KB90, all of the fluid elements travel in the same direction as the screw rotation. Consequently, more intensive transverse mixing occurs in KB30F than KB90. Moreover, Figure 6.9a shows that the velocity gradient near the barrel surface is larger in KB30F than KB90. This implies that the convection of fluid elements near the barrel surface is more intensive in the former than the latter, which would result in a larger heat loss through the barrel in KB30F.

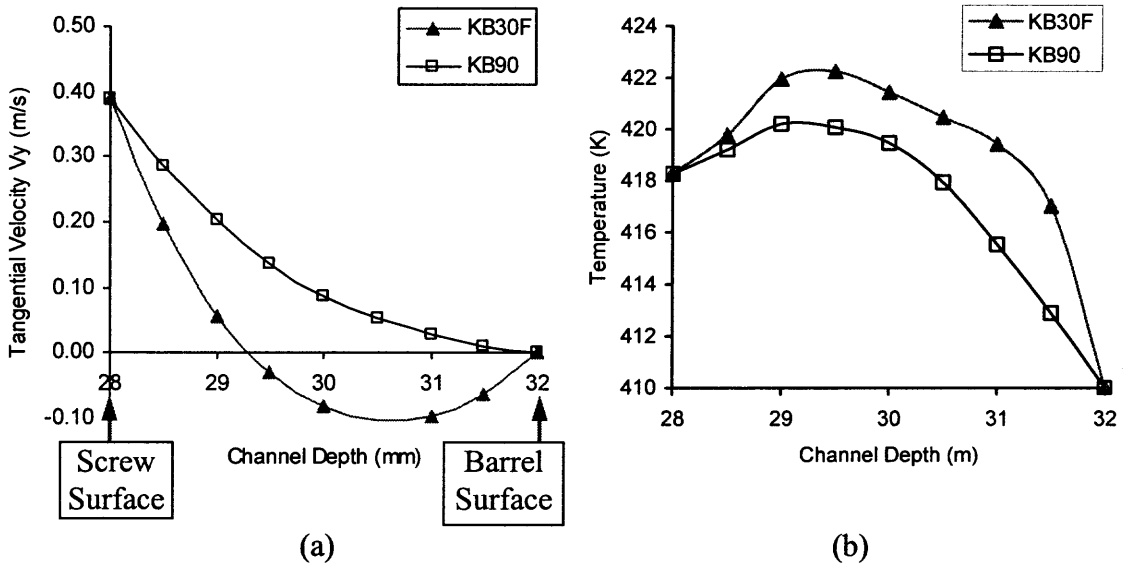

Figure 6.9 (a) Tangential velocity and (b) temperature profiles in KB30F and KB90 at line with Y = 0 m in the axial cross section with Z = 0.04875 m.

Figure 6.9b shows that the temperature in KB30F is higher than that in KB90. This is attributable to the larger heat from reaction at Z = 0.04875 m in the former than in

the latter (i.e. higher conversion ratio in KB30F, as shown in Figure 6.5). However, the temperature gradient near the barrel surface in KB30F is much larger than that in KB90, leading to a more pronounced heat loss through the barrel. As a consequence, the large increase of conversion ratio in the middle of the axial length in KB90 at 287 rpm, as shown in Figure 6.7, could be explained by the poor heat transfer near the barrel surface, although its axial and transverse mixing intensities are lower than those in KB30F.

On the other hand, Figure 6.7 shows that the large increase in conversion in KB90 at 287 rpm does not occur at 48 rpm. The possible reason is as follows. At 48 rpm, both the heat loss at the barrel surface, and the mixing intensity of fluid, are very weak. As discussed in the preceding paragraph, KB90 has poorer heat loss through the barrel than KB30F. Meanwhile, Figure 6.8 shows that the flux-mixing coefficient is the largest in KB30F, and the lowest in KB90. That is, compared with KB90, KB30F has much pronounced mixing intensity and heat loss. The former favors reaction, but the latter hinders it. At current simulation conditions, the competition between mixing intensity and heat loss lead to a faster polymerization progression in KB30F than in KB90. Furthermore, most of the heat from reaction is retained in the reaction system because of the poor heat loss through the barrel. In KB30F, the large heat from reaction could further accelerate the polymerization progression.

The trends in conversion ratio along the axial length in both forward and reversed kneading blocks are demonstrated in Figure 6.10. These plots show that the effect of the helical angle, forward or reversed, of kneading blocks upon the polymerization is not very significant. At 287 rpm, the conversion ratio has a slightly faster increase in the reversed elements than in the forward elements. At 48 rpm, globally, the reversed

elements have slightly slower increase in conversion ratio than the forward ones. The possible explanations for these trends are discussed in the next section (see Figure 6.13a).

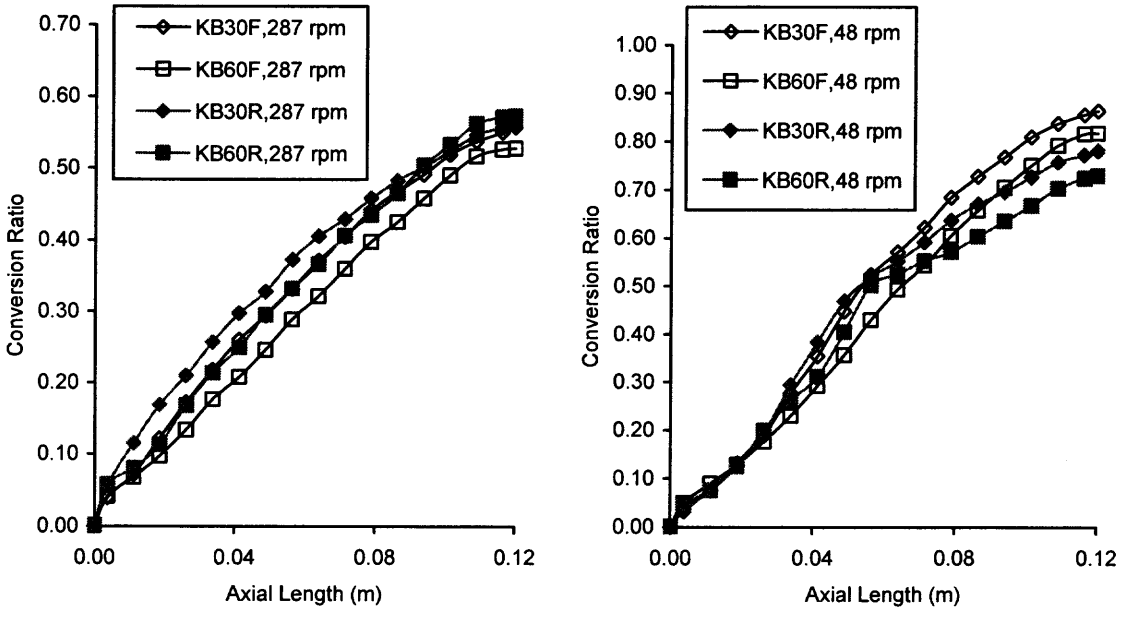

(a) (b)

Figure 6.10 Comparison of conversion ratio profiles in forward and reversed kneading blocks at (a) 287 rpm and (b) 48 rpm.

6.1.2 Polymerization at $[M]/[I]_0 = 800$, $T = 420$ K, $C_0 = 0.6$, and $D = 34$ mm

Figure 6.11 shows the increase of conversion ratio along the axial length in different kneading blocks at an inlet conversion ratio of 0.6, and T = 420 K. It is seen that the conversion ratio drops with decreasing screw rotational speed, which is similar to that in conveying elements (see Figure 5.17a). Furthermore, Figure 6.11 shows that at 287 rpm, the conversion ratio in KB90 has a rapid rise in the middle of the axial length; however, such a rapid rise does not occur in KB90 at 48 rpm. These phenomena are similar to those presented in Figure 6.7. Here, the rapid increase in conversion ratio in KB90 at 287 rpm is attributable to the large viscous dissipation at high screw speed.

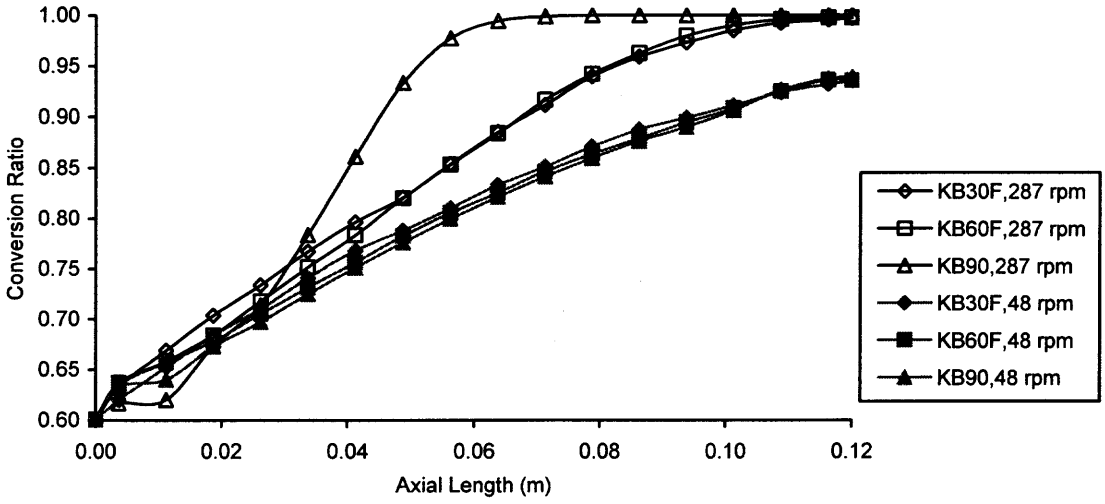

Figure 6.11 Conversion ratios along axial length in kneading blocks at $[M]/[I]_o = 800$, T = 420 K and $C_o = 0.6$.

Figure 6.12 demonstrates the trends of conversion ratio along the axial length in both forward and reversed kneading blocks at 287 rpm, and 48 rpm. At 287 rpm, the conversion ratio has a much faster increase in the reversed kneading blocks than in the forward ones, whereas at 48 rpm, the difference in conversion ratio between the forward and reversed kneading blocks is negligible.

Figure 6.13b illustrates the distributions of conversion ratio in both reversed and forward kneading blocks. At 287 rpm, the reversed kneading block has a broader distribution than the forward one, whereas the distribution at 48 rpm has similar magnitudes in both cases. This can be attributable to the different velocity profiles, which represents the conveying and mixing mechanisms, in the forward and reversed kneading blocks. As displayed in Figure 6.13a, the axial velocity profiles are broader at higher screw speed. At 48 rpm, the velocity profile in the forward kneading block has almost the same shape as that in the reversed one. However, at 287 rpm, the difference in velocity profiles between the forward and reversed elements is significant. The variation in

velocity profiles changes the residence time distribution and mixing mechanism of the reaction system in kneading blocks, and further alters the temperature profiles and conversion ratio distributions.

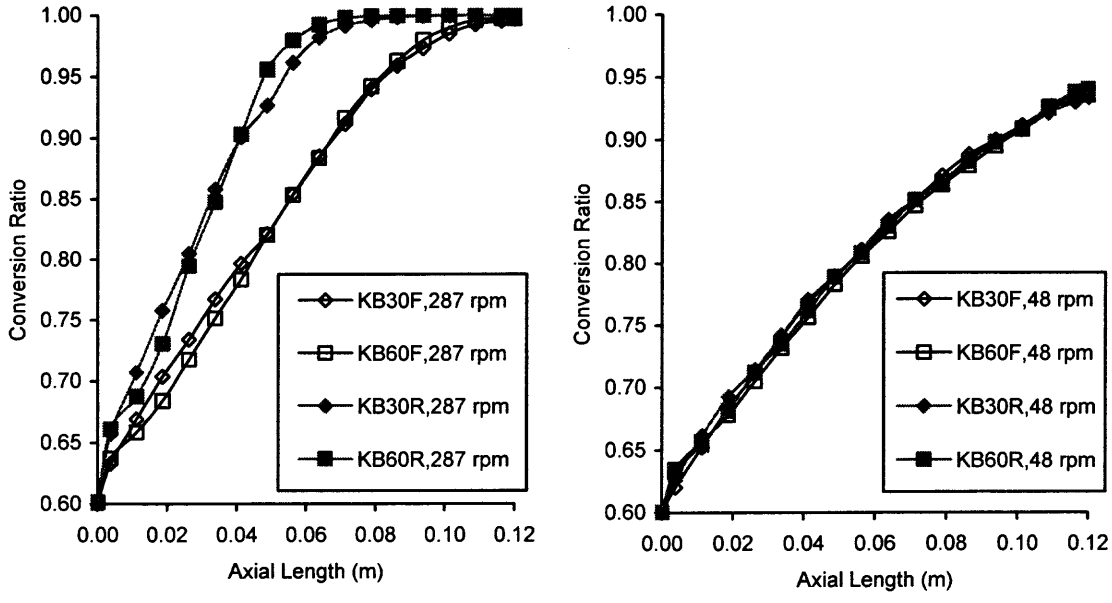

(a) (b)

Figure 6.12 Effect of helical direction of kneading blocks on conversion ratio profiles along the axial length at (a) 287 rpm and (b) 48 rpm.

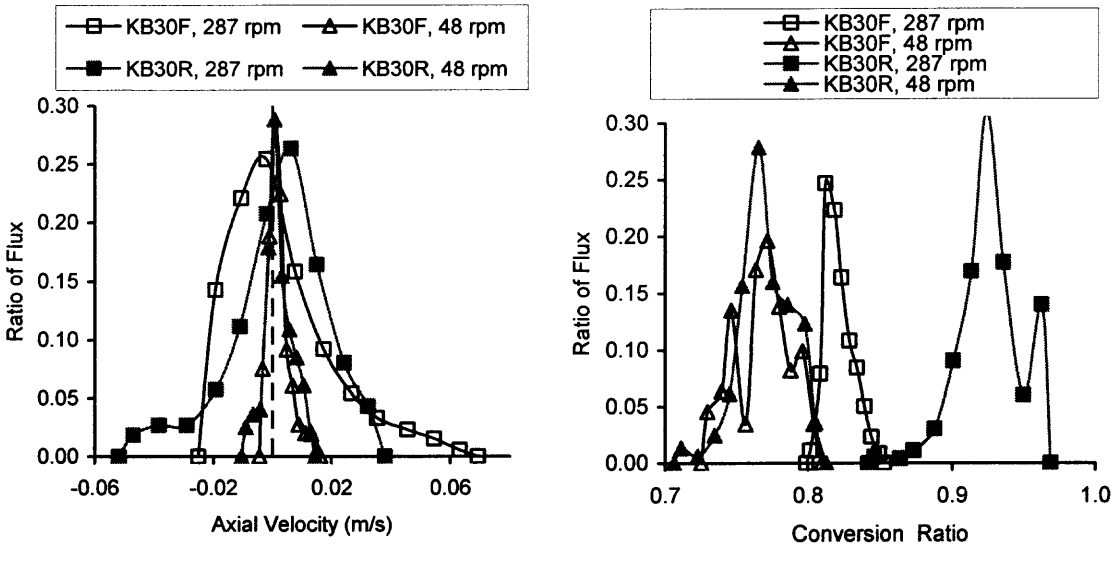

(a) (b)

Figure 6.13 Distributions of (a) axial velocity and (b) conversion ratio at the middle plane of disc No.9 in forward and reversed kneading blocks.

6.1.3 Scale-up Polymerization at $[M]/[I]_0 = 800$, T = 420 K, $C_0 = 0.6$ in Kneading Blocks

Figure 6.14 summarizes the increase of conversion ratio along the axial length with screw diameter of 34 mm and 68 mm, respectively. Figure 6.14 shows that the conversion ratio increases faster with increasing screw diameter. This is due to the fact that the heat loss at barrel surface is weaker and the non-uniformity of temperature in the screw channel becomes more pronounced at D = 68 mm than D = 34 mm, as discussed in the preceding chapter (see section 5.1.5). Furthermore, at D = 68 mm, the effect of kneading block configurations on polymerization progression is smaller than that at D = 34 mm. This suggests that at D = 68 mm, the heat loss at barrel surface and the temperature non-uniformity play more important roles than the kneading block configurations.

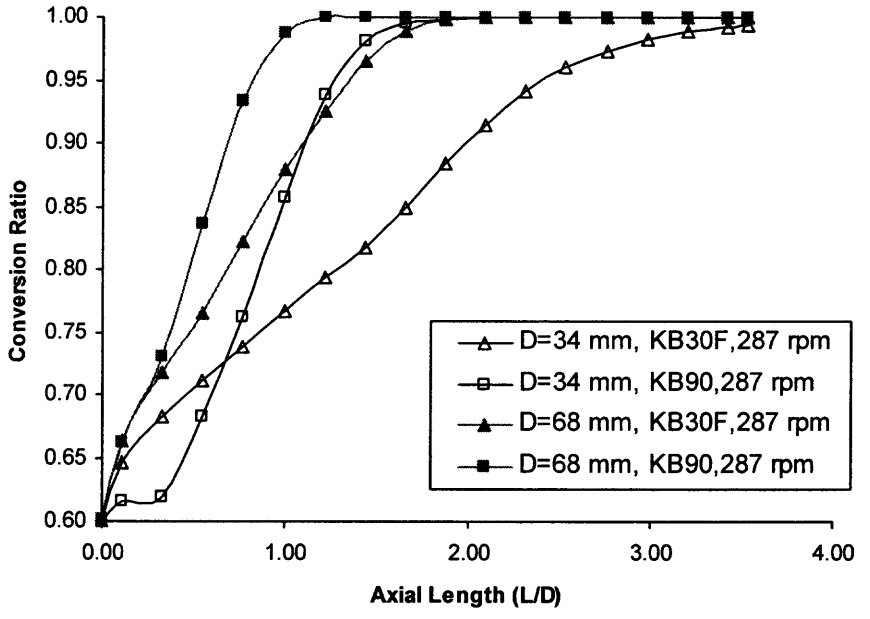

Figure 6.14 Average conversion ratio profiles at 287 rpm with screw diameters of 34 mm and 68 mm.

6.2 Comparison of Polymerization in Conveying Elements and Kneading Blocks

Figure 6.15 demonstrates the comparison of conversion ratio profiles in kneading blocks and conveying elements at T = 410 K and D = 34 mm. At 287 rpm, the conversion ratio is higher in the kneading blocks than the conveying elements, but this trend is reversed at 48 rpm. The possible explanation is as follows. As discussed in the preceding chapters, the reaction progression depends on the competing result among the heat from reaction, viscous heating and heat loss through the barrel. Because the conversion at the channel inlet is zero, viscous heating is not an important energy source to reaction. Meanwhile, both the heat loss through the barrel and the heat from reaction enhance with increasing mixing intensity of fluid in screw elements, which further relies on the geometry of the screw element and operational conditions. Accordingly, the competition between the heat generation and heat loss in kneading blocks could lead to different results, compared with that in conveying elements, even at an identical screw rotational speed. Thus, the effect of screw geometry, i.e. conveying elements or kneading blocks, on the trends of conversion ratio along axial length could diverge at different screw rotational speeds.

On the other hand, when the inlet conversion ratio is 0.6, as shown in Figure 6.16, the screw element geometry has a very little effect on the conversion ratio profiles at 48 rpm. At 287 rpm, the conversion ratio increase in conveying elements is faster than that in the forward kneading blocks, but are lower than that in the neutral kneading block (i.e., with a stagger angle of 90°). There are two possible reasons for this phenomenon. First, the velocity gradient in fluid near the barrel surface is smaller in the conveying elements than the kneading blocks, as displayed in Figures 5.10b and 6.9a, which causes a larger heat loss in the latter. Secondly, as shown in Figure 6.17, the shear rates in conveying

elements are higher than those in kneading blocks at identical screw speed. This indicates that viscous dissipation in kneading blocks could be lower than that in conveying elements, although the former have more intensive mixing capacity. In the current case, viscous dissipation is a critical energy source in reaction. Consequently, the competition between viscous dissipation and heat loss at the barrel surface makes the reaction in the forward kneading blocks slightly slower than that in the conveying elements at 287 rpm. The large increase in conversion ratio in the neutral kneading block (KB90) at 287 rpm is due to the small heat loss at the barrel surface, as presented in Figure 6.9a.

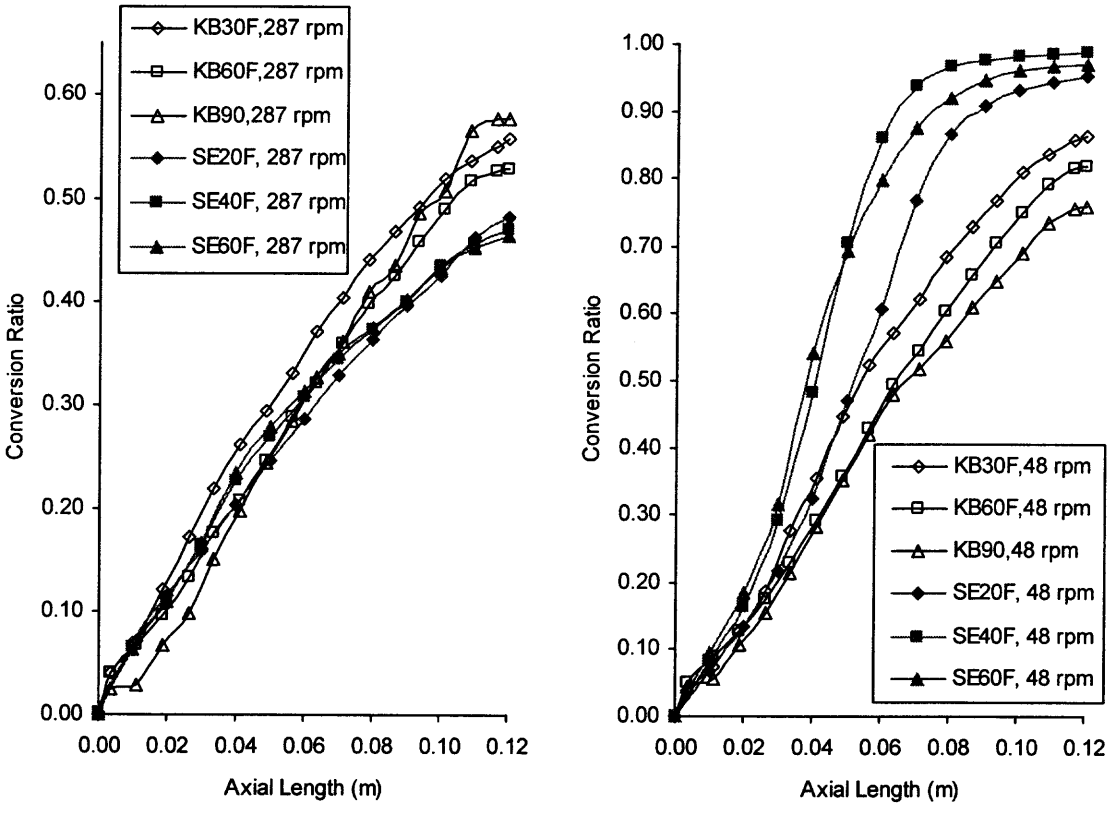

(a) (b)

Figure 6.15 Comparison between conversion ratio profiles in kneading blocks and screw elements at T = 410 K and D = 34 mm with (a) 287 rpm and (b) 48 rpm.

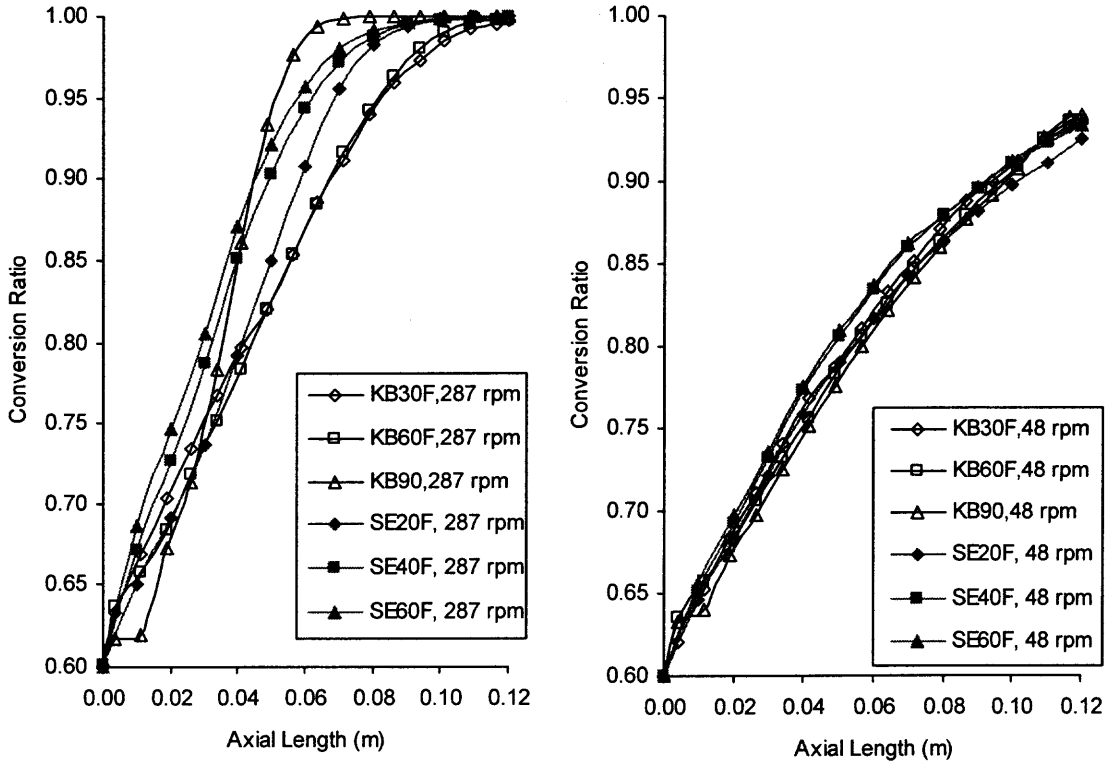

(a) (b)

Figure 6.16 Comparison between conversion ratio profiles in kneading blocks and screw elements at T = 420 K and D = 34 mm with (a) 287 rpm and (b) 48 rpm.

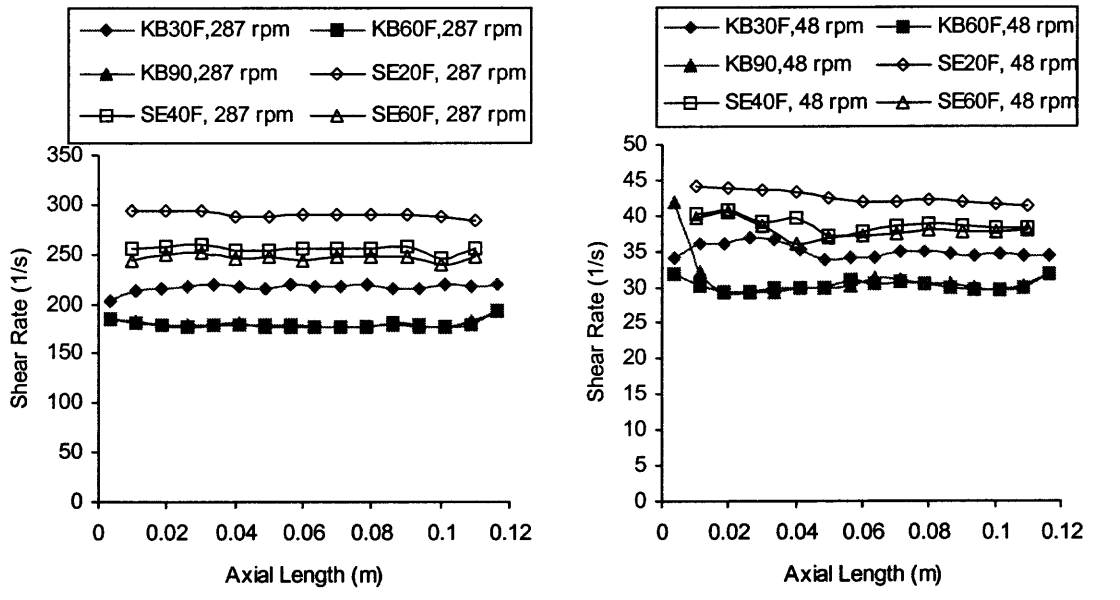

(a) (b)

Figure 6.17 Comparison between shear rates in kneading blocks and screw elements at T = 420 K and D = 34 mm with (a) 287 rpm and (b) 48 rpm.

Figure 6.18 shows the effect of geometry of screw elements on polymerization with a screw diameter of 68 mm, at 287 rpm, when the inlet conversion is 0.6. This plot indicates that SE120F has a much higher conversion ratio than KB30F and KB90, whereas the conversion in SE40F is larger than that in KB30F, but lower than that in KB90. Compared with a screw diameter of 34 mm (as shown in Figure 6.16a), the effect of element geometry on polymerization is less significant at large screw diameters, because the heat loss at the barrel surface is so low that the non-uniformity of temperature in the screw elements might be more important than the back-mixing.

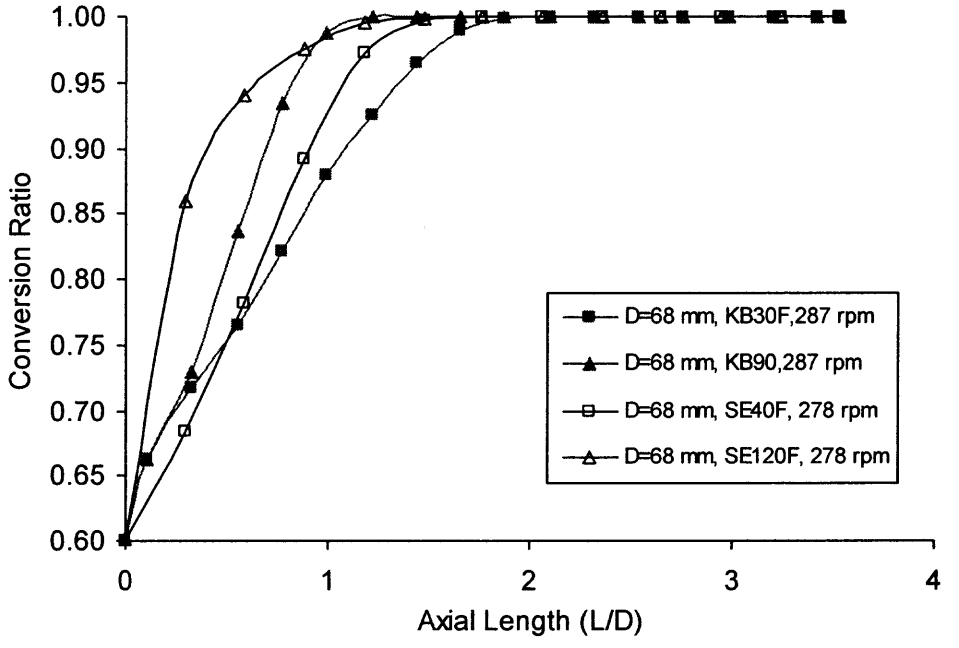

Figure 6.18 Comparison of conversion ratios in kneading blocks and conveying elements at T = 420 K and D = 68 mm.

6.3 Conclusions

In this chapter, the polymerization of ε-caprolactone in various kneading blocks was simulated with a 3-D model, and compared with those in conveying elements. Similar to the conclusions on the studies of reactions in the conveying elements, discussed in the preceding chapter, it has been found that the polymerization progression in kneading blocks not only depends on the mixing mechanisms, but also on both the heat generation in the reaction system and the heat loss at barrel surface.

The trends of conversion ratio in the neutral kneading blocks (KB90) would be different from those of forward and reversed kneading blocks, due to the low heat loss at barrel surfaces. Generally, the conversion ratio in KB90 has a faster increase than those in the forward kneading blocks, especially at high screw speed. The conversion ratio in the reversed kneading blocks may either have a faster, or a slower increase than those in the forward kneading blocks, depending on the conditions of reaction. The effect of screw element geometry, i.e. kneading blocks and conveying elements, on polymerization progression could be significant, relying on the conversion ratio at the let or screw rotational speed.

After scaling up diameter of the kneading blocks, the polymerization becomes faster. Furthermore, the difference in conversion ratio in kneading blocks and conveying elements is less pronounced with increasing diameter. This is attributable to the low heat loss at the barrel surface and the pronounced non-uniformity of temperature in the screw channel.

CHAPTER 7

GLOBAL MODELING AND SCALING UP POLYMERIZATION IN TWIN-SCREW EXTRUSION

When an extruder is used as a polymerization reactor, generally, liquid monomers are fed into the feeding zone, instead of resins in granules or pellets. As mentioned in Chapter 3, the screw channel in a twin-screw extruder is either partially-filled or fully-filled. In the previous two chapters, polymerization of ε-caprolactone in fully-filled conveying elements and kneading blocks was simulated with a 3-D model. In the present chapter, the simulation method for a partially-filled channel is first discussed, followed by the global simulation of polymerization in a twin-screw extruder. The simulated results are then compared with experimental data. Finally, the scaled up polymerization in twin screw extruders is discussed.

7.1 Polymerization in Partially-Filled Channels

According to Janssen (79), twin-screw extruders can be divided into two types: (1) those with positive conveying as the main transportation mechanism, such as in counter-rotating intermeshing twin-screw extruders, and (2) those with drag flow as the main transportation mechanism, such as in co-rotating twin-screw extruders. When the screw channel is partially-filled, the degree of fill, ε, is defined as:

$$\varepsilon = \frac{Q}{Q_{max}} \tag{7.1}$$

where Q is the volumetric flow rate, and Q_{max} is the maximum conveying capacity of the screw element. Accordingly, the residence time for materials in the partially-filled region is given as:

$$t_p = \varepsilon \cdot t_f \tag{7.2}$$

$$t_f = \frac{L}{\bar{V}} = \frac{L}{(Q_{pr}/A)} = \frac{L \cdot A}{Q_{pr}} = \frac{Q_{ch}}{Q_{pr}} \tag{7.3}$$

where t_p and t_f represent the residence time when the channel is partially- and fully-filled, respectively. Q_{ch} is the volume of the screw channel, and Q_{pr} the volumetric flow rate per revolution.

The distribution of fluid in the partially-filled screw channel has two possibilities: materials either remain at the bottom of channels or are dragged up by the pushing flight, depending on the relationship between gravitational force and viscous force. The gravitational force can be evaluated by the Froude number, F_r, and the viscous effect by Reynolds number, R_e:

$$F_r = \frac{\bar{V}^2}{gH_{ch}} \tag{7.4}$$

$$R_e = \frac{\rho \bar{V} H_{ch}}{\eta} \tag{7.5}$$

in which $\bar{V}$ is the average velocity of material in the screw channel; H_{ch} is the depth of the channel, and g the gravitational constant; η and ρ are the viscosity and density of the fluid, respectively. The ratio between these two dimensionless numbers is known as Jeffrey's number (80):

$$J_r = \frac{F_r}{R_e} \tag{7.6}$$

When J_r is larger than a certain value, the viscous force dominates the gravitational force. However, this is only true when the centrifugal force is neglected. When the extruder runs at high speed and the screw diameter is large, the centrifugal force could become a dominant force, which pushes the materials to leave the screw flight.

When the reaction system has low viscosity and is located at the bottom of barrels, the fluid elements are conveyed downstream by the positive displacement mechanism. Consequently, the maximum conveying capacity of the screw channel, Q_{max} in Eq. 7.1, is given as:

$$Q_{\max} = Q_{ch} \cdot N \tag{7.7}$$

where N is the screw rotational speed in revolution per second.

When the reaction system has sufficiently high viscosity, it will stay at the push side of the flight. Accordingly, the maximum conveying capacity of the screw elements is achieved with drag flow mechanism,

$$Q_{\max} = \frac{1}{2}(2n-1)A \cdot V_z \tag{7.8}$$

$$V_z = V_o \cos\varphi = \pi DN \cos\varphi \tag{7.9}$$

where n is the screw tip number, and A is the cross sectional area of a screw channel. V_z is the velocity along the screw channel, and φ the helical angle of the flight. Because the conveying capacity based on the positive displacement (Eq. 7.7) is much larger than that based on the drag flow mechanism (Eq. 7.8), the residence time of materials would be shorter when located at the bottom of barrels than those occupying the push side of the flight.

The simulation results in the previous two chapters indicate that in the fully-filled forward screw elements, both the back-flux and the heat transfer at barrel surfaces play important roles in determining the polymerization progress. It is known that in the partially-filled channel, the pressure gradient along the axial length is zero. This suggests that there is no axial mixing. However, transverse mixing still exists because of the pushing effect of the screw flights, although it is much weaker than that in the fully-filled case. In the current study, a drag flow model and a chamber model are proposed, respectively, to predict the polymerization progression in the partially-filled channel with materials attached to the flight (Figure 7.1), and with materials occupying the bottom of the barrel (Figure 7.2).

When the polymeric materials occupy part of the screw channel, some free surfaces are formed, as shown in Figures 7.1. The shape of the free surface is so complex that it is not easily predicted. In this study, the free surfaces are assumed to be straight planes, either vertically (Figure 7.1) or horizontally (Figure 7.2a).

The 3-D model for the partially-filled channel with materials attached to the screw flight is shown in Figure 7.1. Here, the curved screw channel is unwrapped into a plane. The barrel is fixed, and the screw channel is moving at a velocity of V_z, given by Eq. 7.9. The free surface is assumed to be parallel to the YZ plane. As a consequence, the cross sectional area filled with materials can be determined by the geometry of the conveying element, and the degree of fill. The length of the simulation domain, ΔL, is given by:

$$\Delta L = i \cdot L_z = (2n-1) L_z \tag{7.10}$$

$$L_z = \frac{\Delta Z}{\sin \varphi} \tag{7.11}$$

where ΔZ is the axial length of the partially-filled zone. Similar to what has been assumed in the simulation of the fully-filled screw elements, the barrel has a constant temperature and the screw has adiabatic conditions. The free surface is assumed to have symmetric conditions for velocity and adiabatic conditions for energy.

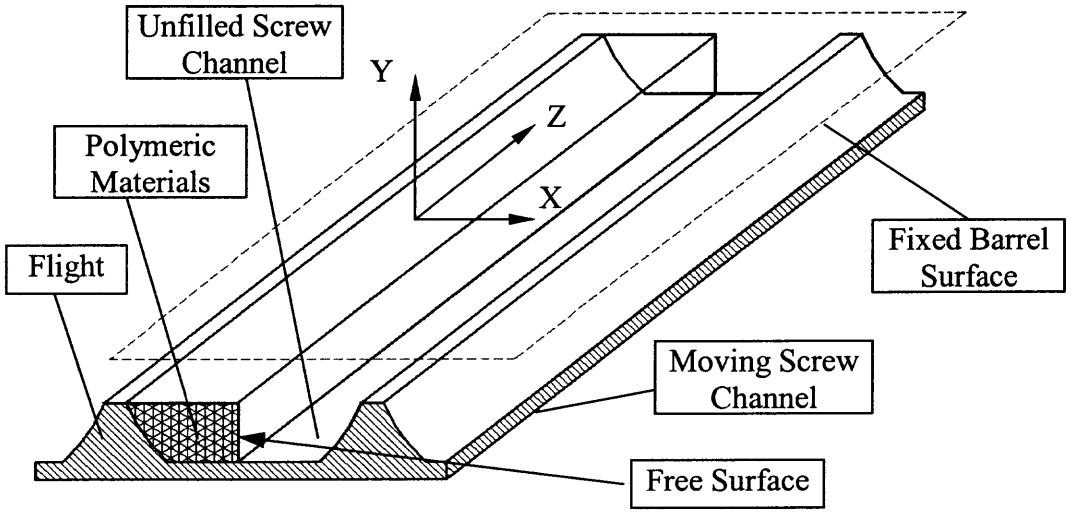

Figure 7.1 Models for partially-filled channels with materials located at pushing flight.

Considering the fact that materials in the screw channel are conveyed with the drag flow mechanism, the 3-D drag flow model presented in Figure 7.1 can be further simplified into a 2-D model. The application of a 2-D model in simulation of reactive extrusion is exposed in detail elsewhere (38-39). It should be noted here that in the 2-D modeling, the width of the channel and the velocity of the moving screw surface should be calculated based on the degree of fill, screw rotational speed, flow rate and geometry of the screw channel.

In the above discussions, the leaking flow in the gaps between the screws and barrels is not included. When leaking flow is taken into consideration, the degree of fill in

the screw channel and the residence time should rise. The leaking flow rate over the screw flight is given as (23):

$$V_L = 0.5 V_o \delta_s \pi D \sin\varphi \cos\varphi \tag{7.12}$$

where δ_s is the gap between the screw and the barrel. Hence, in calculating the degree of fill based on Eq.7.1, Q should be replaced by ($Q + V_L$),

$$\varepsilon = \frac{Q + V_L}{Q_{\max}} \tag{7.13}$$

The average residence time is also corrected to be:

$$t_p^* = t_p \left(1 + \frac{V_L}{V_f} \right) \tag{7.14}$$

where V_f is the volume of the flight. In the 3-D modeling, the correction of the residence time is achieved by adjusting the length of the simulation domain,

$$\Delta L^* = \Delta L \left(1 + \frac{V_L}{V_f} \right) \tag{7.15}$$

Figure 7.2 presents the 3-D chamber model when the materials stay at the bottom of the barrel. The reaction system in a chamber is conveyed forwardly with the positive displacement mechanism. For example, the reaction system initially located at chamber No.1 is conveyed to the location of chamber No.3 due to the screw rotation, as shown in Figure 7.2b. However, there is no exchange of materials between chambers if the leaking flow is neglected. Consequently, when the reaction system occupies the bottom of the barrel, the polymerization can be predicted with tracing the reaction progression in a chamber, i.e. the chamber model.

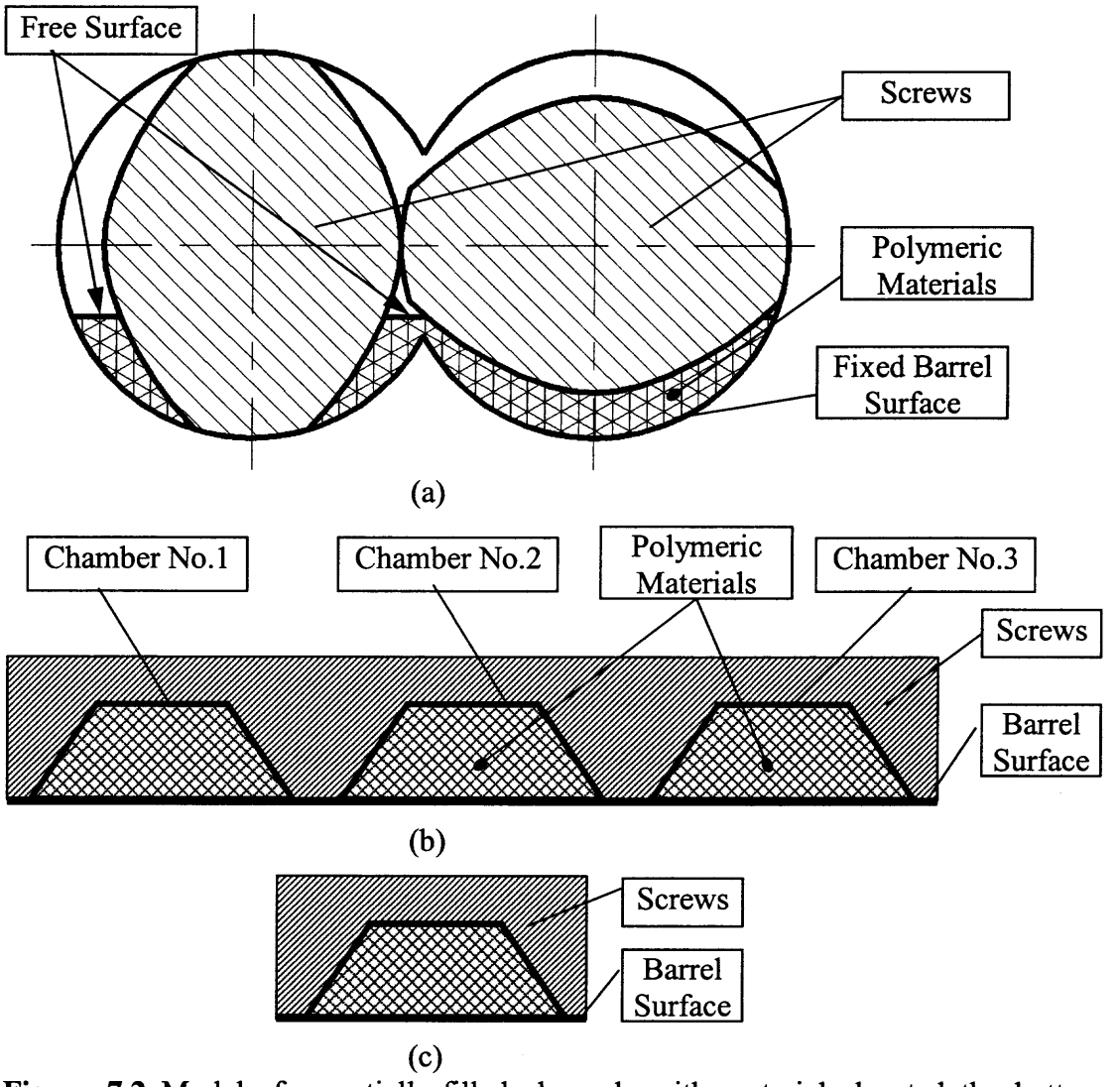

Figure 7.2 Models for partially-filled channels with materials located the bottom of barrel. (a) cross section view, (b) longitudinal view and (c) chamber model.

In the chamber model shown in Figure 7.2c, the temperature and reaction progression of the reaction system in the chamber are functions of time. Hence, the polymerization in a chamber can be calculated by tracing the flow, temperature profile and the degree of reaction at different time. Because the residence time of the reaction system, located at the bottom of barrel, is very short, the increase of temperature/conversion is small. Thus, the effect of simulation method may not have a significant on the simulation results. Consequently, it is feasible to use a simplified

model, such as 1-D model or 2-D model, to predict the reaction progression instead of the chamber model.

7.2 Global Simulation of Polymerization in Twin-screw Extruders

As discussed in Chapter 3, a reversed calculation procedure is used in the simulation of reaction in twin-screw extruders: the calculation starts from the die, and then goes to the upstream elements. Studies in the reactive extrusion with twin-screw extruders (25-32) show that the average residence time in the extruder does not change significantly due to the reaction. This indicates that the distribution of materials along the screw relies on operational conditions, such as feeding rate, screw speed and screw configuration, almost independent of viscosity of the system. This can be explained with the simulation results in the present study. As shown in the previous chapters, the pressure gradient in the fully-filled screw elements depends on the advancement of the reaction, because the viscosity of the system increases with reaction progression. Accordingly, the progress of reaction has a significant effect on pressure and pressure gradient, but not on the length of the fully-filled zones. This implies that the distribution of materials along the screw during reaction can be predicted with a non-reaction system, with a reasonable accuracy.

In the current study, the simulation of polymerization of ε-caprolactone in a co-rotating twin-screw extruder was carried out as follows:

1. Use a 3-D Newtonian, isothermal model to calculate the pressure gradient in the reversed elements and die, and their upstream screw elements under a certain operational condition;

2. Assuming that the die and the reversed elements are fully-filled, calculate the length of fully-filled zone in the elements at the upstream of die and/or reversed elements, based on the equilibrium of pressure;
3. Calculate the degree of fill in the partially-filled zone, and the average residence time in both partially-filled and fully-filled zones; then
4. Starting the numerical simulation from the feeding point of the mixture of monomer and initiator, calculate the temperature and conversion ratio forwardly, with the 3-D simulation model for the fully-filled zones and 1-D or 2-D model for the partially filled channels.

7.3 Validation of Simulation of Polymerization in Twin-screw Extruders

In this section, the simulation results based on the method proposed in the previous section are compared with Vergnes' experimental data (25). In their study, polymerization of ε-caprolactone was carried in a Leistritz LSM 30-34 co-rotating twin-screw extruder. A slit die having a width of 50 mm, 44 mm long and a gap of 2 mm, was fixed at the end of the extruder. The screw profile is given in Table 7.1. The ratio of monomer to initiator, $[M]/[I]_o$, was 1000. The barrel temperatures were 105°C. The flow rate was 1.5 kg/hr or 3 kg/hr, and screw-rotating speed was 100 rpm.

As discussed previously, the first two steps in modeling of reactive extrusion are the calculation of the pressure profile, and the degree of fill along the screw, assuming that die and reversed elements are fully-filled. Table 7.2 summarizes the calculated length of the fully-filled and partially-filled zones along the screw profile at 100 rpm, based on a 3-D model with an isothermal and Newtonian flow conditions. In the element

SE20/307.5, the lengths of both fully-filled and partially-filled zones are zero (i.e. there is no material in this element), because the mixture of monomer and initiator is fed at the downstream of this element. As shown in Table 7.2, the total fully-filled length in the forward screw elements is small. Most of the lengths of the forward elements are partially-filled. This is attributable to the low resistance of the reversed kneading blocks.

Table 7.1 Screw Configuration from Study of Vergnes (25)

Elements	Length (mm)	Pitch (mm)
Feeding Port		
SE20/307.5	307.5	20
SE45/120[1]	120	45
KB45/6/30° (R)	45	KB
SE20/120	120	20
SE30/120[1]	120	30
KB37.5/5/30° (R)	37.5	KB
SE45/120[2]	120	45
SE30/120[2]	120	30
KB22.5/3/30° (R)	22.5	KB
SE45/120[3]	120	20
SE30/67.5	67.5	30
Die		

Table 7.2 Length of Fully-Filled and Partially-Filled Zones Along the Screw

Elements	Length (mm)	Length of fully- or partially-filled zones (mm)			
		Fully	Partially	Fully	Partially
		Q = 1.5 kg/hr		Q = 3.0 kg/hr	
SE20/307.5	307.5	0	0	0	0
SE45/120[1]	120	17.34	102.66	19.66	100.34
KB45/6/30° (R)	45	45	0	45	0
SE20/120	120	0	120	0	120
SE30/120[1]	120	8.26	111.74	9.36	110.64
KB37.5/5/30° (R)	37.5	37.5	0	37.5	0
SE45/120[2]	120	0	120	0	120
SE30/120[2]	120	4.13	115.87	4.68	115.32
KB22.5/3/30° (R)	22.5	22.5	0	22.5	0
SE45/120[3]	120	0	120	0	120
SE30/67.5	67.5	1.47	66.03	3.07	64.43

Table 7.3 shows the predicted residence time in the fully-filled and partially-filled zones along the screw. Because the length of the partially-filled region does not change significantly at different feeding rates (see Table 7.2), the residence time in the partially-filled zones almost remains constant with a flow rate either at 1.5 kg/hr, or at 3.0 kg/hr. Thus, Table 7.3 only gives the residence time at the partially-filled zones with Q = 1.5 kg/hr. As shown in Table 7.3, the total residence time in the fully-filled zones decreases significantly with increasing feeding rate, and it is much higher than that in the partially-filled zones. Moreover, when the materials are located at the bottom of the barrel, the residence time is much shorter than that with materials attached to the screw flight. This is because the materials are conveyed with the positive displacement mechanism when located at the bottom of the barrel, but drag flow when attached to the screw flight.

Table 7.3 Residence Time in Fully-Filled and Partially-Filled Zones Along the Screw

Elements	Residence time (s) in fully- or partially-filled zones			
	Fully-filled		Partially-filled	
	Q = 1.5 kg/hr	Q = 3.0 kg/hr	Model #1	Model #2
SE20/307.5				
SE45/120	21.35	12.21	0.66	1.54
KB45/6/30° (R)	55.42	27.95		
SE20/120			3.60	7.40
SE30/120	10.18	5.81	2.20	4.71
KB37.5/5/30° (R)	46.18	23.29		
SE45/120			1.60	3.74
SE30/120	5.09	2.91	2.30	4.92
KB22.5/3/30° (R)	27.71	13.98		
SE45/120			3.54	7.27
SE30/67.5	1.81	1.91	1.20	2.67
Subtotal (s)	167.74	88.06	15.10	32.25
Die	40	20	0	0

*Model #1 is for the case with materials located at the bottom of barrels, while Model #2 is for the materials at the screw flight.

Janssen's study (79) shows that the materials start to attach to the push side of the flight when the value of F_r/R_e is about 0.04:

$$\frac{F_r}{R_e} \cong 150\frac{N\eta}{\rho} = 0.04 \tag{7.15}$$

In the polymerization of ε-caprolactone, the density ρ of the reaction system is about 1000 kg/m^3. At a screw rotational speed of 100 rpm (i.e. 1.667 rps), F_r/R_e reaches 0.04 when the reaction system has a viscosity of 0.16 Pa-s. This indicates that when the system viscosity is lower than 0.16 Pa-s, the materials prefer to stay at the bottom of the barrel, which are then conveyed forward by the positive displacement mechanism. Vergnes's work (25) shows that the viscosity of the reaction system reaches this critical value of 0.16 Pa-s at the reversed kneading block KB37.5/5/30° (R) (see Table 7.1). This indicates that in the partially-filled zones along the screw, the reaction system is located at the bottom of barrels prior to this element, and stays at the push side of the flight beyond this kneading block. In the former, the residence time should be calculated based on the positive conveying mechanism (Model #1 in Table 7.3), whereas in the latter, it is predicted with the drag mechanism. Consequently, the total residence time of the reaction system in the partially-filled zones is about 25 s.

Considering the fact that the residence time in the partially-filled zones is short, and that there is no axial mixing in the partially-filled channels, the increase in conversion ratio in the partially-filled zones is much smaller than that in the fully-filled regions. In this analysis, the increase in conversion in the partially-filled zones is tentatively neglected; only the conversion increase in the fully-filled zones is calculated.

Similar to what has been done in the previous two chapters, the 3-D mesh for the fully-filled zones was generated with a C++ code. Figure 7.3 shows the geometry of the

reversed kneading blocks and their upstream conveying elements, which are fully-filled in the processing. The mesh for these three sections was generated by 206,080, 147,840, and 103,040 brick elements, respectively.

The length of the conveying elements at the upstream of the reversed kneading blocks in Figure 7.3 was determined based on the calculation results presented in Table 7.2. However, in order to make the mesh generation simple, the length of the fully-filled zone in the conveying elements was slightly increased, as shown in Table 7.4. It should be noted here that the small increase in the fully-filled length would raise the residence time, and thus, partly, make up for the neglected residence time in the partially-filled zones in the analysis.

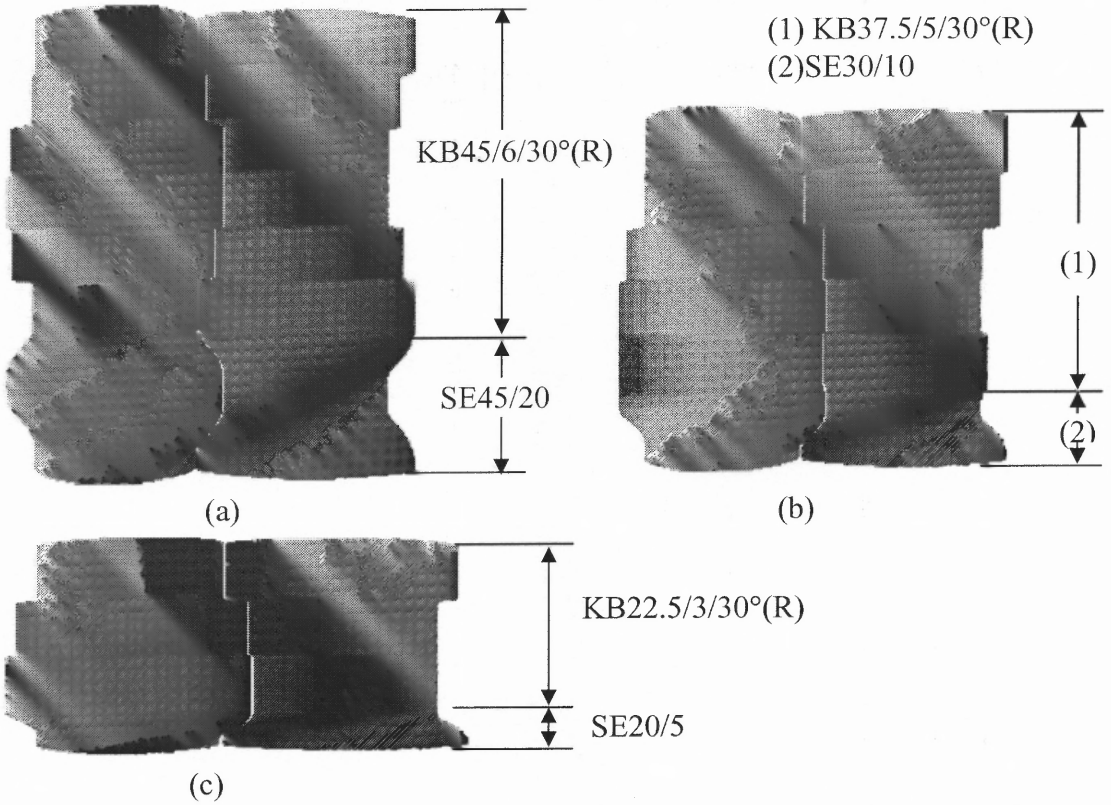

Figure 7.3 Screw geometry for the fully-filled zones of (a) KB45/6/30°(R) and its upstream, (b) KB37.5/5/30° and its upstream, and (c) KB22.5/3/30° and its upstream.

Table 7.4 Length of the Fully-Filled Zone in the Conveying Elements

Elements	Calculated Length of Fully-filled Zone (Table 7.2)		Length in Mesh Generation in 3-D Modeling
	Q = 1.5kg/hr	Q = 3.0 kg/hr	Q = 1.5 or 3 kg/hr
SE45/120[1]	17.34	19.66	20
SE30/120[1]	8.26	9.36	10
SE30/120[2]	4.13	4.68	5

Figure 7.4 shows the profiles of conversion ratio along the axial length based on the 3-D model proposed in the present study, and experimental results from Vergnes (25), at 100 rpm and at a feed rate of 1.5 kg/hr, and 3.0 kg/hr, respectively. Globally, the conversion ratios of ε-caprolactone at the die from the 3-D numerical simulation fit well with the experimental results. This indicates that the numerical simulation method, i.e. 3-D model, proposed in this study is reliable. Moreover, Figure 7.4 shows that the conversion ratios from the simulation are slightly lower than the experimental results, which can be interpreted by the fact that the reactions in the partially-filled zones were neglected in the current analysis.

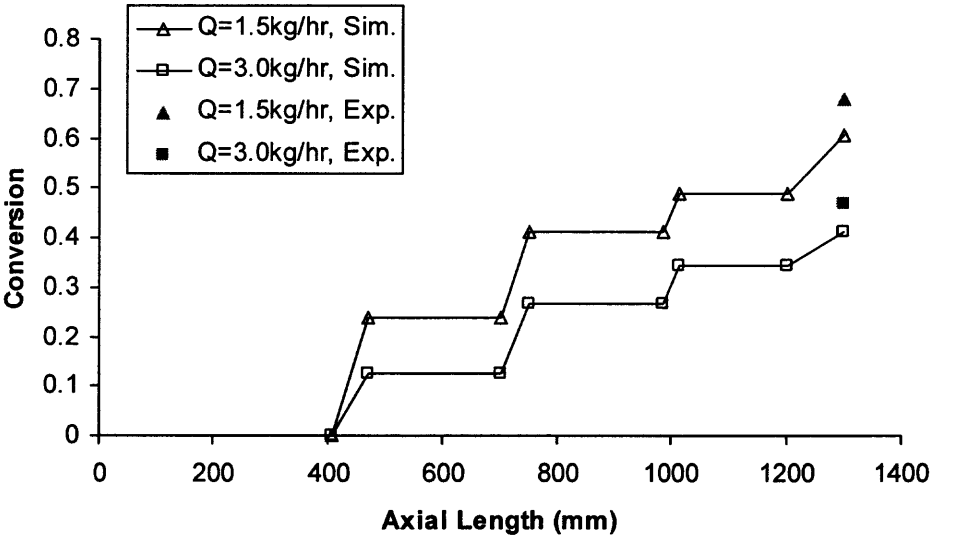

Figure 7.4 Comparison of conversion ratios along the axial length from simulation and experiments.

7.4 Effect of Fully-Filled Length on Polymerization in Reactive Extrusion

In the study of Vergnes (25), the polymerization of ε-caprolactone in a twin-screw extruder was modeled with the 1-D channel model and compared with the experimental results. The simulation results agree well with the experimental data. Accordingly, the authors concluded that the application of 1-D model in predicting polymerization in twin-screw extruders is feasible. However, the simulation results presented in Chapter 5 already showed that the difference in calculated polymerization progression based on 1-D model and 3-D model can be large, depending on the operational conditions. This implies that the 1-D model may not predict the polymerization in twin-screw extruders correctly. Consequently, the question that arises here is: which type of reaction condition is 1-D model applicable?

The conditions for the polymerization used in Vergnes' work (25) are as follows:

1. The diameter of the screw was 34 mm, in which the channel depth was 4.0 mm.
2. The length of fully-filled zone was short. The maximum length of the fully-filled zone was 65 mm.
3. The variation in temperature along the axial length was small.

In the simulation carried out in Chapter 5, the length of the fully-filled elements was 120 mm. Thus, the question here is whether the length of the fully-filled zone is a critical factor, which leads to the deviations in polymerization progression based on 1-D model and 3-D model.

Figure 7.5 shows the predicted conversion ratios of ε-caprolactone along the axial length in conveying elements with a pitch of 45 mm, and at a length of 20 mm, 60 mm and 120 mm, respectively. The simulation conditions are as follows. The inlet and barrel

temperatures were assumed to be 70 °C and 105 °C, respectively. The flow rate was 1.5 kg/hr, and the ratio of monomer to initiator concentration, $[M]/[I]_0$, was 1000. The screw rotational speed was 100 rpm, and the screw elements were fully-filled.

As shown in Figure 7.5, the profiles of the conversion ratio along the axial length depend on the length of the conveying elements; the conversion ratio has a faster rise with increasing length of the elements. For example, the conversion ratio is about 0.19 at an axial location of 0.05 m in the element with a length of 60 mm, whereas it is about 0.26 when the element is 120 mm long. The possible reason for the increase in conversion ratio in the long elements is that the back-flux brings fluid elements with high conversion ratio to the upstream.

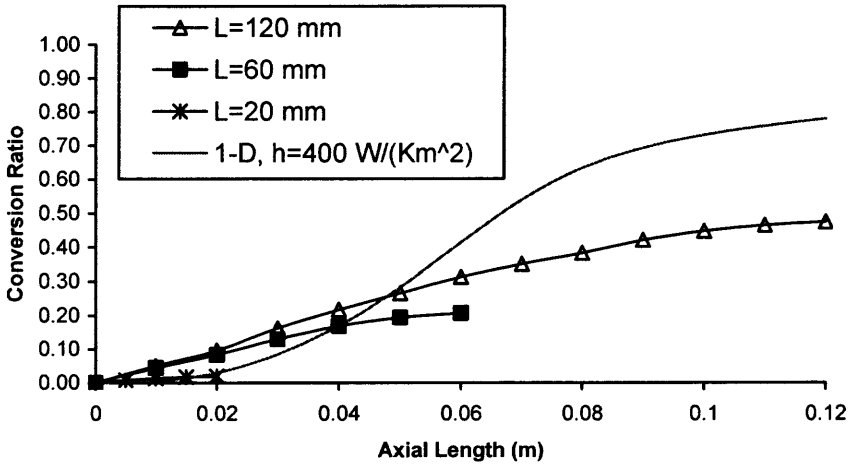

Figure 7.5 Conversion ratios in conveying elements with different axial lengths. (L represents length of the simulation domain in 3-D modeling).

Figure 7.5 also shows that the conversion ratio based on 3-D model differs from that based on 1-D model, with a heat transfer coefficient of 400 J/K m^{-2} at the barrel surface. It is seen that the difference in conversion ratio between 1-D and 3-D model is small when the element has a short length, say, a length shorter than 0.04 m, whereas it is

very significant when the element is longer than 0.08 m. This is because the large heat released from the polymerization changes the heat transfer mechanism at the barrel surface. This indicates that the 1-D channel works well only under certain conditions, namely, a simulation domain with short axial length.

7.5 Scale-up Polymerization in Twin-Screw Extrusion

In order to elucidate the mechanisms in the scaled-up polymerization in twin screw extrusion, a numerical simulation was carried out to trace the polymerization of ε-caprolactone in an extruder with a screw diameter of 68 mm, which is twice that studied in Section 7.3. The condition for the scale up is given in Table 7.5, in which the average residence time of materials in the extruder remains identical after the scaling up.

Table 7.5 Conditions for Scaling up Polymerization

	System before Scaling up	System after Scaling up
Screw Diameter	D	2D
Screw Length	L	2L
Gap	δ	2δ
Screw Speed	N	N
Barrel Temperature	T_b	T_b
Inlet Temperature	T_o	T_o
Feeding Rate	Q	8Q
Average Residence time	t	t

Figure 7.6 summarizes the increase in conversion ratio and temperature along the axial length of the extruder in the polymerization of ε-caprolactone at a screw speed of 100 rpm, at a screw diameter, D, of 68 mm and 34 mm, respectively.

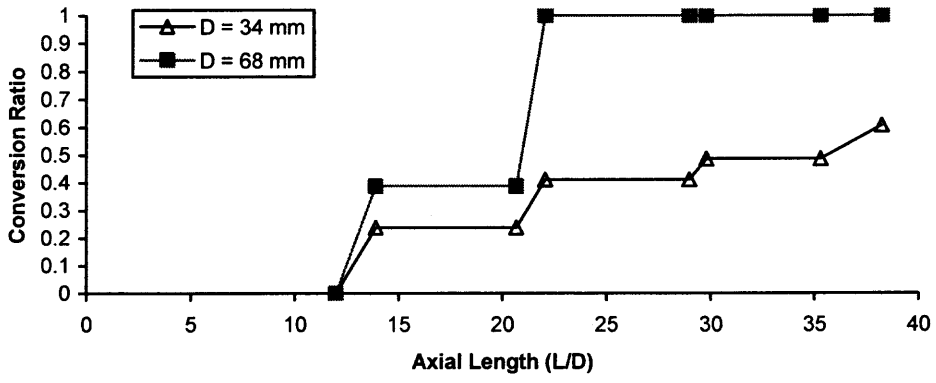

(a)

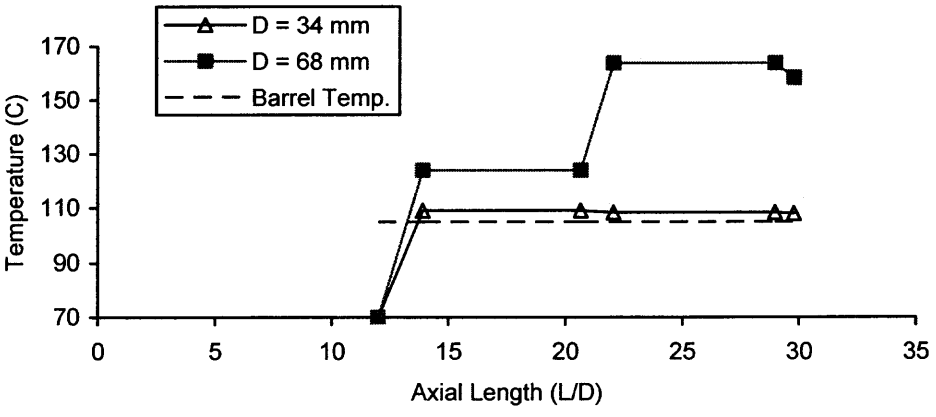

(b)

Figure 7.6 Predicted (a) conversion ratio profile and (b) temperature increase along the axial length during scaling up.

As shown in Figure 7.6a, the conversion ratio has a very fast increase and the reaction is completed at an axial location of about 22D at D = 68 mm. However, the conversion ratio is only about 0.6 at the die of the extruder with D = 34 mm. This indicates that the axial length of the extruder (in unit of D), required to complete the polymerization, is much shorter with increasing screw diameter. This is due to the poor heat loss at the barrel surface at large screw diameter. As a consequence, the temperature has a significant rise with increasing screw diameter. As shown in Figure 7.6b, with D = 34 mm, the temperature of the reaction system is very close to the barrel temperature,

because the heat from reaction is not large so that most of it can be transfer out through the barrel. On the other hand, at D = 68 mm, the conversion ratio has a large increase at a short axial distance (in the fully-filled zone), and the heat from reaction is too large to be released through the barrel surface, resulting in a large increase in temperature.

The large increase in temperature at a short screw length would cause some drawbacks for the polymerization, such as degradation of polymeric macromolecules, and side chain reaction (i.e. branching). This indicates that a good control on temperature increase is very important in carrying out polymerizations in large extruders. Based on the simulation results in this study, it is possible to avoid the large increase in temperature in the large extruders, by the optimization of the screw configuration, operational conditions, and the cooling system.

It is known that the fully-filled zone in twin-screw extruders is formed due to the presence of the reversed screw elements, and the length of the fully-filled zone depends on the configuration of screw element, screw rotational speed and feeding rate. As discussed in Sections 7.3 and 7.4, the residence time is much longer in the fully-filled zones than the partially-filled ones, and the reaction becomes fast with increasing length of the fully-filled zones (see Figure 7.5). This indicates that it is important to reduce the length of the fully-filled zone, especially when the temperature at its inlet is sufficiently high, in order to avoid the rapid increase in conversion ratio and temperature.

On the other hand, the enhancement of heat transfer through the barrel or screw surfaces is also critical to polymerization. This can be achieved by optimizing the design of cooling systems in the screw or the barrel, or even by designing some specific screw elements to enhance the mixing and/or the heat transfer at walls.

7.6 Conclusions

In this chapter, the conveying mechanism in the partially-filled channels was discussed, and the global modeling of polymerization in a co-rotating twin-screw extruder was presented. The comparison between the simulation results and experimental data shows that the conversion ratios of ε-caprolactone based on the numerical simulation agree well with those from the experiments. This indicates that the 3-D simulation method proposed in the current study is reliable.

Scaling up polymerization in twin-screw extruders was also investigated with the 3-D model. The simulation results reveal that polymerization is completed in shorter screw length (in unit of screw diameter, D) with increasing screw diameter. It is also found that the temperature increase is more significant along the screw length when the screw diameter is raised, which would lead to some drawbacks for the polymerization. To solve this problem, an optimization of screw configurations and geometries of screw elements, operational conditions, and the cooling systems in screws and barrels should be carried out, in which the 3-D modeling would be a key tool.

The length of the fully-filled zone has a significant effect on the polymerization progress because of the back-flux. With increasing fully-filled length, the polymerization is accelerated, and the difference in polymerization progress between 3-D and 1-D models becomes pronounced. This implies that the 1-D model can only be used under certain limitations, such as short fully-filled length, small screw diameter, and low heat from reaction. The 3-D model is a powerful method, which can be applied at various reaction conditions.

CHAPTER 8

CONCLUSIONS AND RECOMMENDED WORK

Reactive extrusion is an efficient and environmentally-friendly technique for both polymerization and chemical modification of polymers. However, it is a complex reaction engineering process that combines the traditionally separated operations of polymer chemistry (polymerization or chemical modification) and extrusion, into a single process in a screw extruder. Numerical simulation is a valuable tool in optimizing reactive extrusions, in improving quality and reducing cost of the products. The contributions of the current work are:

1. A 3-D model was developed to simulate the polymerization of ε-caprolactone in fully filled conveying elements and kneading blocks, in which the kinetics equation for polymerization was coupled with continuity equation, momentum equation, and energy equation. Furthermore, the effects of reaction progression, temperature and shear rate upon the system viscosity were incorporated into the modeling.

2. Parametric studies have been carried out to investigate the effects of screw configurations, screw diameter, operational conditions, values of heat from reaction, initiator concentration, and heat transfer conditions at barrel surface, upon the polymerization in fully-filled screw elements of co-rotating twin-screw extruders.

3. Two simulation models were proposed based on the distribution of materials in the partially-filled channels.

4. A global model for reactive extrusion was proposed, combining the models for the fully-filled elements and the partially-filled channels. The predicted conversion ratios at the die agree well with the experimental results from the literature, indicating that the proposed 3-D model for polymerization in twin-screw extruders is reliable.

5. Three indexes, i.e. flux-mixing coefficient, temperature mixing coefficient, and conversion ratio mixing coefficient, were defined for the first time, to evaluate the axial mixing during reactive extrusion; transverse mixing was characterized by the ratio of pressure flow rate to net flow rate in the axial cross section;

6. Scaling up polymerization in twin-screw extruders was studied with the 3-D model, and it was found that 1-D model cannot represent the reaction progress well in the

large machines. 3-D model should be used in scaled up polymerization in reactive extrusion.

The simulation results based on the 3-D model indicate that the polymerization of ε-caprolactone in screw elements depends not only on the mixing mechanism and flow behavior, but also on the heat generation in the reaction system and the heat transfer at the barrel surfaces. Furthermore, the flow and mixing mechanisms affect the heat generation and heat transfer behavior, and vice versa. The increase in mixing intensity generally accelerates the reaction progress, whereas the rise in heat loss through the barrel surface slows down the reaction (Usually the reaction system has a higher temperature than the barrel surface). Consequently, the optimization of polymerization progress in the fully-filled section of twin-screw extruders can be achieved by matching the flow and mixing mechanisms with the energy generation and energy loss.

The method commonly used in the simulation of reactive extrusion, i.e. 1-D channel model, was developed based on the assumption that the reaction system has an ideal mixing in the axial cross section of the flow channel. However, the numerical simulation results based on the 3-D model show that neither the temperature, nor the degree of reaction, is uniform at the axial cross sections in the extruder. The application of 1-D model in predicting the polymerization in reactive extrusion is acceptable only under certain conditions, such as in the cases where the screw diameter is small, or the length of the fully-filled zone is short, or the screw rotational speed and the heat from reaction are low.

The non-uniformity of temperature in the extruder becomes pronounced when the dimension of the machine is scaled up, in which the 1-D model might fail in predicting the reaction progression. This implies that the optimizations of screw configurations,

operational condition, and cooling system design are extremely important to the polymerization carried out in large machines, in which 3-D model is a valuable tool.

The modeling of polymerization in co-rotating twin-screw extruders is very complex, due to the complex flow and mixing behavior, and heat generation and transfer. In the current studies, it was assumed that the polymerization of ε-caprolactone is not sensitive to distributive mixing, and changes in interfacial areas and shear rate; and the model based on the quasi-steady state was used to simulate the dynamic motion of fluid in the twin-screw extrusion. These assumptions could affect the precision of the numerical simulation results.

The following are the recommended future studies, to address some of the issues discussed in this thesis:

1. *Effect of flow mechanism on reactions in reactive extrusion.* The flow in twin-screw extruders is a combination of shear flow and elongational flow. It is important to propose a model to include the presence of elongational flow on reaction.

2. *Heat transfer mechanism in large extruders during reactive extrusion.* Because the non-uniformity in temperature becomes pronounced in large machines, it is necessary to study how to increase the heat transfer through barrel and screw surface, and how to increase the distributive and dispersive mixing in the reaction system.

3. *Modeling of reactive extrusion with the dynamic motion of screws.* In the current study, the dynamic motion of screws was approximated with steady state simulation method. Recently, some technologies, such as Mesh Superposition Technique, have been developed to mimic the dynamic motion of screws in the extruders. However, no work has been carried out to check the feasibility of these techniques in the reactive extrusion yet. It will be a great work if some new mesh generation technologies can be incorporated into the simulation of reactive extrusion, to investigate the effect of the dynamic motion of screws on reactions in the extruders.

REFERENCES

1. S. B. Brown, "Reactive extrusion, a survey of chemical reactions of monomers and polymers during extrusion processing," Chapter 4 in *Reactive Extrusion, Principles and Practice*, M. Xanthos (ed.), Hanser Publishers, Munich, 1992.

2. G.-H. Hu, "Reactive polymer processing: fundamentals of REX", in *Encyclopedia of Materials: Science and Technology*, K. H. J. Buschow et al. (eds.), Elsevier Science, pp. 8049-8057, 2001.

3. C. Tzoganakis, "Reactive extrusion of polymers: a review," Adv. Polym. Tech., 9, pp. 321-330, 1989.

4. F. G. Martelli, *Twin Screw Extruders: A Basic Understanding*, Van Nostrand Reinhold Co., New York, 1983.

5. C. Rauwendaal, *Polymer Mixing, A Self-Study Guide*, Hanser Publishers, Munich, 1998.

6. J. L. White, *Twin Screw Extrusion, Technology and Principles*, Hanser Publishers, Munich, 1990.

7. D. B. Todd, "Features of extruder reactors," Chapter 5 in *Reactive Extrusion, Principles and Practice*, M. Xanthos (ed.), Hanser Publishers, Munich, 1992.

8. D. B. Todd, "Introduction to compounding," Chapter 1 in *Plastic Compounding, Equipment and Processing*, D. B. Todd (ed.), Hanser Publishers, Munich, 1998.

9. T. Sakai, "Extrusion equipment for reactive blending," Chapter 7 in *Reactive Polymer Blending*, W. Baker, C. Scott C., G. H. Hu (eds.), Hanser Publishers, Munich, 2001.

10. P. G. Andersen, "The Werner & Pfleiderer twin-screw co-rotating extruder System," Chapter 4 in *Plastic Compounding, Equipment and Processing*, D. B. Todd (ed.), Hanser Publishers, Munich, 1998.

11. M. L. Booy, "Geometry of fully wiped twin screw equipment," *Polym. Eng. Sci*, 18, pp. 937-984, 1978.

12. M. L. Booy, "Isothermal flow of viscous liquid in corotating twin screw devices," *Polym. Eng. Sci*, 20, pp. 1220-1228, 1980.

13. G. H. Hu, "Reactive blending in screw extruders," Chapter 6 in *Reactive Polymer Blending*, W. Baker, C. Scott C., G. H. Hu (eds.), Hanser Publishers, Munich, 2001.

14. M. Xanthos, "Process analysis from reaction fundamentals: Examples of polymerization and controlled degradation in extruders," Chapter 2 in *Reactive Extrusion, Principles and Practice*, M. Xanthos (ed.), Hanser Publishers, Munich, 1992.

15. J. A. Biesenberger, "Principles of reaction engineering," Chapter 6 in *Reactive Extrusion, Principles and Practice*, M. Xanthos (ed.), Hanser Publishers, Munich, 1992.

16. R. C. Kowalski, "Fit the reactor to the chemistry, case histories of industrial studies of extruder reactions," Chapter 1 in *Reactive Extrusion, Principles and Practice*, M. Xanthos (ed.), Hanser Publishers, Munich, 1992.

17. G. S. Meyhaus, A. Moses, Y. Reibenbach and Z. Tadmor, "Continuous polymeization in extruder reactor," *J. Polym. Sci., Polym. Lett. Ed.*, 11, pp. 103-111, 1973.

18. B. Siadet, M. Malone and S. Middleman, "Some performance aspects of the extruder as a reactor," *Polym. Eng. Sci*, 19, pp. 787-794, 1979.

19. J. Biesenberger and C. Gogos, "Reactive polymer processing," *Polym. Eng. Sci*, 20, pp. 838-846, 1980.

20. J. T. Lindt, "Circular Couette flow of a polymerizing fluid," *Polym. Eng. Sci*, 21, pp. 424-432, 1981.

21. C. Tzoganakis, J. Vlachopoulos and A. E. Hamielec, "Production of controlled rheology polypropylene resins by peroxide promoted degradation during extrusion," *Polym. Eng. Sci,* 28, pp. 170-180, 1988.

22. C. Tzoganakis, J. Vlachopoulos and A. E. Hamielec, "Modeling of the peroxide degradation of polypropylene in a single screw plasticating extruder," *Intern. Polym. Proc.*, 3, pp. 141-154, 1988.

23. W. Michaeli and A. Grefenstein, "Twin-screw extruders for reactive extrusion," *Polym. Eng. Sci.*, 35, pp. 1485-1504, 1995.

24. W. Michaeli and A. Grefenstein, "Engineering analysis and design of twin-screw extruders for reactive extrusion," *Adv. Polym. Tech.*, 14, pp. 263-276, 1995.

25. A. Poulesquen, B. Vergnes, Ph. Cassagnau, J. Gimenez and A. Michel, "Polymerization of ε-caprolactone in a twin screw extruder, experimental study and modeling," *Intern. Polym. Proc.*, XVI, pp. 31-38, 2001.

26. B. Vergnes, G. D. Valle and L. Delamare, "A global computer software for polymer flows in co-rotating twin-screw extruders," *Polym. Eng. Sci.*, 38, pp. 1781-1792, 1998.

27. F. Berzin, B. Vergnes, P. Dufosse and L. Delamare, "Modeling of peroxide initiated controlled degradation of polypropylene in a twin screw extruder," *Polym. Eng. Sci*, 40, pp. 334-356, 2000.

28. F. Berzin and B. Vergnes, "Transesterification of ethylene acetate copolymer in a twin screw extruder," *Intern. Polym. Proc.*, XIII, pp. 13-22, 1998.

29. T. Fukuoka, "Numerical simulation of a reactive extrusion processing. Part I. Kinetics study on grafting of vinysilane to polyethylene," *Polym. Eng. Sci.* 40, pp. 2511-2523, 2000.

30. T. Fukuoka, "Numerical simulation of a reactive extrusion processing. Part II. Simulation and verification for the twin screw extrusion," *Polym. Eng. Sci.* 40, pp. 2524-2538, 2000.

31. H. Kye and J. L. White, "Simulation of continuous polymerization in a modular intermeshing co-rotating twin screw extruder, application to caprolactom conversion to polyamide 6," *Intern. Polym. Proc.,* XI, pp. 129-138, 1996.

32. B. Kim and J. L. White, "Simulation of thermal degradation, peroxide induced degradation, and maleation of polypropylene in a modular co-rotating twin screw extruder," *Polym. Eng. Sci.*, 37, pp. 576-589, 1997.

33. H. Kye and J. L. White, "Simulation of reactive extrusion: polymerization of carprolactam in a modular co-rotating twin screw extruder," *Proceedings of 54th SPE ANTEC*, pp. 309-313, 1996.

34. Z. Chen and J. L. White, "Simulation of non-isothermal flow in modular co-rotating twin screw extrusion," *Polym. Eng. Sci.*, 34, pp. 229-237, 1994.

35. P. Kim and J. L. White, "Transesterification of ethylene vinyl acetate copolymer in a modular intermeshing corotating twin screw extruder with different screw configurations," *J. Appl. Polym. Sci.*, 54, pp. 33-45, 1994.

36. J. P. Puaux and Ph. Cassagnau, "Modeling a reactive extrusion in a twin-screw extruder," *Proceedings of 17th Annual Meeting of Polymer Processing Society* (CD-ROM), Montreal, Canada, May, 2001.

37. J. P. Puaux, G. Bozga and A. Ainser, "Residence time distribution in a corotating twin-screw extruder," *Chem. Eng. Sci.*, 55, pp. 1641-1651, 2000.

38. L. Zhu and K. S. Hyun, "Numerical simulation of bulk polymerization of ε-caprolactone in extrusion," *Proceedings of 60th SPE ANTEC,* pp. 204-208, 2002.

39. L. Zhu, K. S. Hyun and K. A. Narh, "Modeling of Bulk Polymerization of ε-Caprolactone in Shear Flow," *Proceedings of 18th Annual Meeting of Polymer Processing Society* (CD-ROM), Guimaraes, Portugal, June, 2002.

40. D. Strutt, C. Tzoganakis and T. A. Duever, "Mixing analysis of reactive polymer flow in conveying elements of a co-rotating twin screw extruder," *Adv. Polym. Tech.*, 19, pp. 22-33, 2000.

41. D. Strutt, C. Tzoganakis and T. A. Duever, "Mixing analysis of reactive polymer flow in a single-screw extruder channel," *Polym. Eng. Sci.*, 40, pp. 992-1003, 2000.

42. D. B. Todd, "Heat transfer in twin screw extruders," *Proceedings of 34th SPE ANTEC*, pp. 54-59, 1988.

43. J. L. White, E. Kim, J. Keum and H. Jung, "Modeling heat transfer in screw extrusion with special application to modular self-wiping co-rotating twin screw extrusion," *Polym. Eng. Sci.*, 41, pp. 1448-1455, 2001.

44. T. Domschke and C. Justus, "Heat transfer in single and twin screw extruders," *Intern. Poly. Proc.*, VIII, pp. 294-307, 1993.

45. W. M. Davis, "Heat transfer in extruder reactors," Chapter 7 in *Reactive Extrusion, Principles and Practice*, M. Xanthos (ed.), Hanser Publishers, Munich, 1992

46. J. Gimenez, Ph. Cassagnau and R., Michel, "Bulk polymerization of caprolactone: Rheological predictive law", *J. Rheol.*, 44, pp. 527-547, 2000.

47. J. Gimenez, M. Boudris, Ph. Cassagnau and A. Michel, "Control of bulk ε-caprolactone polymerization in a twin screw extruder," *Polymer Reaction Engineering*, 8, pp. 35-157, 2000.

48. R. Kricheldorf, M. Berl and N. Scharnagl, "Poly(lactones). 9. Polymerization mechanism of metal alcoxide, initiated polymerization of lactides and various lactones," *Macromolecules,* 21, pp. 286-293, 1988.

49. Ph. Dubois, N. Ropson, R. Jerome and Ph. Teyssie, "Macromolecular engineering of polylactones and polylactides. 19. Kinetics of ring opening polymerization of ε –caprolactone initiated with functional aluminum alkoxides," *Macromolecules*, 29, pp. 1965-1975, 1996.

50. G. Rafler and J. Dahlmann, "Biodegradable polymers. Polymerization of ε-caprolactone," *Acta Polym.*, 43, pp. 91-95, 1992.

51. N. Ropson, Ph. Dubois, R. Jerome and Ph. Teyssie, "Macromolecular engineering of polylactones and polylactides. 17. Cryometric and viscosimetric analysis of the species active in the ring-opening polymerization of lactones, lactides, and cyclic anhydrides as initiated by aluminum triisoporpoxide," *Macromolecules*, 27, pp. 5950-5956, 1994.

52. K. Y. Yasuda, R. C. Armstrong and R. E. Cohen, "Shear flow properties of concentrated solution of linear and star branched polyesters," *Rheol. Acta*, 20, pp. 163-178, 1981.

53. C. A. Hieber and H. H. Chiang, "Shear rate dependence modeling of polymer melt viscosity," *Polym. Eng. Sci.*, 32, pp. 831-838, 1992.

54. G. Marin, W. W. Graessley, J. P. Montfort and Ph. Monge, "Linear viscoelastic properties of polybutadiene solutions," *Plastics in Medical Surgery (International Conference)*, 2, pp. 285-289, 1980.

55. V. R. Raju, E. V. Menezes, G. Marin, W. W. Graessley and L. J. Fetters, "Concentration and molecular weight dependence of viscoelastic properties in linear and star polymer," *Macromolecules*, 14, pp. 1668-1676, 1981.

56. M. Daoud, J. P. Cotton, B. Farnoux, G. Jannink, G. Sarma, H. Benoit, R. Duplessix, C. Picot and P. G. de Gennes, "Solutions of flexible polymers. Neutron experiments and interpolation," *Macromolecules*, 8, pp. 804-810, 1975.

57. S. Bidstrup and C. W. Macosko, "Chemorheology relations for epoxy-amine crosslinking," *J. Poly. Sci., Part B: Polym. Phy.*, 28, pp. 691-709, 1990.

58. I.-K. Yang and J. D. Lin, "Effects of flow on polymeric reactions," *Polym. Eng. Sci.*, 42, pp. 753-759, 2002.

59. K. J. Ganzeveld and L.P. B. M. Janssen, "A mixing model for multi component reactions in twin screw extruders applied to the polymerization of urethanes," *Polym. Eng. Sci.*, 32, pp. 457-466, 1992.

60. H. Yang and I. Manas-Zloczower, "Flow field analysis of the kneading disc region in a corotating twin screw extruder," *Polym. Eng. Sci.*, 32, pp. 1411-1417, 1992.

61. H. Cheng and I. Manas-Zloczower, "Distributive mixing in conveying elements of a ZSK-53 co-rotating twin screw extruder," *Polym. Eng. Sci.*, 38, pp. 926-935, 1998.

62. T. Li and I. Manas-Zloczower, "Flow field analysis of an intermeshing counterrotating twin screw extruder," *Polym. Eng. Sci.*, 34, pp. 551-558, 1994.

63. H. Cheng and I. Manas-Zloczower, "Study of mixing efficiency in kneading discs of co-rotating twin screw extruders," *Polym. Eng. Sci.*, 37, pp. 1082-1090, 1997.

64. Th. Avalosse, Y. Rubin and L. Fondin, "Non-isothermal modeling of co-rotating and contra-rotating twin screw extruders," *Proceedings of 58th SPE ANTEC,* pp. 19-24, 2000.

65. D. M. Kalyon, A. D. Gotsis, U. Yilmazer, C. G. Gogos, H. Sangani, B. Aral and C. Tsenoglou, "Development of experimental techniques and simulation methods to

analyze mixing in co-rotating twin screw extrusion," *Adv. Polym. Tech.*, 8, pp. 337-353, 1988.

66. Y, Wang and J. L. White, "Non-newtonian flow modeling in the screw regions of an intermeshing corotating twin screw extruder," *J. Non-Newtonian Fluid Mechanics*, 32, pp. 19-38, 1989.

67. H. Potente and J. Flecke, "Analysis and modeling of the residence time distribution in intermeshing co-rotating twin screw extruders based on finite element simulations," *Proceedings of 55th SPE ANTEC*, pp. 110-114, 1997.

68. D.J. Wal, D. Goffart, E.M. Klomp, H.W. Hoogstraten and L.P.B.M. Janssen, "Three-dimensional flow modeling of a self-wiping corotating twin-screw extruder. Part II: The kneading section," *Polym. Eng. Sci.*, 36, pp. 912-924, 1996.

69. D. Goffart, D.J. Wal, E.M. Klomp, H.W. Hoogstraten, L.P.B.M. Janssen, L. Breysse and Y. Trolez, "Three-dimensional flow modeling of a self-wiping corotating twin-screw extruder. Part I: The transporting section," *Polym. Eng. Sci.* 36, pp. 901-911, 1996.

70. V. L. Bravo, A. N. Hrymak, A.N. and J.D. Wright, "Numerical simulation of pressure and velocity profiles in kneading elements of a co-rotating twin screw extruder," *Polym. Eng. Sci.*, 40, pp. 525-541, 2000.

71. T. Ishikawa, T. Amano, S.-I. Kihara and K. Funatsu, "Flow patterns and mixing mechanisms in the screw mixing element of a co-rotating twin-screw extruder," *Polym. Eng. Sci.*, 42, pp. 925-939, 2002.

72. T. Ishikawa, S.-I. Kihara and K. Funatsu, "3-D non-isothermal flow field analysis and mixing performance evaluation of kneading blocks in a co-rotating twin screw extruder," *Polym. Eng. Sci.*, 41, pp. 840-849, 2001.

73. T. Ishikawa, S.-I. Kihara and K. Funatsu, "3-D numerical simulations of nonisothermal flow in co-rotating twin screw extruders," *Polym. Eng. Sci.*, 40, pp. 357-364, 2000.

74. M. Yoshinaga, S. Katsuki, M. Miyazaki, L. Liu, S-I Kihara and K. Funatsu, "Mixing mechanism of three-tip kneading block in twin screw extruders," *Polym. Eng. Sci.*, 40, pp. 168-178, 2000.

75. K. Funatsu, S.-I. Kihara, M. Miyazaki, S. Katsuki and T. Kajiwara, "3-D numerical analysis on the mixing performance for assemblies with filled zone of right-handed and left-handed double-flighted screws and kneading blocks in twin-screw extruders," *Polym. Eng. Sci.*, 42, pp. 707-723, 2002.

76. T. Ishikawa, S.-I. Kihara, K. Funatsu, T. Amaiwa and K. Yano, "Numerical simulation and experimental verification of nonisothermal flow in counter-

rotating nonintermeshing continuous mixers," *Polym. Eng. Sci.*, 40, pp. 365-375, 2000.

77. R. Ma, A. N. Hrymak and P. E. Wood, "Numerical simulation and experimental verification of flow field in a twin screw extruder," *Proceedings of 17th Annual Meeting of Polymer Processing Society* (CD-ROM), Montreal, Canada, May, 2001.

78. L. Zhu, K. A. Narh and K. S. Hyun, "3-D modeling of polymerization in conveying element in twin-screw extruder," *Proceedings of 61st SPE ANTEC*, pp. 147-151, 2003.

79. R. A. D. Graaf, D. J. Woldringh and L. P. B. M. Janssen, "Material distribution in the partially filled zone of a twin screw extruder," *Adv. Polym. Tech.*, 18, pp. 295-302, 1999.

80. J. A. O'Keefe, "Water on the moon and a new nondimensional number," *Science*, 173, pp. 669-670, 1969.